DANMARKS OG GRØNLANDS GEOLOGISKE UNDERSØGELSE RAPPORT 2011/10

Geochemistry of the supracrustal rocks and the associated intrusive TTG suites of the Archaean craton in South-West Greenland and southern West Greenland, 61°30′ - 64°N

Kristoffer Szilas, Alfons Berger, Thomas F. Kokfelt,
Tomas Næraa, Anders Scherstén
& Martin Klausen

GEOLOGICAL SURVEY OF DENMARK AND GREENLAND
MINISTRY OF CLIMATE AND ENERGY

GEUS

DANMARKS OG GRØNLANDS GEOLOGISKE UNDERSØGELSE RAPPORT 2011/10

Geochemistry of the supracrustal rocks and the associated intrusive TTG suites of the Archaean craton in South-West Greenland and southern West Greenland, 61°30′ - 64°N

Kristoffer Szilas, Alfons Berger, Thomas F. Kokfelt,
Tomas Næraa, Anders Scherstén
& Martin Klausen

GEOLOGICAL SURVEY OF DENMARK AND GREENLAND
MINISTRY OF CLIMATE AND ENERGY

G E U S

Geochemistry of the supracrustal rocks and the associated intrusive TTG suites of the Archaean craton in South-West Greenland and southern West Greenland, 61º30’ - 64ºN

Contributing authors:

Kristoffer Szilas, Alfons Berger, Thomas F. Kokfelt, Tomas Næraa, Anders Scherstén & Martin Klausen

Edited by:

Thomas F. Kokfelt

Table of contents

Editorial note

This GEUS report is a partial contribution within the framework of the 'Homogenisation' project, which is a co-financed project by GEUS and Greenland's Bureau of Minerals and Petroleum (BMP) that has had the main goal to reassess the geology in the area of SW Greenland between 61.5 and 64.0N.The aim of this report is to present and discuss various aspects of the rocks from the SW Greenland Archaean craton from a geochemical and petrological perspective. The data presented represent some of the results coming out of the field work carried out in the area over the last three years (2008-2010), and which involved a geologists from GEUS as well as from external universities/research institutions.

The report is divided into four parts that each discusses geochemical data sets to illustrate various geological processes relevant to the understanding of the SW Greenland Archaean craton, but also to provide more detailed information obtained from specially investigated areas.

The first part provides a regional geochemical dataset from supracrustal rocks in the area between Grædefjord and Sermiligaarsuk (Tartoq) and is to a large extent based on the work that is in progress by Kristoffer Szilas as his Ph.D. project. This regional dataset consist of 220 whole rock geochemical data (major and trace elements) from six different areas of supracrustal rocks, and represents a significant contribution to the existing data set for the entire Archaean craton of SW Greenland.

The second and third parts discuss various processes related to the formation of TTG gneisses in a regional (part 2), as well as, a local (part 3) perspective. In the regional study, the SWG TTG's are compared to a global literature dataset and differences are pinpointed that provide possible clues to their petrogenesis. In part four (by A. Berger, T. Kokfelt and M. Klausen) a local study is presented from a single locality at Dalagers Nunatakker (Frederikshåb Isblink). The rocks at this locality comprise ultramafic rocks and associated felsic rocks of which some show field and geochemical evidence of in situ partial melting processes. The study highlights some possible petrogenetic links between the rocks of the suite using both whole rock geochemistry and mineral chemistry data.

Thomas F. Kokfelt

Geochemistry of Archaean supracrustal belts in South-West and southern West Greenland

Kristoffer Szilas (1), Thomas F. Kokfelt (1) and Anders Scherstén (2)

(1) Geological Survey of Denmark and Greenland, Øster Voldgade 10, DK-1350 Copenhagen K, Denmark, (2) Department of Earth & Ecosystem Sciences, Lund University, 223 62 Lund, Sweden

Introduction

The supracrustal belts of the Archaean craton of SW Greenland occur within the tonalite-trondhjemite-granodiorite (TTG) gneisses that make up the majority of the craton. The supracrustal belts comprise metamorphic rocks primarily of volcanic and intrusive origins, and with subordinate occurrences of ultramafic rocks and rocks of presumed metasedimentary origin. All rocks have experienced metamorphism, mostly under amphibolite facies conditions, but also include greenschist and granulite facies metamorphic grade. Consequently, the prefix 'meta' in all lithologies is taken as implicit throughout this text. The relationship between the supracrustal belts and the surrounding TTG's have been the topic of several studies since the area was first mapped out in the late 1960 and early 1970'es. It is commonly argued that the supracrustal belts represent remnants or slivers of oceanic crust, but it is debated if it formed in relation to mid-oceanic or arc-related spreading centres (Kusky and Polat 1999; Furnes et al. 2007; 2009; Polat et al. 2008), or in association with oceanic plateau systems (Campbell et al. 1989; Bickle et al. 1994; Arndt et al. 1997), whereas the TTG suites are regarded as intrusions into the more mafic crust (e.g., Windley and Garde, 2009; Polat et al., 2009). Crustal growth occurred through the progressive amalgamation of individual arc systems with the final stabilisation occurring at ca. 2.7 Ga (e.g., Nutman et al. 2007 and references therein).

In this chapter we present an overview of the whole rock geochemistry of the supracrustal belts that were visited between Grædefjord and Sermiligaarsuk during the 2008 to 2010 fieldwork seasons. The geochemical data includes volcanic and mafic intrusive rocks found in six supracrustal belts (see Figure 1): (1) Tartoq, (2) Ravns Storø, (3) Bjørnesund, (4) Perserajoorsuaq, (5) Grædefjord, and (6) Nunatak 1390. The presented dataset from these areas are compared and used to discuss possible models for the primary geological setting in which these rocks formed. A major part of the dataset represents a corner stone in a Ph.D. project (2009-2012), which currently is undertaken by Kristoffer Szilas at GEUS and which has run parallel to the overall GEUS/BMP financed 'Homogenisation' project in South West Greenland. The Ph.D. project, entitled "Archaean supracrustals, SW Greeland", uses geochemical and geochronological data to unravel the geological formation history of the supracrustal belts in South-West and southern West Greenland.

The geochemical dataset

The geochemical data consists of major and trace element data for samples from the following supracrustal belts, with the number of analytical data obtained for each area in parenthesis: Tartoq (33), Ravns Storø (43), Bjørnesund (45), Perserajoorsuaq (18), Grædefjord (39) and Nunatak 1390 (42). The location of the various belts can be seen on Figure 1. Data for 16 TTG gneiss samples that were intruded into the supracrustal rock sequences (marginally or within the belts) are reported for reference from Ravns Storø, Tartoq and Grædefjord. Szilas et al. (2011a) reports the geochemical characteristics of TTGs from SW Greenland.

Preliminary Hf and Nd isotopic data suggest ages of these supracrustal belts ranging from ca. 2.9 to 3.2 Ga (K. Szilas, unpublished data). This is in general agreement with zircon age dating of TTG sheets that intrude into the supracrustal belts (Windley and Garde 2009 and references therein; Kokfelt et al 2011).

Analytical methods and data quality

The final dataset was compiled from several analytical rounds, and thus acquired over an extended period of time and from different laboratories, implying some extent of heterogeneity within the data set. To address this issue, we compared the data obtained for the Disko-1 ‘in house’ standard from the various laboratories involved (see Appendix Tables A.1-A.3).

Geology of the supracrustal belts

In this section we give a brief overview of the geology of the different supracrustal belts that are presented data for.

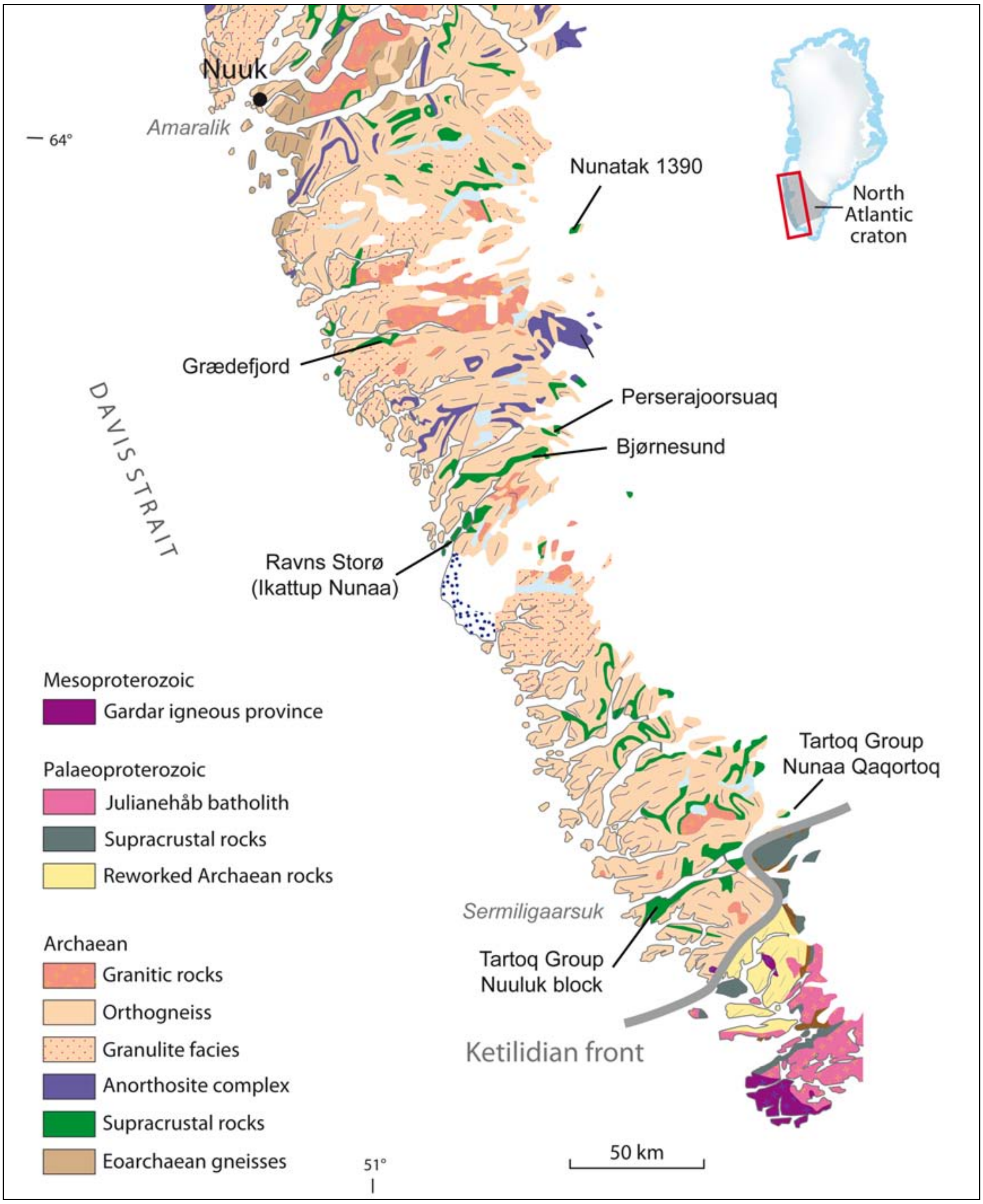

Figure 1. *Overview of the southern part of the North Atlantic Craton in West Greenland. Red stars mark the location of the supracrustal belts discussed in this text.*

Figure 2. *Field photographs of meta-volcanic rocks (amphibolites) in some of the investigated supracrustal belts. (a) Greenschist facies tholeiitic rocks at Nuuluk block in the Tartoq Group, (b) Pillow lava on Nunaa Qaqortoq in the Tartoq Group, (c) Layered amphibolites at Bjørnesund, (d) Possible lithic tuff at Ravns Storø, (e) Pillow lava at Ravns Storø, (f) Calc-alkaline amphibolite at Perserajoorsuaq.*

Tartoq

The Tartoq Group is situated around the fjord of Sermiligaarsuk in the southern part of the area at ca. 61.5° N (Figure 1). The Tartoq Group comprises supracrustal rocks variably metamorphosed under mainly greenschist facies grade (Fig 2a), but with metamorphic grade generally increasing from west to east (van Hinsberg et al. 2010). However, it not entirely clear, to what extent the low metamorphic facies may reflect retrogression. Detailed geological descriptions of the Tartoq Group supracrustal belt can be found in Higgins (1968), Berthelsen and Henriksen (1975), Petersen (1992), Lie (1994), van Hinsberg et al. (2010), Kisters et al. (2011) and Szilas et al. (2011b). The samples for this data set were collected in 2009 and 2010 during GEUS fieldwork in the region. The main lithologies include mafic greenschists and amphibolites that are interpreted as lava flows (Fig. 2b), dykes and gabbroic intrusions. Additionally large ultramafic bodies are found in the Bikuben block, likely represent cumulate rocks, but they are not included in the present data set, nor in the discussion. Felsic schists occur as intrusive sheets in the mafic sequence ranging from 1 to 80 meters in thickness and they are interpreted to represent high strain zones where TTG basement have been sheared into the supracrustal belt (van Hinsberg et al. 2010). The oldest intrusive TTG gives a minimum age of 2996.3 ± 5.9 Ma (Szilas et al. 2011b) and grains in some of the mylonitic felsic schists give ages up to about 3.7 Ga, which points towards a very old basement in the area (K. Szilas, unpublished data). One major difference between the Tartoq Group and the other supracrustal belts described below is that it appears that only tholeiitic rocks occur in Tartoq rather than the bimodal tholeiitic and calc-alkaline assemblage of rocks known elsewhere in SW Greenland (Szilas et al. 2011b).

Ravns Storø

The Ravns Storø supracrustal belt, or the Ikkattup Nunaa belt, was described by Windley (1966), Dawes (1969), Andersen and Friend (1973) and Friend (1975). Samples for this data set were collected by GEUS in 2008 and 2009. Well preserved pillow structures (Fig. 2e) are present in the western part of the belt, indicating that at least some of the volcanic rocks formed in a subaqueous environment. Consequently, caution must be taken regarding the use of more fluid-mobile elements for the petrological interpretations, as they might have been remobilised shortly after extrusion and later during metamorphism. The supracrustal belt mainly comprises amphibolites of variable composition that show variable degrees of deformation. Possible lithic tuffs occur (Fig. 2d), which might be taken as evidence for at least parts of the volcanic sequence being extruded under subaerial conditions. Also present in the southeastern part of the belt are ultramafic rocks, as well as, some aluminous schists that contain cordierite, staurolite, garnet and anthophyllite. The latter group of rocks has been interpreted as metamorphosed volcanic rocks that were hydrothermally-altered prior to metamorphism (Friend 1976; Schumacher et al. 2011) and are thus not included in the present data set.

Generally the field relations and geochemistry is very similar to the Bjørnesund supracrustal belt located about 10 km to the north. U-Pb dating of zircons from a cross-cutting felsic sheet yield an age 2905.3 ± 4.9 Ma (Szilas et al. 2011c).

Bjørnesund

This supracrustal belt is characterised by dark amphibolites, calc-silicate amphibolites and felsic sheets. The main lithologies and field relations are very similar to the Ravns Storø supracrustal belt, but compared to those, they show generally higher degrees of deformation, which makes good examples of primary volcanic structures rare. Nonetheless, there could be made a clear distinction between dark tholeiitic and light calc-alkaline amphibolites in the field (Fig. 2c). The supracrustal belt is in direct intrusive contact with a large anorthosite body. On the basis of similar field relations as in the Fiskenæsset anorthosite complex, found immediately to the north, a link between this and Bjørnesund has been suggested by several authors (Myers, 1985; Keulen et al., 2010; Szilas et al., 2011c). The samples for this data set were collected by GEUS in 2009. The main age peaks in some gneisses and quartz diorites that intrude into the supracrustal belt are about 2.90 - 2.92 Ga (Szilas et al. 2011c; Kokfelt et al. 2011), providing a minimum age for the formation of the supracrustal sequence.

Perserajoorsuaq

No previous geochemical data have been published from this area and it is believed that this locality has not been visited since it was first mapped by H. R. Williams in the beginning of the 1970s. The new samples were collected during a brief reconnaissance (reco-stop for ca. 2 hours) by GEUS in 2009. Generally these rocks record high strain (Fig. 2f) preventing a proper recognition of primary igneous structures. The two main lithologies are mafic amphibolites and leucocratic amphibolites in a repeated succession. No geochronology data exist for this area until now.

Grædefjord

This supracrustal belt is characterised by intense E-W trending cataclastic deformation and brittle-ductile mylonites (Kolb et al. 2010). The high degree of deformation in this region makes the identification of primary igneous (volcanic) features rather difficult. The area has been reported to contain agglomerates and volcanic breccias (Wilf 1982). However, a revisit to the area by GEUS in 2009 did not unequivocally confirm a subaeral volcanic origin of these described occurrences. U-Pb zircon dating of felsic gneisses within the supracrustal sequence generally gives ages of just over 2.7 Ga, but some intrusive TTG sheets have main peaks of about 2.9 Ga that are skewed towards 2.7 Ga (K. Szilas unpublished data). The ~2.9 Ga age agrees with the timing of the early TTG formation in the Grædefjord area (Kisters et al. 2010), whereas the 2.7 Ga age is likely to represent the latest thermal overprinting event.

Nunatak 1390

This locality contains well-preserved pillow structures, ash layers and ultramafic rocks mainly at greenschist metamorphic conditions. The lower pillow lava sequence is over 500 meters thick and calc-silicate alteration is seen throughout and comprise up to 20% of the rocks. Stratigraphically higher there is a 700 meter thick sequence of laminated ash that could be a subaerial deposit. Samples were collected by GEUS in 2006 and 2007. Some preliminary geochemical data were published by Scherstén and Stendal (2008) and field descriptions are given by Stendal (2007). Intrusive orthogneisses consistently yield U-Pb zircon ages around 2.9 Ga (Næraa and Scherstén 2008; K. Szilas unpublished data).

Geochemistry of the supracrustal belts

The data set comprises 220 whole rock geochemical analyses of major elements and trace elements of relatively mafic (111) and felsic (109) rock samples. In the field these rocks were all interpreted as being of either volcanic or shallow intrusive origin (Fig. 2). In addition, 16 analyses of TTG gneiss sheets collected from the same region and which are mainly intrusive into the supracrustal belts were included as a reference group.

The data set was filtered for felsic intrusive rocks, or so-called TTG sheets, based on crosscutting relations and TTG-like chemistry. Despite of this screening procedure, some of the felsic samples that are categorised as calc-alkaline amphibolites are, however, likely to represent deformed TTG sheets that intruded the mainly mafic supracrustal sequences and later, were deformed beyond recognition (i.e., sheared, stretched and likely mechanically mixed with the surrounding supracrustals). Nonetheless, the vast majority of calc-alkaline amphibolites does not overlap with either the ‘reference’ TTG gneiss samples, or the other group of more mafic amphibolites, tholeiites, and are therefore likely to represent a distinct rock group, arguably with a distinct petrogenetic history. The more mafic tholeiitic rocks appear to represent the most juvenile component of supracrustal belts.

The bimodal distribution of the supracrustal rocks is especially evident from the rare earth element (REE) patterns (Fig. 3), where a tholeiitic group of rocks have a very flat pattern (La_N/Sm_N ~ 1) with minor Eu-anomalies and a calc-alkaline group of rocks have a steeper pattern (La_N/Sm_N 2-6). This classification is consistent with the field observation that tholeiitic rocks are generally dark mafic rocks and that the calc-alkaline rocks are felsic schists or leucocratic amphibolites. No transitional samples have been found indicating that these rocks formed by two fundamentally different processes. The TTG gneisses have patterns that are even steeper (La_N/Sm_N > 8) compared to the calc-alkaline rocks, but some extent of overlap does exist (Fig. 3).

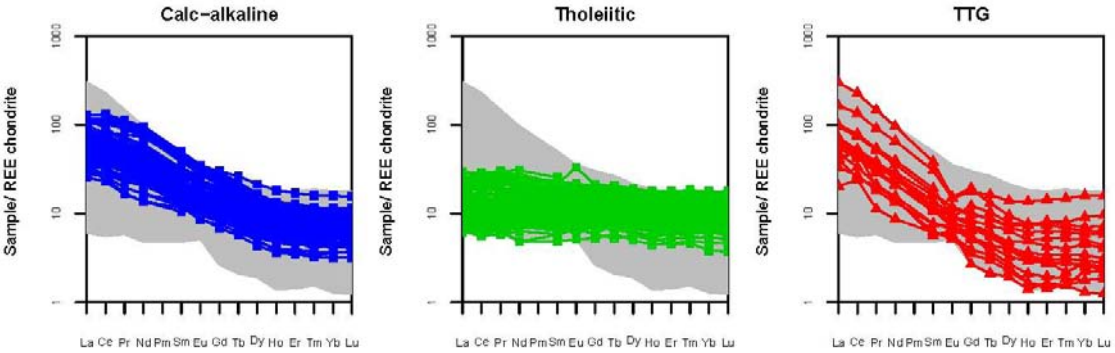

Figure 3. *Chondrite normalised (Boynton 1984) REE patterns showing the bimodal distribution of the supracrustal rocks follow a tholeiitic or a calc-alkaline trend with 111 and 120 samples, respectively 19 TTG gneiss samples for reference.*

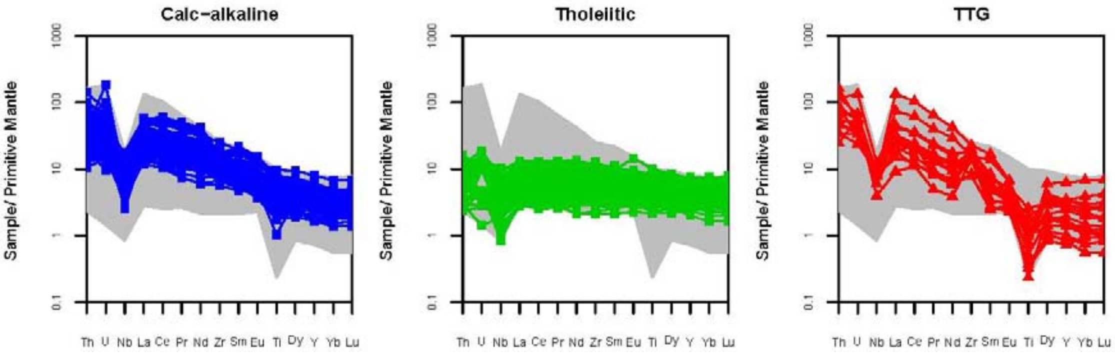

Figure 4. (previous page) *Primitive mantle normalised (Sun and McDonough 1989) trace element diagram showing only the relatively fluid-immobile elements.*

On a primitive mantle (PM) normalised 'spidergram' (Fig. 4), where only the relatively fluid-immobile elements are shown (due to the likely disturbance of the large ion lithophile elements (LILE) during metamorphism and seafloor alteration) the same trends are seen as in the REE diagrams. The tholeiitic rocks have flat patterns at ~3-10 times PM values, and with a fairly pronounced negative anomaly for Nb (Nb/La < 1). The calc-alkaline rocks have steeper patterns with up to 100 times PM for the most incompatible elements (Th and U) and lower levels for the least incompatible elements (Dy, Y, Yb and Lu ~ 5-10 times PM), comparable to the tholeiites. The calc-alkaline rocks have pronounced negative anomalies for Nb (Nb/La << 1) and Ti (Ti/Dy << 1), and variably negative anomalies for Eu. The TTG gneisses show a great deal of similarity to the calc-alkaline rocks, but with even more distinct negative Nb- and Ti-anomalies and with generally lower concentrations of middle to heavy REE's.

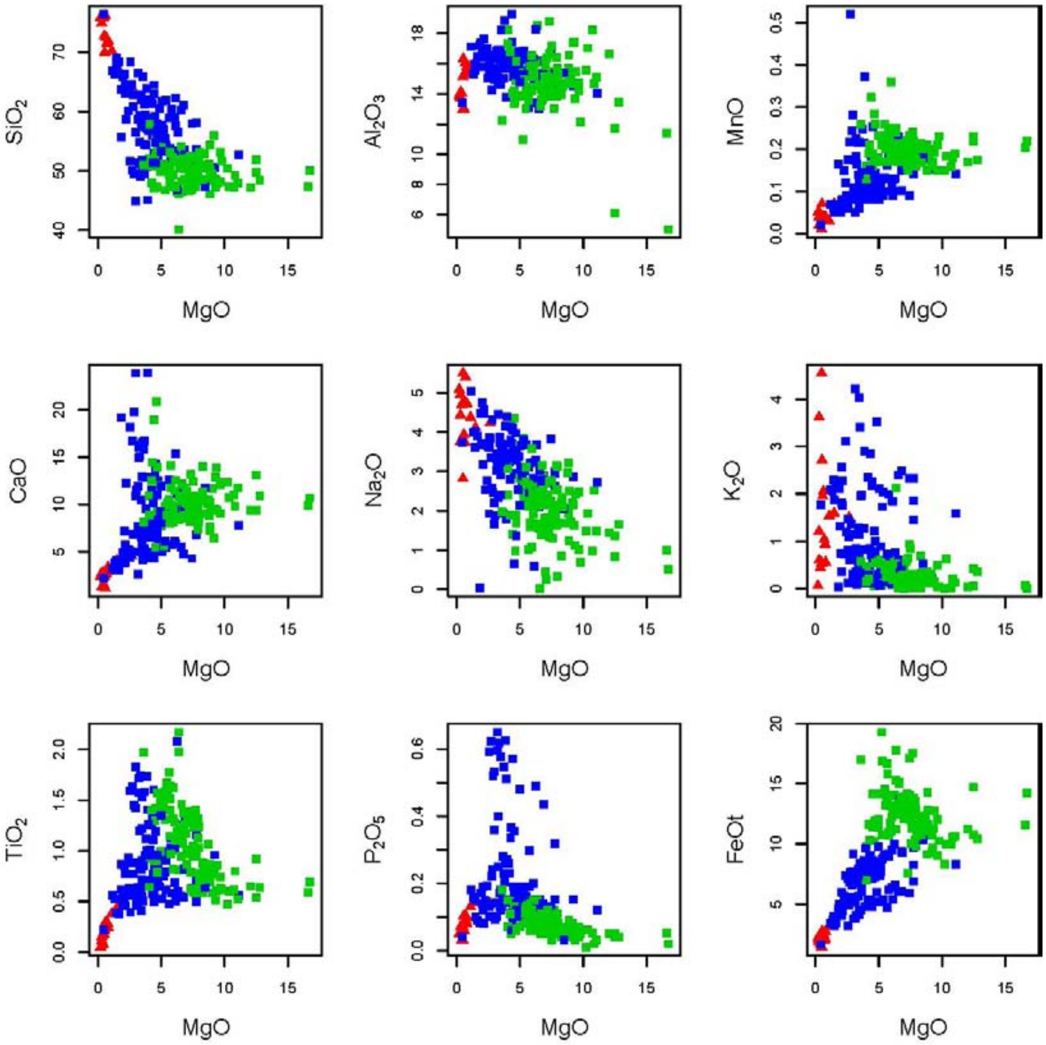

Figure 5. *Major element concentrations for the tholeiitic and calc-alkaline amphibolites and TTG gneisses plotted against MgO (all in wt.%). The calc-alkaline rocks (blue squares) have intermediate MgO contents relative to the tholeiites (green squares) and the TTG gneisses (red triangles), and define in most diagrams a fan of mixing arrays between these*

two components. An exception to this is a group of calc-alkaline rocks from the Bjørnesund area that have relatively high P_2O_5 *and CaO.*

Major elements plotted against MgO (Fig. 5) show fairly systematic variations with the tholeiitic rocks and the TTG gneisses forming end members and the calc-alkaline rocks plotting in between. The tholeiitic rocks have median values of around 50 wt.% SiO_2, 7.2 wt.% MgO, 14.8 wt.% Al_2O_3 and 1 wt.% TiO_2, whereas the calc-alkaline rocks have median values of about 58 wt.% SiO_2, 3.9 wt.% MgO, 15.7 wt.% Al_2O_3 and 0.75 wt.% TiO_2.

The same systematics are displayed for the trace elements on Fig. 5, although there are certain elements that plot off the otherwise linear array. However, the calc-alkaline rocks that fall outside of this array are restricted to certain calc-silicate amphibolites found at Bjørnesund and a few samples from Ravns Storø with high Nb and REE as well as high P_2O_5 and CaO.

The tholeiitic rocks have a median trace element content of about 232 ppm Cr, 36 ppm Ni, 2.4 ppm Nb, 60 ppm Zr and 3.8 ppm La, while the calc-alkaline rocks have a median trace element contents of about 144 ppm Cr, 26 ppm Ni, 5.6 ppm Nb, 131 ppm Zr and 20 ppm La.

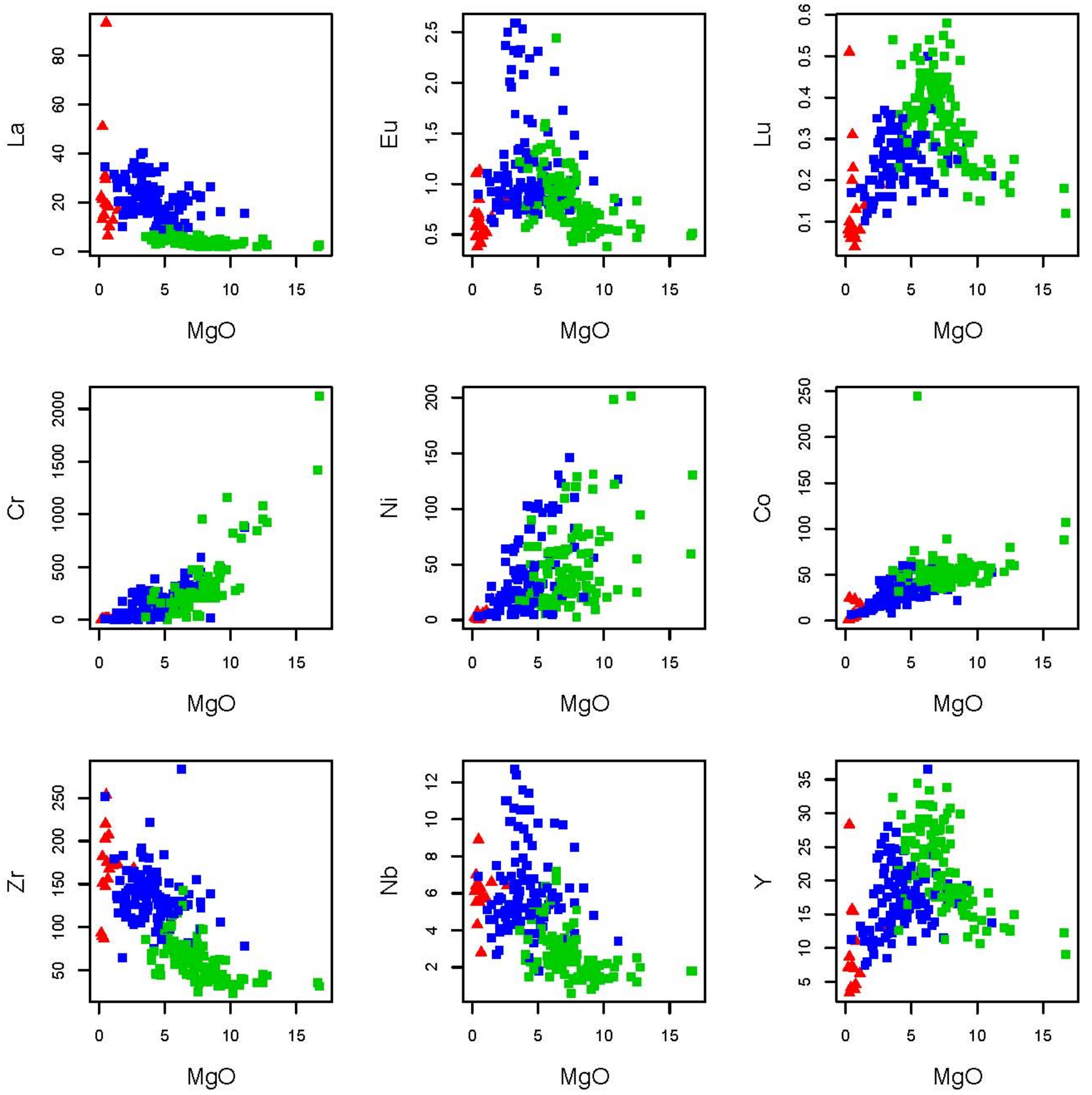

Figure 6. *Trace element concentrations for the tholeiitic and calc-alkaline amphibolites and TTG gneisses plotted against MgO. As for the major elements it appears that the calc-alkaline rocks can be explained by mixing of tholeiites with TTG gneisses. One group of calc-alkaline rocks from Bjørnesund tend to have anomalously high concentrations of Nb and generally have high REE concentrations.*

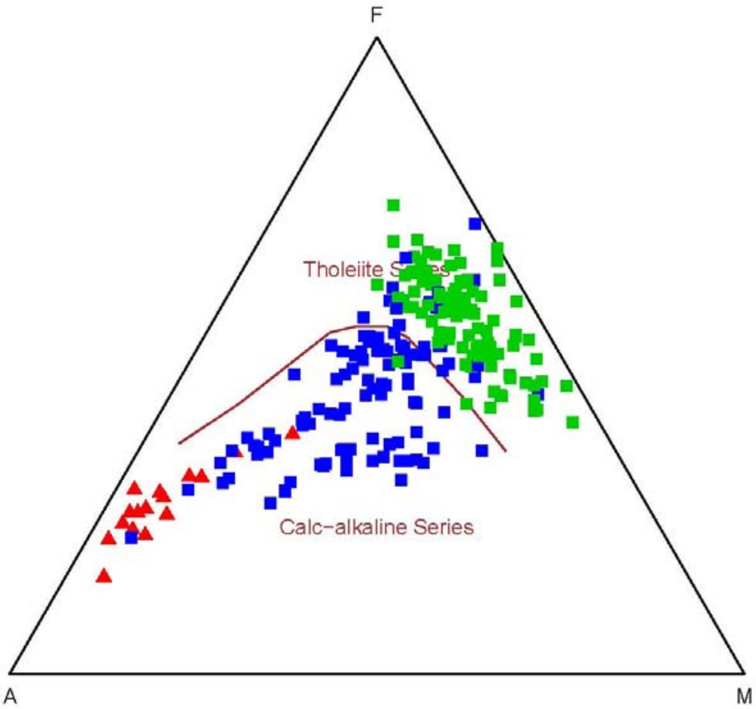

Figure 7. *AFM plot (after Irvine and Baragar 1971) with (Na_2O+K_2O), FeOt and MgO in each apex. The red line separates volcanic rocks of tholeiitic and calc-alkaline series and there is good agreement with the supracrustal data that was grouped on the basis of REE-patterns.*

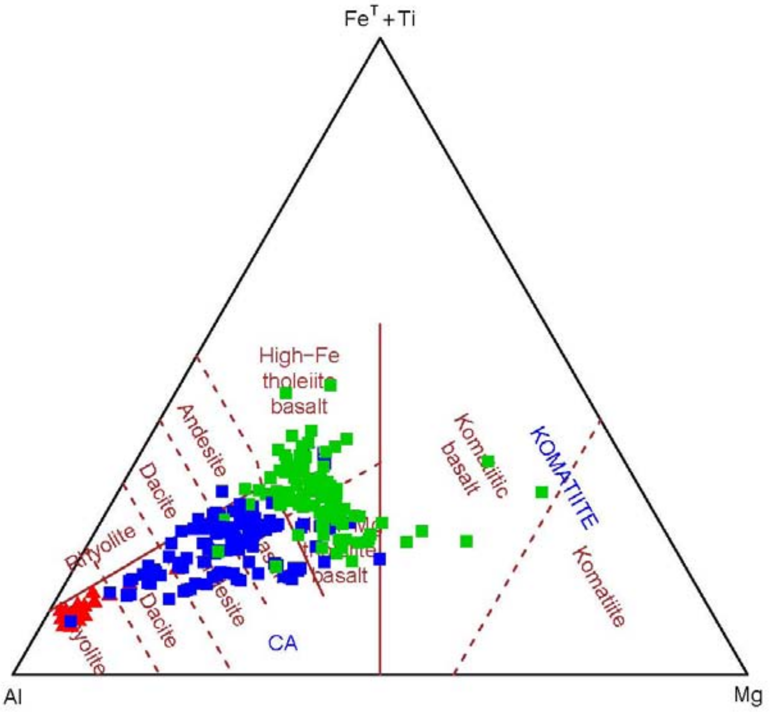

Figure 8. *Jensen plot (Jensen 1976) with Al, (Fe^T + Ti) and Mg at the apexes shows a good classification of the supracrustal rocks into a tholeiitic and a calc-alkaline trend.*

The AFM-plot (Fig. 7) roughly divides the supracrustal rocks into two groups, generally consistent with the division based on the REE-patterns. Some of the scatter and overlap observed in the AFM diagram between the calc-alkaline and the tholeiitic rocks can be attributed to slight mobility of K_2O and Na_2O, as would be expected. A more reliable classification diagram is that of Jensen (1976) shown in Figure 8, which is based on relatively more fluid-immobile major elements. There is good agreement between how the rocks have been grouped according to their REE-patterns and this classification diagram into a tholeiitic and a calc-alkaline trend.

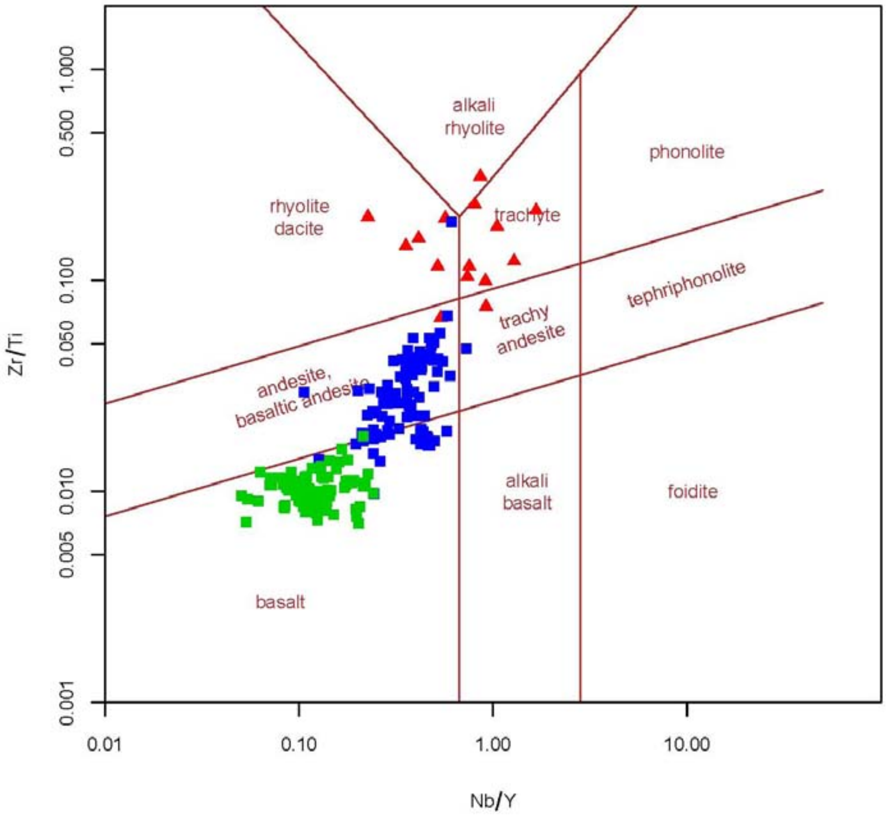

Figure 9. *Nb/Y vs. Zr/Ti diagram after Winchester and Floyd (1977) and modified by Pearce (1996). The supracrustal rocks plot largely in two distinct groups, as basalts and basaltic andesites / andesites. Note double-logarithmic axes.*

To get an idea about how evolved the supracrustal rocks are the Nb/Y – Zr/Ti classification diagram is shown in Figure 9. The 'Winchester and Floyd' diagram is usually preferred over the TAS-diagram for classifying metamorphic rocks, because it relies on ratios between immobile elements. From Fig. 9 it is clear that there is a bimodal distribution in the data and that the tholeiitic amphibolites are basaltic in composition, whereas the calc-alkaline rocks are generally more evolved with compositions in the andesitic field.

Various attempts to make tectonic discrimination diagrams can be found in the literature and several of the most commonly used ones have been summarised by Rollinson (1993). The principle behind these types of diagrams is to use the chemical fingerprint in rock suites of known tectonic affinity as a 'predictive' tool to determining the geological setting of (often older) rocks of unknown heritance. Going back in the rock record to the Archaean times, a main caveat in applying such tectonic discrimination methods lie in the assumption of 'uniformitarism', i.e. the assumption that rocks formed by the same processes in Archaean times as they do today. There is generally a consensus that subduction zones were in operation by at least 3.12 Ga (Smithies et al. 2005), and some authors even suggest extending the onset of this event back to about 3.8 Ga (Polat et al. 2002). Thus, it seems plausible that tectonic discrimination diagrams could be used for these ca. 3 Ga old rocks from South West Greenland, although some level of skepticism is sensible (e.g. Moyen 2010).

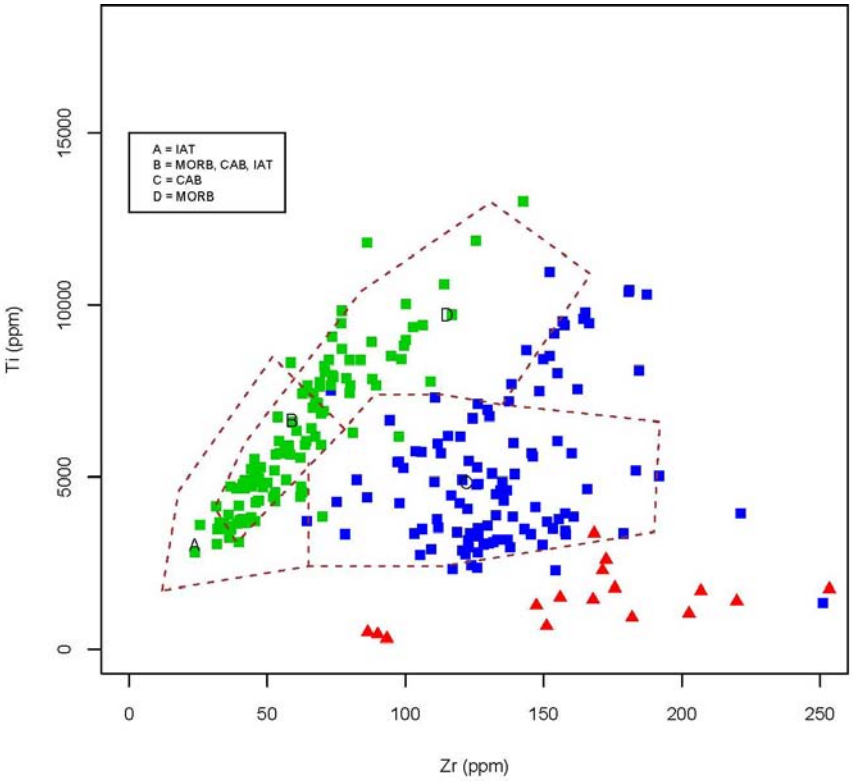

Figure 10. *Tectonic discrimination diagram using Ti against Zr concentration (after Pearce and Cann 1973). The calc-alkaline amphibolites plot in the CAB field characteristic of volcanic arcs and the tholeiitic amphibolites plot in several fields, covering IAT and MORB, but also a field with overlap from CAB. IAT = island arc tholeiite; MORB = mid-ocean ridge tholeiite; CAB = calc-alkaline basalt.*

Figure 10 shows the use of Ti and Zr to group rocks of similar setting. The calc-alkaline amphibolites do fall in the predicted calc-alkaline basalt (CAB) field, which is most common in a volcanic arc settings and the tholeiitic amphibolites plot in several overlapping fields from island arc tholeiites (IAT) to mid ocean ridge basalt (MORB).

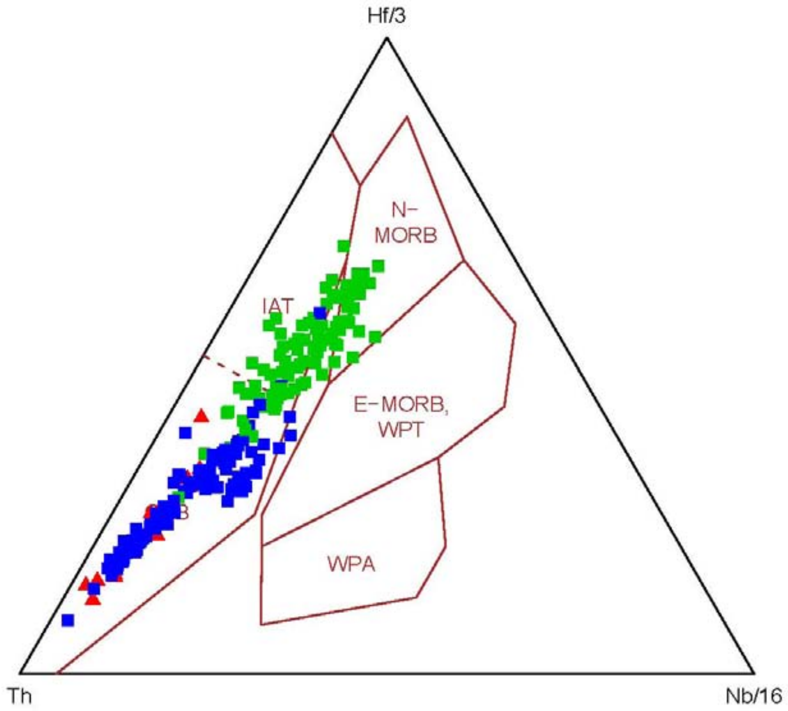

Figure 11. *Tectonic discrimination diagram using Th, Hf and Nb concentrations (Wood 1980). The calc-alkaline amphibolites plot in the CAB field as expected and the tholeiitic amphibolites plot mainly in the IAT field and some plot in the N-MORB field.*

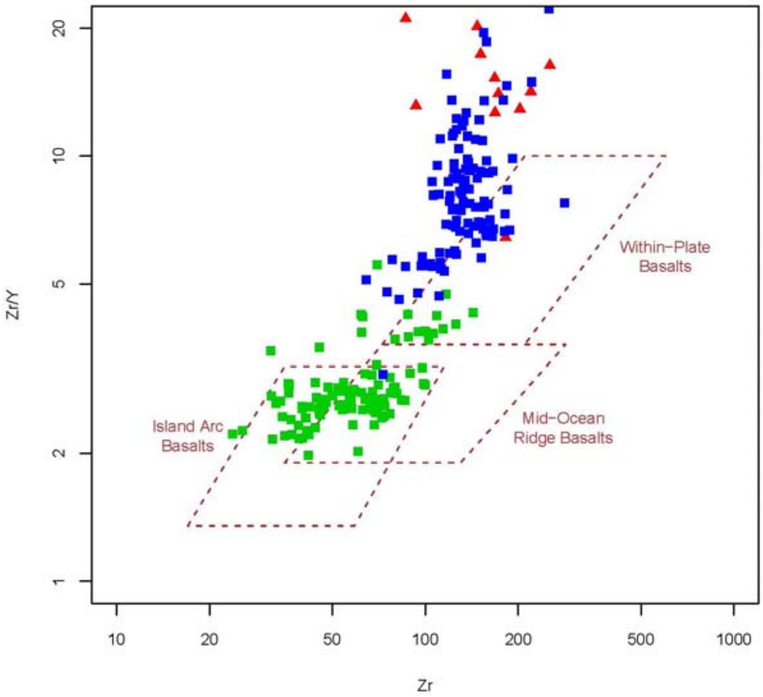

Figure 12. *Tectonic discrimination diagram using Zr/Y against Zr (Pearce and Norry 1979). The calc-alkaline amphibolites plot near the field of within-plate basalts. The tholeiitic amphibolites plot in the IAT field and where this overlaps the MORB field.*

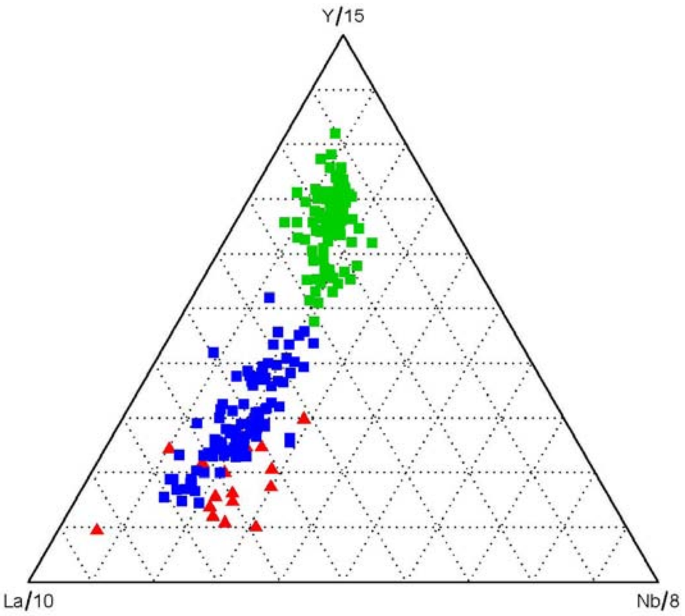

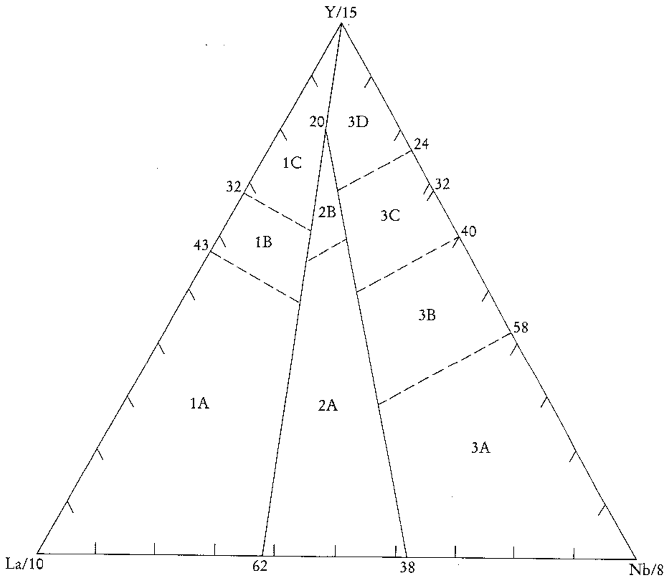

The La/10–Y/15–Nb/8 discrimination diagram for basalts (after Cabanis and Lecolle, 1989). The plotting coordinates are shown around the margin of the diagram; the broken lines are drawn normal to the sides of the triangular diagram. Field 1 contains volcanic-arc basalts, field 2 continental basalts and field 3 oceanic basalts. The subdivisions of the fields are as follows: 1A, calc–alkali basalts; 1C, volcanic-arc tholeiites; 1B is an area of overlap between 1A and 1C; 2A, continental basalts; 2B, back-arc basin basalts (although this is less well defined); 3A, alkali basalts from intercontinental rift; 3B, 3C, E-type MORB (3B enriched, 3C weakly enriched), 3D, N-type MORB.

Figure 13. *Tectonic discrimination diagram using La, Y and Nb (Cabanis and Lacolle 1989). The calc-alkaline amphibolites plot in the region of normal calc-alkaline basalts from the volcanic arc environment and the tholeiitic amphibolites mainly plot in the region expected for back-arc basalts and extend slightly into the N-MORB region.*

Figure 11 uses Th, Hf and Nb and the calc-alkaline amphibolites plot in the CAB field as expected. The tholeiitic amphibolites plot mainly in the IAT field and some of the samples plot in the N-MORB field.

Figure 12 uses Zr/Y against Zr. The calc-alkaline amphibolites plot near the within-plate basalt field, which generally comprise basalts that have erupted through continental crust and have been contaminated during this process. The tholeiitic amphibolites plot in the IAT field and where this overlaps with the N-MORB field.

Figure 13 uses La, Y and Nb concentrations and the calc-alkaline amphibolites plot in the CAB region of the diagram and the tholeiitic amphibolites plot mainly in the region of back-arc basin basalts.

Discussion

This data set, comprising 220 samples from supracrustal belts in SW Greenland, consistently shows two distinct geochemical groups that furthermore is correlated with their field classification; namely dark mafic rocks of tholeiitic affinity and light coloured felsic schists to leuco-amphibolites of calc-alkaline affinity. They are best distinguished by their REE patterns, but show systematic differences in both major and trace elements.

It is interesting to observe the similarities in geochemistry of the supracrustal belts from different terranes and even of different ages. They are presently located up 300 km apart and this could be interpreted as the same processes having operated in the region for a long period of time (at least from 2.9 to 3.2 Ga ago).

It is also worth noting that the bimodal distribution of rocks from Bjørnesund was observed very early on by Williams (1976), who showed that poorly banded gneisses and amphibolites were connected by a linear array of transitional rocks. However, this idea was not pursued by later workers, likely because they worked with smaller and more focused data sets. With a total number of 236 analyses (TTG sheets included) this data set is likely the most comprehensive to date for the Archaean supracrustal belts of SW Greenland and gives new insights to the general heterogeneity of these rocks, but similar volcanic setting across the various supracrustal belts. Here we explore processes that are likely to explain the observed geochemical variation and outline models that can explain the formation of the supracrustal belts of SW Greenland.

The tholeiitic rocks have flat trace element patterns and generally have MORB-like major element composition which at first hand would suggest a normal ocean floor environment, but the distinct negative Nb-anomaly and undepleted character for the light REE combined with the IAT-affinity on the discrimination diagrams (Fig. 10, 11 and 12) suggest that it differs from N-MORB. On Figure 13 a BAB-affinity is suggested, which is in agreement with the arc-flavour that was suggested from the IAT affinity. A back-arc basin (BAB) environment similar to the Lau and Mariana basins (Taylor and Martinez 2003) is thus a more likely candidate for the setting of the tholeiitic amphibolites and comparison of the Greenland data with similar Archaean tholeiitic rocks from Canada (Hollings et al. 2000; Sandeman et al. 2006), that were interpreted to have formed in a back-arc environment, show good overlap of the data.

Another explanation for Archaean tholeiites in general in the literature (Campbell et al. 1989; Kerr et al. 1996; Arndt et al. 1997) is the oceanic plateau setting (e.g. Ontong Java-style plateaus), but such a setting is generally associated with abundant komatiites in all of the Archaean examples. Komatiites are generally lacking in the supracrustal belts of SW Greenland, and such rocks generally have positive Nb-anomalies whereas this data set has negative anomalies.

A back-arc environment is also more likely to be preserved over time rather than actual MORB or oceanic plateaus since the crust is generally thinner (Martinez and Taylor 2003) and more prone to obduction as it is already present in a collisional setting.

The sharp contrast between the REE-patterns (Fig. 3) in the tholeiitic amphibolites and the calc-alkaline amphibolites cannot be explained by fractional crystallisation, because the slope is very different. Such difference in LREE/MREE enrichment are likely to reflect different sources and/or different degrees of partial melting, thus suggesting the calc-alkaline rocks to have been derived from generally more enriched sources and possibly also by smaller degrees of partial melting compared to the tholeiites. Fractional crystallisation would on the other hand be a possible mechanism to explain part of the concentration variations found within each of the two rock groups, including the fractionation (removal/addition) of plagioclase to explain the negative or positive Eu-anomalies. The negative Nb-anomalies which are most clearly seen in the calc-alkaline rocks could be explained as the result of partial melting at the presence of a residual phase retaining Nb in the mantle source region, such as rutile or cpx (Baier et al. 2008).

On the major and trace element variation diagrams (Fig. 5 and 6), it is clear that the tholeiitic rocks and the TTG gneisses form compositional end members, whereas the calc-alkaline rocks plot with intermediate positions. Thus, much of the compositional range observed in the calc-alkaline rocks could possibly be explained as a result of some kind of mixing processes involving tholeiitic and TTG-like compositional end members. This model is further supported by the REE-patterns for the tholeiites and calc-alkaline rocks that show two distinct groups that cannot be related by fractionation, thus a possible way of explaining the observed liniar arrays, or fans of arrays, is by binary mixing and/or contamination processes, where the TTG gneisses are the mixing end member/contaminant. A similar association of rocks was described by Wang et al. (2004) in the North China Craton and they envisaged mixing of basaltic rocks with adakitic melts to produce intermediate melts similar to our calc-alkaline volcanics.

The TTG gneisses show similar trace element patterns as generally reported from Greenland and elsewhere by other authors and it is generally agreed that the most likely source for the Archaean TTG gneisses was partial melting of hydrous metabasaltic rocks as either garnet amphibolite of eclogite (Rapp et al. 1991; Martin et al. 2005; Rapp et al. 2010), but there is still debate over what the actual setting of these melts was (Condie 2005; Bédard 2006; Moyen 2011).

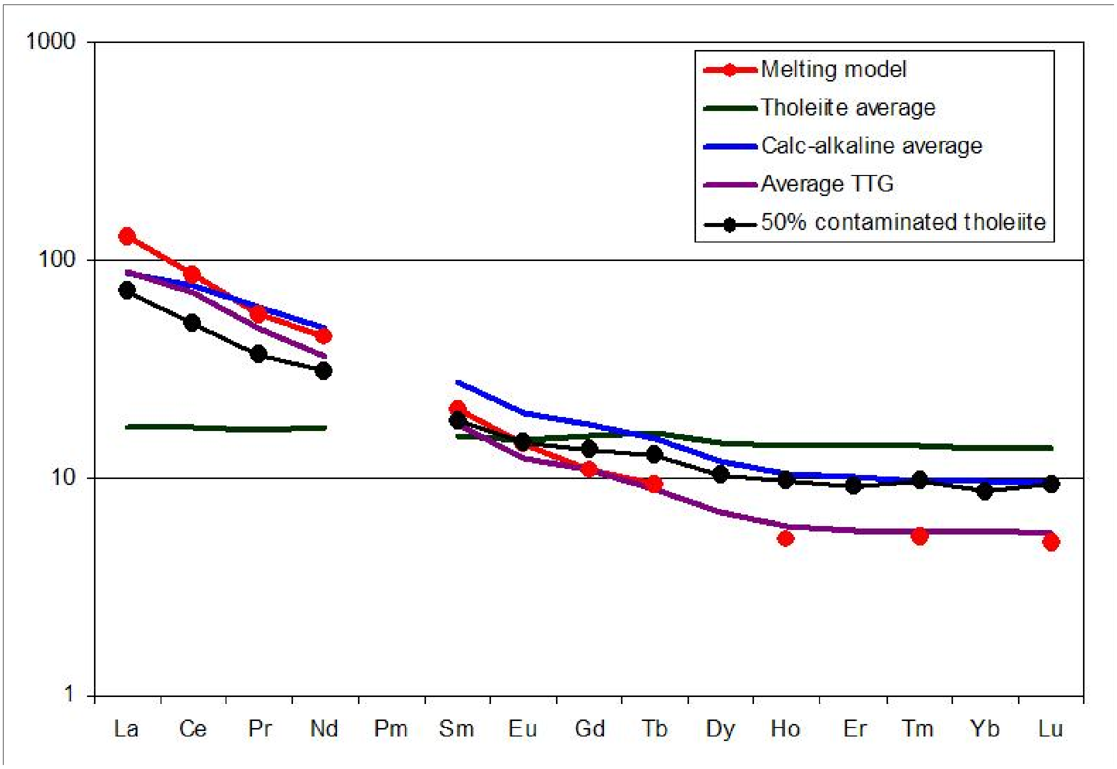

Figure 14. *Chondrite normalised (Boynton 1984) REE patterns for average compositions of the data previously shown for tholeiitic amphibolites, calc-alkaline amphibolites and TTG gneisses. Additionally a partial melt model and a mixture of this melt and the average tholeiitic amphibolite is plotted.*

In a simple attempt to model the formation of the local TTGs as well as the calc-alkaline amphibolites a batch melt model for the REE was made using the average tholeiitic amphibolite as a source and 5% partial melting with the residual of Rapp et al. (1991) and partition coefficients of Bedard (2006). A more detailed melt model of the SW Greenland TTGs can be found in Szilas et al. (2011a). The result is seen in Figure 14 where it is clear that the melting model show a good fit with the local TTGs, consistent with the consensus in the literature that metabasaltic rocks are indeed the source of TTG magmas. More interesting, however, is the fact that calc-alkaline amphibolites can be approximated by a mixture of this TTG melt and the tholeiitic amphibolites in equal proportions. The fit is almost perfect if the high-Nb samples from Bjørnesund are excluded from the calc-alkaline data set.

Three scenarios for the genesis of the calc-alkaline rocks are possible:

(1) The melt modelling (Fig. 14) together with the remarkably well-defined mixing trends on the variation diagrams (Fig. 5 and 6) does suggest that the calc-alkaline amphibolites in the supracrustal belts are the result of contamination of tholeiitic rocks by TTG-like melts. This could either be mixing between tholeiitic basalts with younger TTG, while they intruded and later sheared to be homogenised or it could be the result of low degree in-situ partial melting of tholeiites that produce TTG-like melts that then mixes with the surrounding tholeiitic rocks. This could certainly be the case in some of the more deformed supracrustal belts, but in areas where primary structures such as pillows and ash layers are observed in the calc-alkaline rocks, such volcanics must be a primary feature of

the supracrustal belts. Additionally if such mixing was indeed the case the rocks would plot as a continuum in the previous diagrams, but instead three distinct groups are observed and thus late mechanical mixing of TTG with tholeiitic basalts does not explain the formation of the calc-alkaline rocks adequately.

(2) The calc-alkaline rocks might simply reflect volcanic arc generated magmas from a source that is different than the one responsible for the tholeiitic amphibolites, much in the same way as modern day island arcs, where the mantle wedge above the subduction slab is fertilised with fluid mobile elements to yield enriched volcanics with relative depletion in fluid immobile elements such as Nb, Ta and Ti. However, there is recent controversy over what the calc-alkaline differentiation trend actually means in the arc environment, because this can be produced either by the presence of 2-3 wt.% water in a fractionating basalt or by mixing of basaltic magmas and felsic magmas generated by underplating (Tatsumi and Suzuki 2009; Reubi and Blundy 2009). It is widely accepted that melting in a subduction zone environment today is caused by fluid flux from the dehydration of the subduction slab, which fertilises the mantle wedge with fluid mobile elements and lowers the solidus temperature of the mantle to produce melt. One major uncertainty is that subduction zones might not have operated in the Archaean, because from thermal constraints the oceanic crust might have been too buoyant to actually be subducted (van Hunen et al. 2008) and if subduction was possible it would be short termed (~10Ma) as the slabs would break off due to lithospheric weakness (van Hunen and van den Berg 2008). In the latter case pulses of upwelling asthenosphere in response to slab breakoff might be able to explain mixing or mafic and felsic melts to produce the distinct calc-alkaline volcanics and periodic TTG formation as seen in Figure 15.

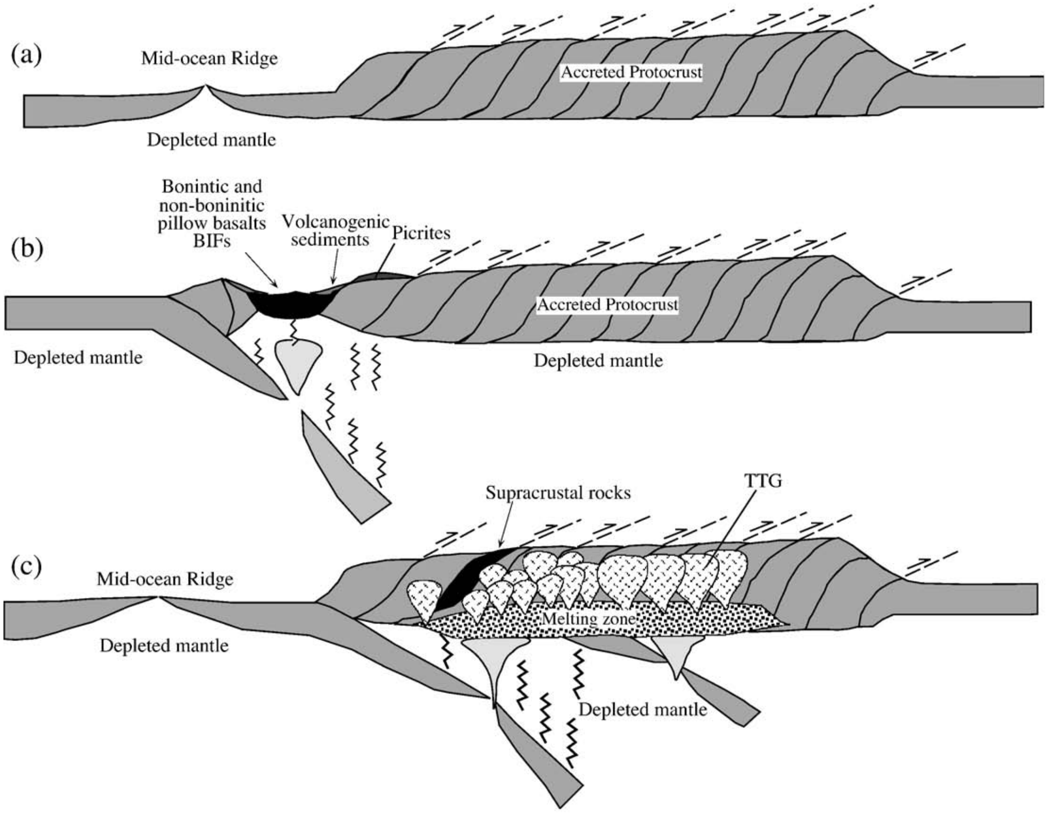

Figure 15. (previous page) Progressive evolution of an Archaean subduction zone, where modern style processes were operating as proposed in model (2). Slab break-off would lead to TTG formation. From Kerrich and Polat (2006).

(3) A recent model that considers the thermal constraints of the Archaean Earth (van Hunen et al. 2008) suggests that oceanic crust in the Archaean did not subduct, but rather was scraped off in a collision zone by so-called flake tectonics and that only the denser lithospheric mantle was subducted. Piled up oceanic crust would reach P-T conditions of eclogite facies at the base, which would be so dense that it delaminated and caused asthenosphere upwelling (Fig. 16). This could create basaltic melts by decompression melting as well as melting of the base of the basaltic crust, which would produce TTG-like felsic melts. Mixing of these two different melts could create the observed calc-alkaline magmas that in turn would be expected to erupt onto the pre-existing tholeiitic crust. If the delamination process continued the entire crust would eventually be processed to consist almost entirely of TTG, with belts of supracrustal rocks that escaped melting. This model also explains why the tholeiitic rocks appear to be mainly submarine (dark mafic rocks often with pillow structures) and the calc-alkaline rocks often are subaerial (felsic schists and leucocratic amphibolites that could represent ash and tuff).

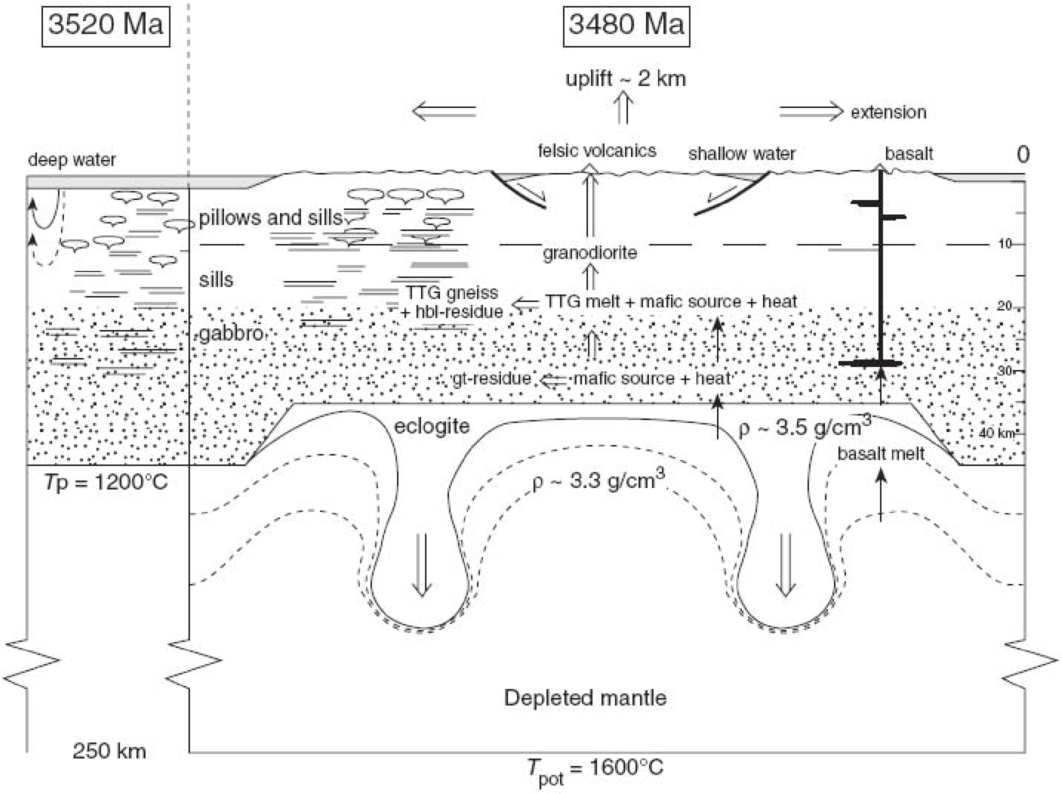

Figure 16. *Thick oceanic crust or stacks of oceanic crust would have a base within the eclogite metamorphic field and this could delaminate to cause asthenosphere upwelling as proposed in model (3). Decompression melting and under plating would then cause mafic and felsic melts to mix and could lead to calc-alkaline magmas that would erupt on top of the tholeiitic oceanic crust. Eclogite and melt residues would fall back into the mantle and cause more upwelling as well as lowering the solidus, which would promote more melt production. This process might have gone on until complete exhaustion of the mafic to felsic volcanic sequence and result in a TTG crust. From van Hunen et al. (2008).*

Given the systematic variations of the calc-alkaline rocks between the tholeiitic rocks and the TTG gneisses as end members it is likely that they represent a mixture of mafic and felsic melts produced through one of the three models above. We can reject model (1) with late mechanical mixing, because the data lack continuity, but at the present time we cannot separate model (2) and (3), because they would yield essentially the same characteristics in terms of geochemistry.

Conclusions

The Archaean supracrustal rocks of SW Greenland show a bimodal distribution in terms of major and trace elements, which suggest that magma mixing is a likely explanation of the data. This means that the calc-alkaline rocks found in the generally tholeiitic supracrustal belts are not a primary feature, but are rather produced by the mixing of basaltic and felsic melts and model (2) and (3) featuring subduction and delamination, respectively, as outlined in the discussion above can both explain the observations. This suggests that the formation of the tholeiitic and calc-alkaline rocks happened at slightly different times and by different processes perhaps related to a volcanic arc.

Future research will be undertaken to test which of the two models is responsible for the calc-alkaline rocks in the supracrustal belts. The timing of events as well as source compositions might be too similar to be resolvable with current isotopic systems, but geochemical modelling to explain trace element variations and to get estimates of pressures and temperatures might be a way to set constraints on the formation processes of the supracrustal belts of SW Greenland.

Hopefully these questions will be resolved in the near future and a Ph.D.-thesis at GEUS is in progress on this very topic.

Acknowledgements

We would like to acknowledge the Bureau of Minerals and Petroleum (BMP) for financial support of the field work and the analytical work. We would also like to thank Geocenter Danmark for funding of two PhD-projects at GEUS, which have contributed to this work.
Agnete Steenfelt is greatly acknowledged for reading through a draft version of this chapter, which helped to improve it.

References

Andersen, L.S. & Friend, C. 1973: Structure of the Ravns Storø amphibolite belt in the Fiskenæsset region. Geological Survey of Greenland report 51, 37-40.

Arndt, N.T., Kerr, A.C. & Tarney, J., 1997: Dynamic melting in plume heads: the formation of Gorgona komatiites and basalts. Earth and Planetary Science Letters 146, 289-301.

Baier et al. 2008: The origin of the negative niobium tantalum anomaly in subduction zone magmas. Earth and Planetary Science Letters 267, 290-300.

Bédard, J.H. 2006: A catalytic delamination-driven model for coupled genesis of Archaean crust and sub-continental lithospheric mantle. Geochimica et Cosmochimica Acta 70, 1188-1214.

Berthelsen, A & Henriksen, N. 1975: Geological map of Greenland, 1:100,000 Ivittuut 61 V.1 Syd (with description), Geological Survey of Greenland, Copenhagen, 169 pp.

Bickle, M.J., Nisbet, E.G. & Martin, A. 1994: Archean greenstone belts are not oceanic crust. The journal of geology, vol. 102, 121-138.

Boynton, W.V. 1984: Cosmochemistry of the rare earth elements: meteorite studies. In: Henderson, P. (ed.). Rare Earth Element Geochemistry, Elsevier, Amsterdam (1984), 63–114.

Cabanis, B. & Lecolle, M. 1989: Le diagramme La/10-Y/15-Nb/8: un outil pour la discrimination des series volcaniques et la mise en evidence des processus de melange et/ou de contamination crustale. C.R. Acad. Sci. Ser. II, 2023-2029.

Campbell, I.H., Griffiths, R.W. & Hill, R.I. 1989: Melting in an Archean mantle plume: heads it's basalts, tails it's komatiites. Nature 369, 697–699.

Condie, K.C. 2005: TTGs and adakites: are they both slab melts? Lithos 80, 33-44.

Dawes, P.R. 1969: Age and correlation of supracrustal rocks in the Frederikshåbs Isblink area. Grønlands geologiske undersøgelser rappoprt 19, 31-33.

Furnes, H., de Wit, M., Staudigel, H., Rosing, M., Muehlenbachs, K. 2007: A vestige of Earth’s oldest ophiolite. Science, 315, 1704-1707.

Furnes, H. Rosing, M., Dielk, Y. & de Wit, M. 2009: Isua supracrustal belt (Greenland) – A vestige of a 3.8 Ga suprasubduction zone ophiolite, and the implications for Archean geology. Lithos 113, 115-132.

Friend, C.R.L. 1975: The geology and geochemistry of the Preketilidian basement complex in the Ravns Storø area, Fiskenaesset region, southern West Greenland. Unpublished Ph.D. thesis, University London, 233 pp.

Friend, C.R.L. 1976: Field relationships and petrology of leucocratic schists from the Ravns Storø Group near Fiskenæsset. Rapport Grønlands Geologiske Undersøgelser 73, 81-85.

Higgins, A.K. 1968: The Tartoq Group on Nuna Qaqertoq and in the Iterdlak area, South-West Greenland. Geological Survey of Greenland report 17, 17 pp.

Hollings, P., Stott, G. & Wyman, D. 2000: Trace element geochemistry of the Meen-Dempster greenstone belt, Uchi subprovince, Superior Province, Canada: back-arc development on the margins of an Archean protocontinent. Canadian journal of earth science 37, 1021-1038.

Irvine, T. N. & Baragar, W. R. A. 1971: A guide to the chemical classification of the common volcanic rocks. Canadian Journal of Earth Sciences 8, 523–548.

Jensen, L. S. 1976: A New Cation Plot for Classifying Subalkalic Volcanic Rocks. Ontario Geological Survey Miscellaneous Paper 66.

Kerr, A.C., Marriner, G.F., Arndt, N.T., Tarney, J., Nivia, A., Saunders, A.D. & Duncan, R.A. 1996: The petrogenesis of Gorgona komatiites, picrites and basalts: new field, petrographic and geochemical constraints. Lithos 37, 245–260.

Kerrich, R. & Polat, A. 2006: Archean greenstone-tonalite duality: Thermochemical mantle convection models or plate tectonics in the early Earth global dynamics? Tectonophysics 415, 141-165.

Keulen, N. Schumacher, J.C., van Hinsberg, V., Szilas, K., Windley, B. & Kokfelt, T.F. 2010: The Bjørnesund anorthosite-greenstone belt – linking the Fiskenæsset complex to the Ravn Storø metavolcanic belt. In: Kokfelt, T.F. & Kolb, J. 2010.

Annual workshop on the geology of southern West Greenland related to field work: abstract volume II. GEUS report 2010/58.

Kisters, A.F.M., Bergen, A., Kokfelt, T.F. & Kolb, J. 2010: Structural geology of the Grædefjord area, southern West Greenland. In: Kokfelt, T.F. & Kolb, J. 2010. Annual workshop on the geology of southern West Greenland related to field work: abstract volume II. GEUS report 2010/58.

Kisters, A.F.M., Szilas, K. & van Hinsberg, V.J. 2011: Structural geology and emplacement of the Tartoq Group, SW Greenland. Geological survey of Denmark and Greenland report 2010/47.

Kokfelt T.F., Keulen, N. Næraa, T., Nilsson, M., Scherstén, A. Szilas, K. & Heijboer, T. 2011: Geochronological characterisation of the felsic rocks of the Archaean craton in South-West Greenland and southern West Greenland, 61°30′ - 64°N, Geological survey of Denmark and Greenland report 2011/12.

Kolb, K., Dziggel, A., Koppelberg, M., Stoltz, N.B., Kisters, A.F.M. & Bergen, A. 2010: Controls of hydrothermal quartz vein mineralisation and wall rock alteration between Sermilik and Grædefjord, southern West Greenland. Geological survey of Denmark and Greenland report 2010/47, 73 pp.

Kusky, T.M. & Polat, A. 1999: Growth of granite-greenstone terranes at convergent margins, and stabilization of Archean cratons. Tectonophysics 305, 43-73.

Lie, A. 1994: Guld-mineraliseringer i det Arkæiske Nuuluk grønstensbælte, Târtoq-gruppen, sydvest Grønland. Unpublished M.Sc. thesis, Århus University, 126 pp.

Martin, H., Smithies, R.H., rapp, R., Moyen, J.-F. & Champion, D. 2005: An overview of adakite, tonalite-trondhjemite-granodiorite (TTG), and sanukitoid: relationship and some implications for crustal evolution. Lithos 79, 1-24.

Martinez, F. & Taylor, B. 2003: Controls on back-arc crustal accretion: insights from the Lau, Manus and Mariana basins. In: Larter, R.D. & Leat, P.T. (eds.). Intra-oceanic subduction systems: tectonic and magmatic processes. Geological Society, London, Special Publications, 219, 19-54.

Moyen, J.-F. 2010: Can discrimination diagrams tell us something about Archaean geodynamics? Geophysical research abstract, vol. 12, EGU2010-8045, EGU general assembly 2010.

Moyen J.-F. 2011: The composite Archaean grey gneisses: Petrological significance, and evidence for a non-unique tectonic setting for Archaean crustal growth. Lithos (in press).

Myers, J.S. 1985: Stratigraphy and structure of the Fiskenæsset Complex, southern West Greenland. Grønlands Geologiske Undersøgelser Bulletin 150, 72.

Nutman, A.P. & Friend, C.R.L. 2007: Adjacent terranes with c. 2715 and 2650 Ma high pressure metamorphic assemblages in the Nuuk region of the North Atlantic craton, southern West Greenland: complexities of Neoarchaean collisional orogeny. Precambrian Research 155, 159–203.

Næraa, T. Scherstén, A. 2008. New Zircon ages from the Tasiusarsuaq terrane, southern West Greenland. Geological survey of Denmark and Greenland bulletin 15, 73-76.

Pearce, J. A. 1996: A user's guide to basalt discrimination diagrams. In: Wyman, D. A. (editor) Trace element geochemistry of volcanic rocks: applications for massive sulphide exploration. Geological Association of Canada, short course notes 12, 79-113.

Pearce, J. A. & Cann, J. R. 1973: Tectonic setting of basic volcanic rocks determined using trace element analyses. Earth and Planetary Science Letters 19, 290-300.

Pearce, J. A. & Norry, M. J. 1979: Petrogenetic implications of Ti, Zr, Y, and Nb variations in volcanic rocks. Contributions to Mineralogy and Petrology 69, 33-47.

Petersen, J.S. 1992: Nuuluk-Iterlak gold and massive-sulfide project, Taartoq Archaean greenstone belt, SW Greenland. Field report, Nunaoil A/S, 164 pp.

Polat, A., Hofmann, A.W. & Rosing, M.T. 2002: Boninite-like volcanic rocks in the 3.7-3.8 Ga Isua greenstone belt, West Greenland: geochemical evidence for intra-oceanic subduction zone processes in the early Earth. Chemical Geology Volume 184, 231-254.

Polat, A. Frei, R., Appel, P.W.U., Dilek, Y., Fryer, B., Ordóñez-Calderón, Yang, Z. 2008: The origin and composition of Mesoarchean oceanic crust: Evidence from the 3075 Ma Ivisaartoq greenstone belt, SW Greenland. Lithos 100, 293-321.

Polat, A., Appel, P.W.U., Fryer, B., Windley, B., Frei, R., Samson, I.M. & Huang, H. 2009: Trace element systematics of the Neoarchean Fiskenæsset anorthosite complex and associated meta-volcanic rocks, SW Greenland: Evidence for a magmatic arc origin. Precam. Res. 175, 87-115.

Reubi, O. & Blundy, J. 2009: A dearth of intermediate melts at subduction zone volcanoes and the petrogenesis of arc andesites. Nature 461, 1269-1273.

Rapp, R.P., Norman, M.D., Laporte, D., Yaxley, G.M., Martin, H. & Foley, S.F. 2010: Continent formation in the Archean and chemical evolution of the cratonic lithosphere: melt-rock reaction experiments at 3-4 Gpa and petrogenesis of Archean Mg-diotites (Sanukitoids). Journal of Petrology, vol. 51, 1237-1266.

Rapp, R.P, Watson, E.B. & Miller, C.F. 1991: Partial melting of amphibolite/eclogite and the origin of Archean trondhjemites and tonalites. Precambrian research 51, 1-25.

Rollinson, H.R. 1993: Using geochemical data: evaluation, presentation, interpretation. Longman, UK. 352 pp.

Sandeman, H.A., Hanmer, S.m Tella, S., Armitage, A.A., Davis, W.J. & Ryan, J.J. 2006: Petrogenesis of Neoarchaean volcanic rocks of the MacQuoid supracrustal belt: a back-arc setting for the northwestern Hearne subdomain, western Churchill Province, Canada. Precambrian research 144, 140-165.

Scherstén, A. & Stendal, H. 2008: Geochemistry of the Tasiusarsuaq ‘greenstone-granite’ terrane, southern West Greenland. Geological survey of Denmark and Greenland report 2008/15, 40 pp.

Schumacher, J.C., van Hinsberg, V.J. & Keulen, N. 2011: Metamorphism in supracrustal and ultramafic rocks in southern West Greenland and South-West Greenland, 64-61.5°N. Geological survey of Denmark and Greenland report 2011/6.

Smithies, R.H., Champion, D.C., van Kranendonk, M.J., Howard, H.M. & Hickman, A.H. 2005: Modern-style subduction processes in the Mesoarchaean: geochemical evidence from the 3.12 Ga Whundo intraoceanic arc. Earth and Planetary Science Letters 231, 221-237.

Stendal, H. (ed.) 2007: Characterisation of selected geological environments. Mineral resourse assessment of the Archaean Craton (66° to 63°30’N) SW Greenland contribution no. 1. Geological Survey of Denmark and Greenland report 2007/20, 90 pp.

Sun, S. & McDonough, W. F. 1989: Chemical and Isotopic Systematics of oceanic basalts: implications for Mantle Composition and Processes. In A.D. Saunders & M.J. Norry (eds.): Magmatism in the Ocean Basins, Spec. Publ. Vol. Geol. Soc. Lond., 42, 313-345.

Szilas, K., Kokfelt, T.F., Næraa, T. & Scherstén, A. 2011a: Geochemistry of the Archaean felsic crust with implications for TTG formation. Geological Survey of Denmark and Greenland report 2011/10.

Szilas, K., van Hinsberg, V.J., Kisters, A.F.M., Kokfelt, T.F., Scherstén, A. & Windley, B.F. 2011b: Remnants of Mesoarchaean oceanic crust in the Tartoq Group, North Atlantic Craton, SW Greenland. Geological survey of Denmark and Greenland Bulletin 21, (in review).

Szilas, K., Scherstén, A., Hoffmann, J.E., Kokfelt, T.F., van Hinsberg, V.J., Windley, B.F., & Münker, C. 2011c. Linking the Ravns Storø and Bjørnesund supracrustal belts (SW Greenland) using Lu-Hf and Sm-Nd isotopic data and whole-rock geochemistry. Geophysical Research Abstracts, vol. 13, EGU2011-11114-1.

Tatsumi, Y. & Suzuki, T. 2009: Tholeiitic vs calc-alkalic differentiation and evolution of arc crust: constraints from melting experiments on a basalt from the Izu-Bonin-Mariana arc. Journal of petrology, vol 50, 1575-1603.

Taylor, B. & Martinez, F. 2003: Back-arc basin basalt systematics. Earth and Planetary Science Letters 210, 481-497.

van Hinsberg, V.J., Szilas, K. & Kisters, A.F.M. 2010: The Tartoq Group, SW Greenland: Mineralogy, textures and a preliminary metamorphic to hydrothermal history. Geological Survey of Denmark and Greenland report 2010/120, 52 pp.

van Hunen, J. & van den Berg, A.P. 2008: Plate tectonics on the early Earth: Limitations imposed by strength and buoyancy of subducted lithosphere. Lithos 103, 217-235.

van Hunen, J., Keken, P.E., Hynes, A. & Davies, G. 2008: Tectonics of early Earth: Some geodynamic considerations. Geological society of America, Special paper 440, 157-171.

Wang, Z., Wilde, S.A., Wang, K. & Yu, L. 2004: A MORB-arc basalt-adakite association in the 2.5 Ga Wutai greenstone belt: late Archean magmatism and crustal growth in the North China Craton. Precambrian Research 131, 323-343.

Wilf, C.I.Z. 1982: Geokemien af de grå amphiboliter, en del af en supracrustal bjergartsenhed, ved Grædefjorden, nord for bygden Qeqertarsuatsiaat (Fiskenæsset) i den centrale del af Sydvestgrønland. Unpublished M.Sc. thesis, Aarhus University, 145 pp.

Williams, H.R. 1976: Granitisation of basic rocks in the Bjørnesund area, near Fiskenæsset, West Greenland. Rapport Grønlands Geologiske Undersøgelser 73, 47-54.

Winchester, J. A. & Floyd, P. A. 1977: Geochemical discrimination of different magma series and their differentiation products using immobile elements. Chemical Geology 20, 325–343.

Windley, B.F. 1966: Anorthosites and polymetamorphism between Ravns Storø and Sukkertoppen, West Greenland. Grønlands geologiske undersøgelser rapport 11, 27-29.

Windley, B. & Garde, A.A. 2009: Arc-generated blocks with sections in the North Atlantic craton of West Greenland: Crustal growth in the Archean with modern analogues. Earth-science reviews 93, 1-30.

Wood, D. A. 1980: The application of a Th–Hf–Ta diagram to problems of tectonomagmatic classification and to establishing the nature of crustal contamination of basaltic lavas of the British Tertiary volcanic province. Earth and Planetary Science Letters 50, 11–30.

Geochemistry of the Archaean felsic crust with implications for TTG formation

Kristoffer Szilas, Thomas F. Kokfelt, Tomas Næraa, Anders Scherstén

Introduction

Globally the Archaean crust can be divided into supracrustal units and high-grade gneiss terranes. Supracrustal rocks represent surface environments and in areas where these deposits are abundant (e.g. Norseman-Wilunain in Australia; Barberton in South Africa; Abitibi in Canada) they constitute an association of volcanic rocks intruded by granites and are therefore sometimes referred to as granite-greenstone belts. The high-grade gneiss terranes are mainly composed of igneous plutonic rocks (orthogneisses) that have crystallised within a thickened crust. The two associations reflect different processes of crust formation, and represent different levels within the crust. This section is primarily concerned with geochemical data from the high-grade gneiss terranes; however, felsic sheets situated within the supracrustal units have been included in the discussion as they are demonstrably linked to the same TTG forming events based on field relations, geochronology and geochemistry.

The high-grade gneiss terranes consist primarily of felsic orthogneisses, often referred to as ‘grey gneisses’ (e.g. Windley 1984; Garde 1997; Steenfelt et al. 2005), and they constitute the majority (maybe up to 85%) of the exposed crust in southern West Greenland and South-West Greenland. The primary gneissic fabric is composed of either a continuous or a banded foliation, and the gneisses often contain inclusions of more mafic lithologies, usually amphibolite. Typical orthogneisses have a mineral assemblage composed of quartz, plagioclase, biotite ± hornblende ± minor K-feldspar. Accessory phases are allanite, apatite, zircon, sphene, and titanomagnetite. The strong deformational and metamorphic overprinting is usually evident in form of one or more deformational episodes. The main regional metamorphic grade is that of amphibolite to granulite facies. In areas of highest metamorphic grade, the gneissic basement was partially melted as witnessed by abundant migmatites. Only in few areas, where the deformation is less intense, original igneous textures are occasionally preserved in the rocks.

It has been shown that the Archaean crust and mantle are different from their Phanerozoic counterparts and thus different processes or conditions must have operated during their formation (Rollinson 2008; Griffin et al. 2009). Additionally it has been proposed in a number of recent studies that over 70% of the continental crust was formed before 2.5 Ga (e.g. Belousova et al. 2010; Hawkesworth et al. 2010; Griffin et al. 2010) making the understanding of Archaean high-grade gneiss terranes even more critical to gain insight in Earth’s evolution.

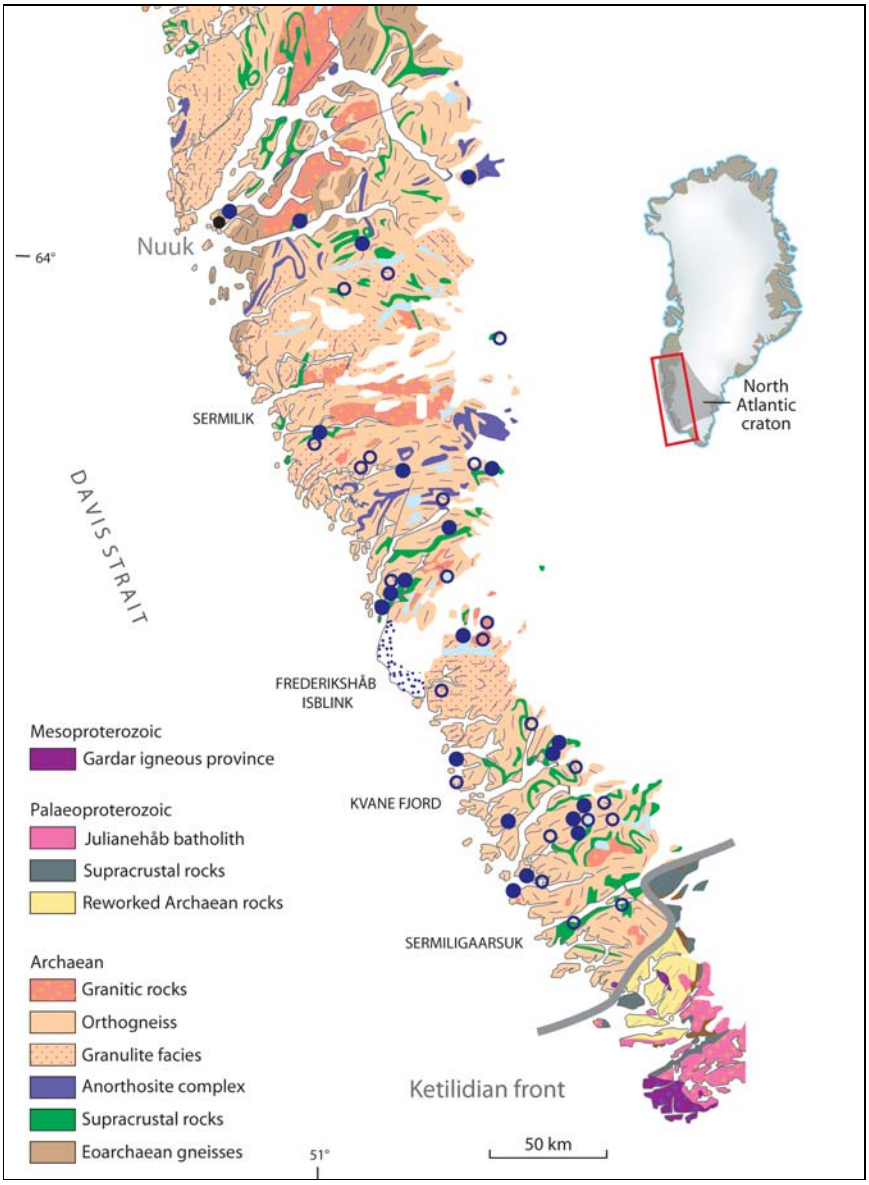

Figure 1. *Simplified geological map of SW Greenland showing the positions of rock samples discussed in this report; TTG samples sensu strictu (filled blue circles), and other felsic samples, mainly migmatites and granites (open blue circles). Where several samples are from localities near each other they have be shown as one position. Place names of selected fjords are shown.*

The global Archaean TTG suite

The grey-gneisses are generally thought to represent juvenile crustal components with igneous protoliths (orthogneisses) and a number of studies have shown that a large proportion of the orthogneisses in Archaean high-grade gneiss terranes belong to a suite of rocks with a tonalite-trondhjemite-granodiorite composition, known as the 'TTG suite' (e.g. Martin 1993; Martin 1999; Martin et al. 2005). The global Archaean TTG suite is characterised by $SiO_2 > 64$ wt%, Fe_2O_3+MgO+MnO+$TiO_2 < 5$ wt%, $K_2O/Na_2O < 0.5$, high Na_2O and low Mg# (average of

0.43), Ni (14 ppm) and Cr (29 ppm) (Martin et al. 2005). They also have negative Nb-Ta anomalies that are generally associated with a negative Ti anomaly. They normally have strongly fractionated upwards concave rare earth element (REE) patterns with enrichment in light REE (LREE) over heavy REE (HREE) with $La_N/Yb_N > 150$ and Yb_N ~0.3 - 8.5.

Geochemical similarities exist between the Archaean TTG suite and modern high-silica adakites, which are mainly believed to have formed through direct melting of the slab in subduction zones (Defant and Drummond 1990; Martin et al. 2005). Martin and Moyen (2002) suggested a secular evolution from Archaean TTG's that show little evidence for mantle interaction, to post-Archaean adakites and island arc basalts that show evidence for larger mantle contributions and greater average depths of melting, as reflected in relatively high Mg#, Ni and Cr contents and MREE/HREE's in these rock types. In their model, they explained the secular change by a steepening of subduction zones through time, with the Archaean being characterised by a relatively flat subduction style (due to thicker, hotter and more buoyant oceanic plates in the Archaean), leaving no space for a mantle wedge above the subducting plate. In comparison, steeper subduction styles in post-Archaean (and modern) times imply that partial melts derived from the subducting plate to a larger extent interact with the overlying mantle wedge to generate the chemical signature of adakites. In the case of normal arc basalts, it is generally believed that partial melting is localised within the mantle wedge, where it is triggered by the introduction of fluids from the subducting dehydrating slab.

A number of experimental studies have shown that TTG compositions can be produced by low to moderate (10-20%) degrees of partial melting of a hydrous metabasalt with a garnet amphibolite to eclogite residual chemistry depending on the pressure (Rapp et al. 1991; 2003; 2010; Rapp and Watson 1995; Moyen 2011).

Results – geochemical data

64 samples of TTG gneisses collected during field work by GEUS from SW Greenland, between Ameralik fjord in north and Sermiligaarsuk fjord in south, were analysed for major and trace elements (Appendix Table B.1). The data were acquired over a longer period (2008-2010) and from different laboratories, accentuating the need for a comparison of the standard data (see Appendix A).

For the purpose of discussing the petrogenesis of TTGs, a screening of the dataset was carried out in order to exclude samples that were suspected of being affected by post magmatic processes such as: low temperature alteration, mechanical mixing during deformation, and migmatisation which could affect the petrologenetic interpretations.

Firstly, samples containing leucosomes, veins, xenoliths and restite were rejected from the data set (n=8). Secondly, a large number of the TTG samples have been age determined by zircon U/Pb dating (Kokfelt et al. 2011); samples with complex age patterns were filtered out, because these are likely to represent multiple melt components and/or crustal remelts, and are thus not likely primary melts candidates (n=4). Thirdly, a screening based on the chemical criterias established for TTG's (see above) was applied removing samples (n=21) with $SiO_2 < 64$ wt%, significant Ce-anomalies (alteration), Eu/Eu* > 2 (reflecting plagioclase accumulation), Cr > 30 ppm, Ni > 25 ppm, $Al_2O_3/CaO+Na_2O+K_2O > 1.2$ and $K_2O/Na_2O > 1$. The samples removed by this filtering procedure included several relatively mafic samples unrelated to TTG magmatism, such as possible diorites, sanukitoids and samples that may have been contaminated with enclaves of supracrustal rocks. The filtered data set consists of 32 samples that in ‘all likelihood’ represents TTG magmas, *sensu stricto,* i.e. that have not been affected to any significant degree by crustal contamination or post-magmatic alteration processes. The location of all of the TTG samples (65) cover the entire area of SW Greenland from 61°30’ and up to ~64° (Fig. 1).

In the major element variation diagrams (Fig. 2) Al_2O_3, CaO, MgO, FeO_t and TiO_2 form general negative trends versus SiO_2, whereas Na_2O shows more scatter. The trace elements generally produce scattered variations with SiO_2, except for Ni and Cr that show inverse rough correlations with SiO_2 (Fig. 3). In the chondrite-normalised REE diagram (Fig. 4), the TTGs are LREE enriched with La_N/Sm_N ~3-9 and variable Gd_N/Lu_N of 1-5 and small positive or negative Eu-anomalies (Eu/Eu* = 0.64-1.69). In a primitive mantle-normalised ‘spidergram’ (Fig. 5), the TTGs samples have pronounced negative Nb and Ti anomalies, as well as, generally positive Zr-anomalies (Nb_N/La_N = 0.05-0.6; Ti_N/Dy_N = 0-4; Zr_N/Sm_N= 1.2-8.7; Nb/Ta = 4.2-25).

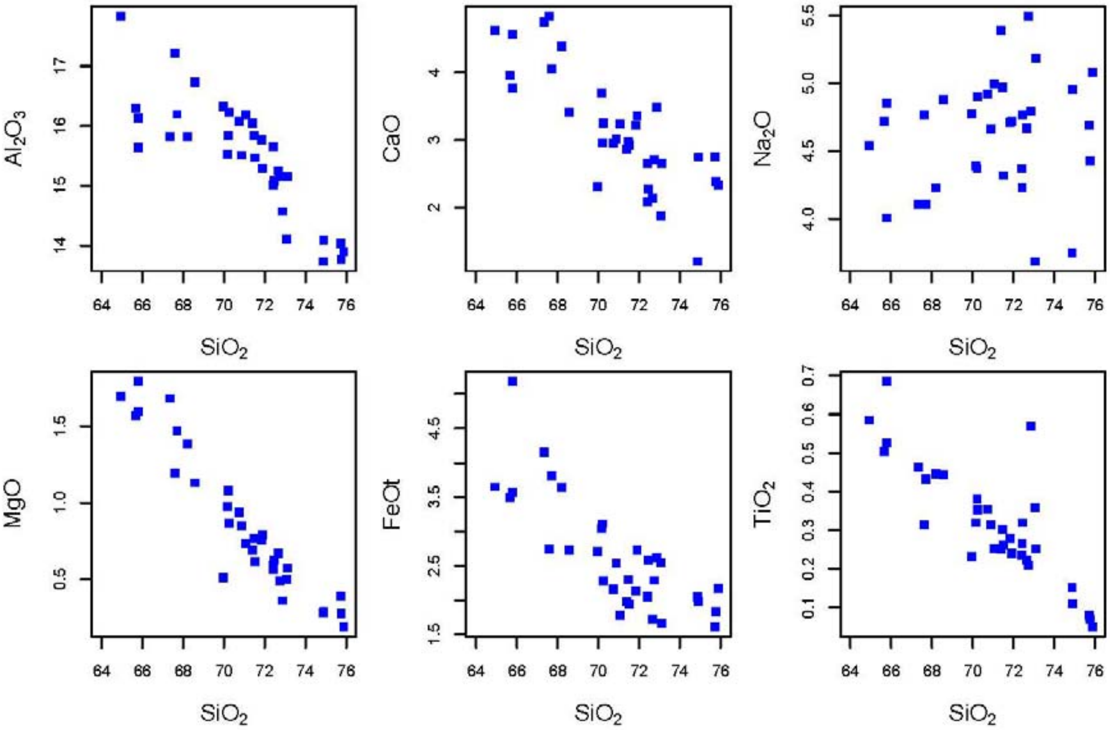

Figure 2. *Major element variation of the 34 screened TTG samples showing inverse correlation with SiO_2, except for Na_2O, which is likely related to an increasing albite component in the plagioclase.*

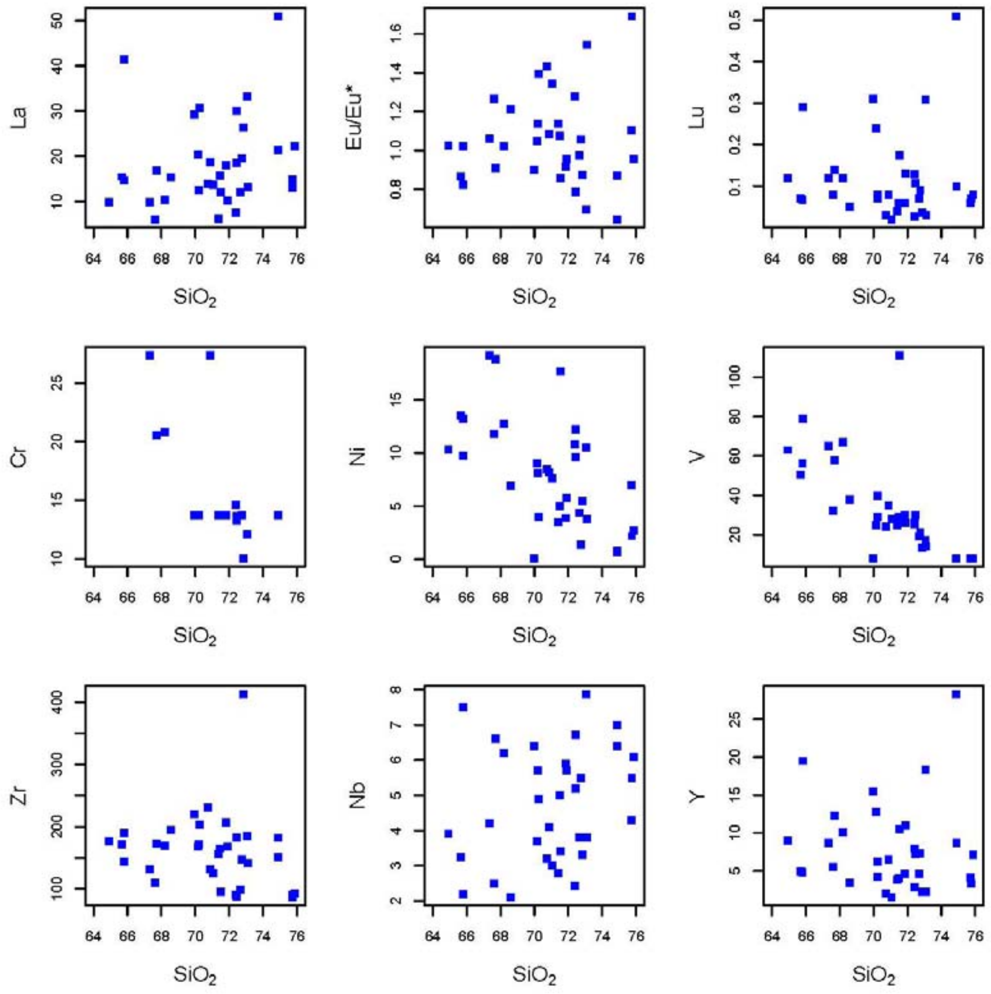

Figure 3. *Trace elements variation of the screened TTG samples showing general positive correlation with* SiO_2 *although there is significant scatter, except for Cr, Ni and V which show strong inverse correlation with* SiO_2.

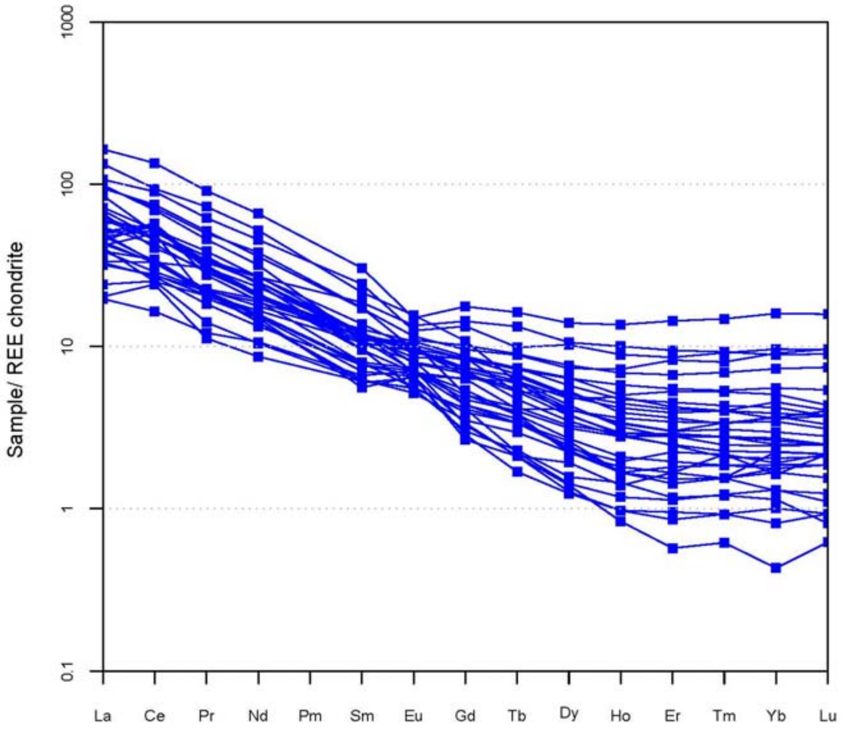

Figure 4. *Chondrite-normalised (Boynton 1984) REE diagram. The TTG samples from SW Greenland show a ~10x concentration range in the light to heavy REEs.*

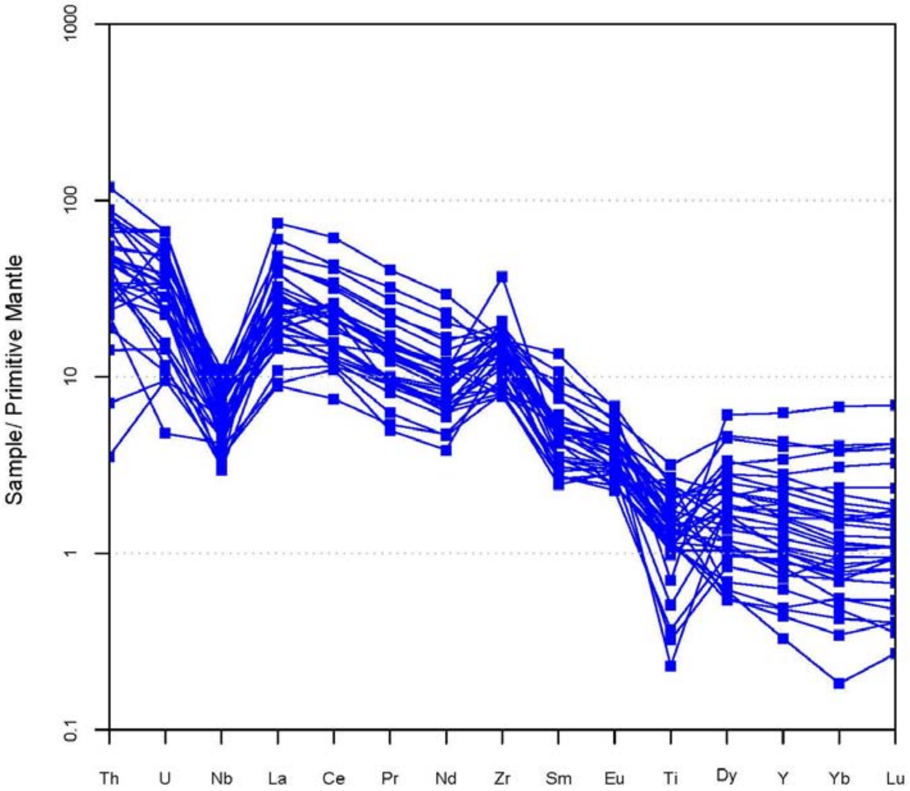

Figure 5. *Primitive mantle-normalised (Sun and McDonough 1989) trace element diagram. The screened TTG samples show distinct negative anomalies for Nb and Ti, and a positive anomaly for Zr.*

In the feldspar diagram the normative composition of the TTG samples plot mainly at the border between the tonalite-trondhjemite-granodiorite fields (Fig. 6), but a few samples also plot within the granite field, reflecting their somewhat higher K_2O contents in these biotite-bearing samples. In geotectonic discrimination diagrams (Fig. 7) the TTGs plot in the volcanic arc/active continental margin setting.

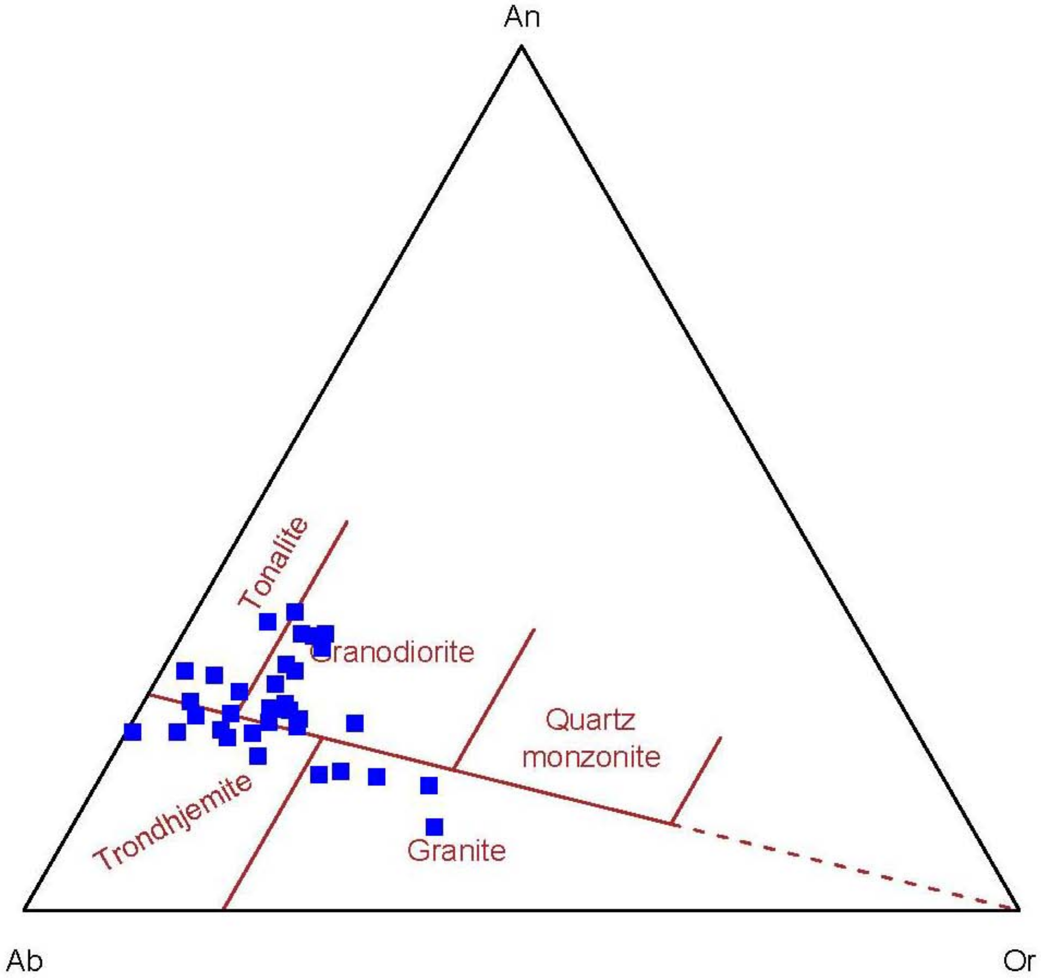

Figure 6. *The screened TTG samples plotted in a normative feldspar diagram (O´Connor 1965). Most plot in the TTG-suite field, but a few plot in the granite field, although they might not contain orthoclase, but rather biotite, which disturbs the norm-calculation.*

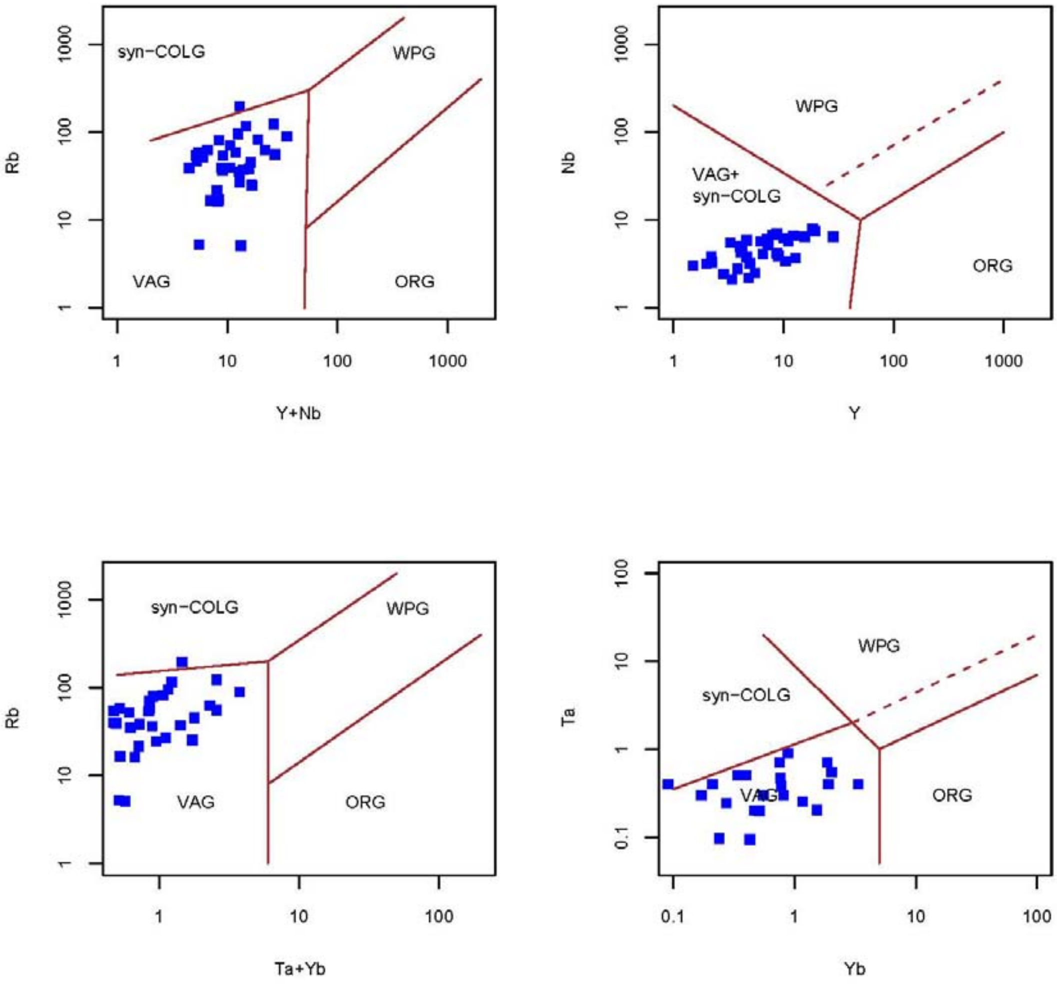

Figure 7. *Screened TTG samples plotted in various tectonic discrimination diagrams for plutonic rocks (Pearce et al. 1984). The SW Greenland TTG samples plot consistently in the VAG field, indicating a volcanic arc affinity.*

Modelling the partial melting process

It is well-established from experimental data that hydrous metabasalts are the most likely source of TTG magmas (Moyen and Stevens 2006), but there is considerable debate about the geotectonic setting in which they formed; this could involve either (1) a subduction zone environment (Drummond 1990; Foley et al. 2002; Rapp et al. 2003), (2) melting of the lower part of a thickened mafic crust (Defant and Condie 2005), or (3) melting related to a mantle plume (Bédard 2006). To address the relevance of each of these three scenarios in relation to SW Greenland, we modelled the REE element data to obtain estimates of the range in temperatures and pressures under which TTG’s are likely to have formed.

For the modelling, we applied a batch melt model (Shaw 1970), which is considered the most realistic melting model for TTG formation given the high SiO_2 contents in these melts (Foley et al. 2002). The modelling involved the REEs, and the procedure was to constrain the range of P-T-x conditions for which the REE patterns could be reproduced. The obtained results constraining the melting conditions were then compared to the results from published experimental studies. Various estimates of residual mineralogies (Drummond and Defant 1990; Rapp et al. 1991) were used to simulate different pressure conditions (Table 1), which together with incremental melt fractions (*F*, or the degree of melting) represent the two main variables.

Table 1. Compositions of restites used for the melt modelling.

Amph	Plag	Cpx	Opx	Garnet	Reference:
-	-	61%	-	39%	Rapp et al. (1991) ~ 22 kbar
17%	15%	52%	-	15%	Rapp et al. (1991) ~ 16 kbar
41%	48%	-	11%	-	Rapp et al. (1991) ~ 8 kbar
84%	5%	-	-	10%	Drummond and Dufont (1990)
50%	40%	-	-	10%	Our estimate of grt-amphibolite

Following experimental studies between 10-40% partial melting of basalt will produce TTG-like melts (Rapp et al. 1991), but a more reasonable melt fraction would be 10-20% (Rollinson 2010), in agreement with mass balance calculations from average crust, which indicates a melt fraction about 14% from a basaltic source (Hawkesworth and Kemp 2006). In our calculations the partition coefficients of Bédard (2006) were used, because they form an internally consistent dataset and have been used for the specific task of calculation TTG-formation from metabasalts previously. Two different starting compositions were tested: (1) a purely tholeiitic basaltic composition, and (2) a composition that represents a mixture of tholeiitic basalts and calc-alkaline rocks as usually found in the supracrustals belts of SW Greenland (Szilas et al. 2011). These two source estimates are based on the median values of 111 tholeiites and 109 calc-alkaline rocks described by Szilas et al. (2011). The mixture estimate (2) relies on the assumption that none of the two groups were preferentially sampled, which is reasonable given the large sample population and the fact that the bimodality was not known at the time of sampling. The proportion of tholeiites and calc-alkaline rocks in the mixture estimate (2) is about 50:50, which is more or less consistent with mapping of the various lithologies and we thus believe this estimate to be a reasonable composition for the average supracrustal belts of SW Greenland, although the exact composition does not affect the modelling much.

The results of the modelling are shown in Figures 8 and 9, which plots the calculated melting trajectories for the two different source compositions in a La_N/Sm_N versus Gd_N/Lu_N diagram. These two REE ratios are sensitive to the degree of partial melting and to the average depth of melting, respectively. Shown in Figures 8 and 9 are the screened TTG samples (blue filled circles) as well as melting trajectories (lines with filled diamonds) calculated for two different source compositions, and a range of residual mineralogies and depths of melting. For each melt trajectory, increased degrees of melting leads to decreasing La/Sm, and at 100% of melting the melt composition is equal to that of the initial source composition. Increasing depths of melting mainly effect the Gd/Lu ratio as deeper melting will involve larger proportions of residual garnet in the source region which will retain HREE and Lu relative to MREE and Gd. Also shown for reference in Figures 8 and 9 are the average global TTG compositions of Martin et al. (2005), as well as, the filtered out part of the SW Greenland data that were filtered away from the TTG data set (small red dots).

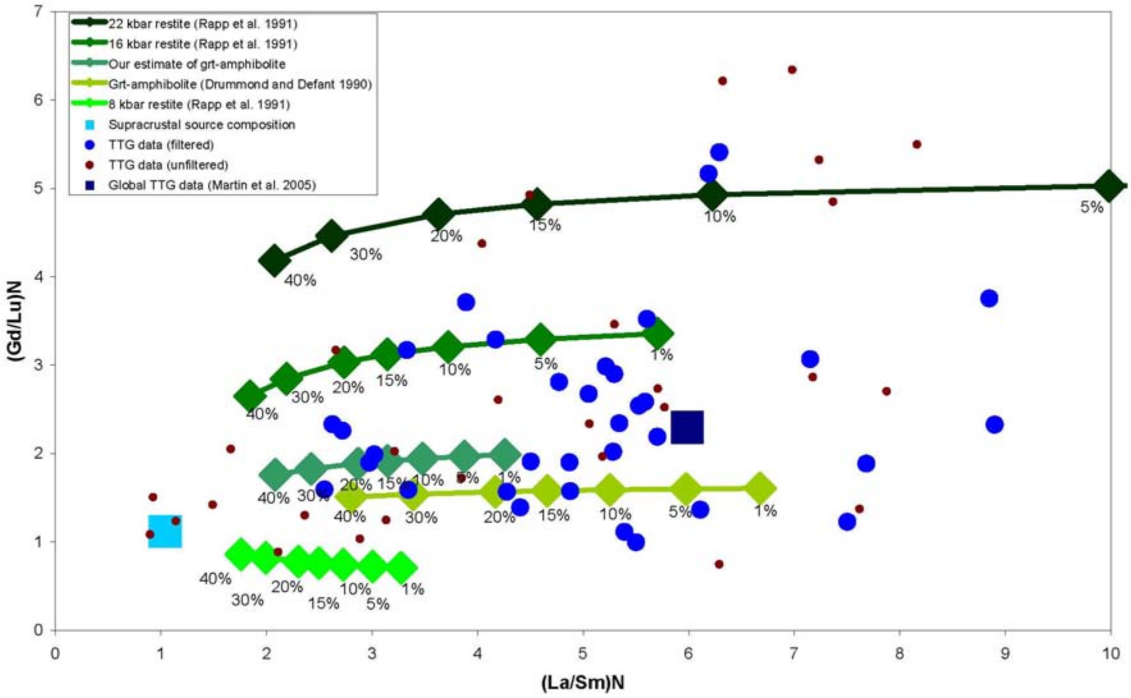

Figure 8. *Modelling of the SW Greenland TTG compositions in a La/Sm versus Gd/Lu diagram. The subscript N denotes chondrite normalisation of Boynton (1984). Melt models with a tholeiitic source composition and the residual mineralogy is listed in Table 1. Increments mark the degree of melting (F) from 1% to 40% in the melting model. The results indicate that very low melting degrees (1-5%) are required to explain the SW Greenland TTG compositional range with a tholeiitic source rock.*

The large range in Gd_N/Lu_N displayed by the filtered TTG samples indicates that TTG formation took place over a range of pressures. However, the tendency is that TTG compositions plot with low Gd_N/Lu_N values reflecting pressures below 16 kbar (correspondin to >50km depth).

Similarly, the range in La_N/Sm_N suggests that different melt fractions and/or source compositions are involved to explain/generate the SW Greenland TTG compositions. By comparing the melting models displayed in Figure 8 and 9, it is seen that the tholeiitic source, produces melts with lower La_N/Sm_N at a given melting degree compared to the more LREE-enriched mixed tholeiitic - calc-alkaline source, which is generally preferred as a source of TTGs (Moyen 2010). Noteworthy, some of the more mafic samples that were filtered out of the TTG data set (diorites or samples contaminated by supracrustal enclaves) are seen to plot close to the starting composition consistent with their more mafic compositions.

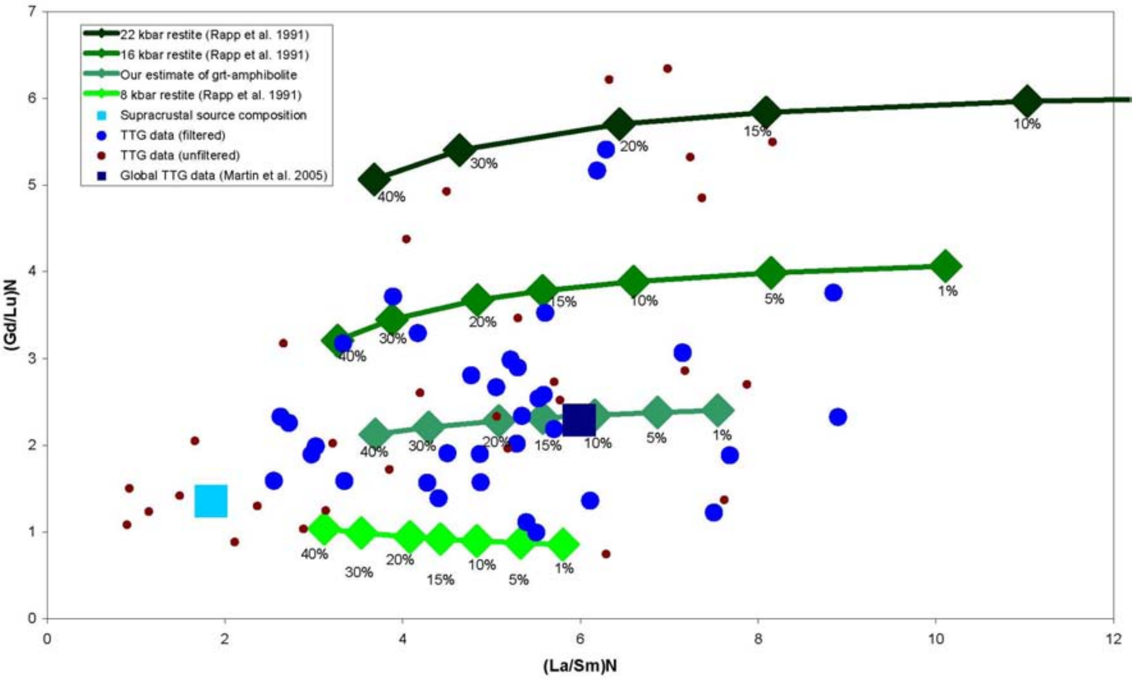

Figure 9. *Melt models with a combined tholeiitic and calc-alkaline source composition. This model requires higher degrees of melting than the models assuming a pure tholeiitic source. Note that some TTG samples with low La/Sm seem to require either higher degrees of partial melting (>60%) or derivation from a less enriched source rock (eg. tholeiite).*

Discussion of the geochemical data and melt model

In the following section we first discuss the possible petrogenetic implications of the melt modelling presented above. In a subsequent section we explore the SW Greenland TTG data set in a wider context by giving a short literature review of petrogenetic models for TTG formation.

We have compared our TTG data with that of previously reported data from SW Greenland (Garde 1997; Steenfelt et al. 2005) and a global data set of Martin et al. (2005) and found similar ranges in major and trace element concentrations confirming that our data represent 'normal' Archaean TTGs.

The major element variations of our data (Fig. 2) seem to primarily reflect variable degrees of partial melting or source composition rather than melting depth, due to lack of correlation between SiO_2 and Gd_N/Lu_N (not shown), or differentiation, which would likely be stalled by the high viscosity of these felsic magmas.

Low degree melts of an enriched source would result in higher SiO_2 and Na_2O and lower MgO, FeO_t and TiO_2 than higher degree of melting, which lowers the SiO_2 content and increase the MgO, FeO_t and TiO_2 as well as the CaO component of the melt. These major element variations are consistent with melting experiments in which temperature/degree of partial melting show similar trends during TTG formation (Springer and Seck 1997; Moyen and Stevens 2006) and similar trends are found in recent granitoids (Annen et al. 2006; Bea 2010), although interpreted to represent magma chamber processes such as fractional crystallisation.

This trend seems to be compatible with the variation in Ni, Cr and V, whereas incompatible trace elements like La, Lu, Zr, Nb and Y show some scatter although they seem to be correlated somewhat positively with SiO_2 (Fig. 3). Source variations (eg. tholeiitic vs. calc-alkaline basalts) could be responsible for this scatter, because these sources have much greater difference in their incompatible trace element content than for the compatible trace elements. Alternatively these trace element variations could reflect variable interaction with a mantle wedge during ascent of TTG-like slab melts as proposed by Martin and Moyen (2002).

Kemp et al. (2007) showed that even I-type granites are dominated by incorporation of older supracrustal material and thus production of new crust almost always represents reworking of material. This is consistent with isotopic data from Archaean TTGs that they almost always represent reworking of older volcanic rocks (Whalen et al. 2002; Næraa 2011). Thus a combination of variable melting of a heterogenous supracrustal source with addition of juvenile melt that mixed and possibly fractionated in a magma chamber is a likely scenario that explains the geochemical data for the SW Greenland TTGs.

The TTGs can be divided into two separate groups based on their Sr/Y vs. La/Yb ratios (Fig. 10), which according to Moyen (2011) relates to the depth of melting. Although Sr can be mobilised in fluids and/or melts being a large ion lithophile element, it is locked up in plagioclase, which is a major component of TTGs and is thus not expected to be strongly affected by post-magmatic processes without the formation of abundant clay minerals. It is thus unlikely that Sr has been mobilised significantly in our samples, as the presence of sericite would have resulted in exclusion of the samples from the dataset.

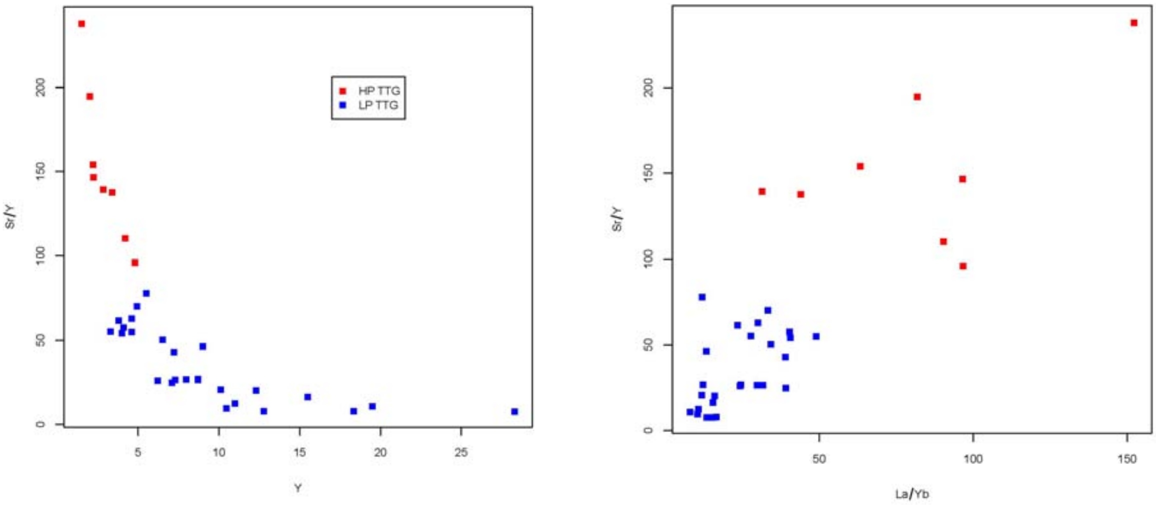

Figure 10. *Sr/Y vs. Y diagram (left-hand side) and Sr/Y vs. La/Yb (right-hand side) with the high Sr/Y TTG samples grouped as high-pressure TTGs and the low low-pressure TTG based on the distinct jump in values seen in the Sr/Y vs. La/Yb on the right.*

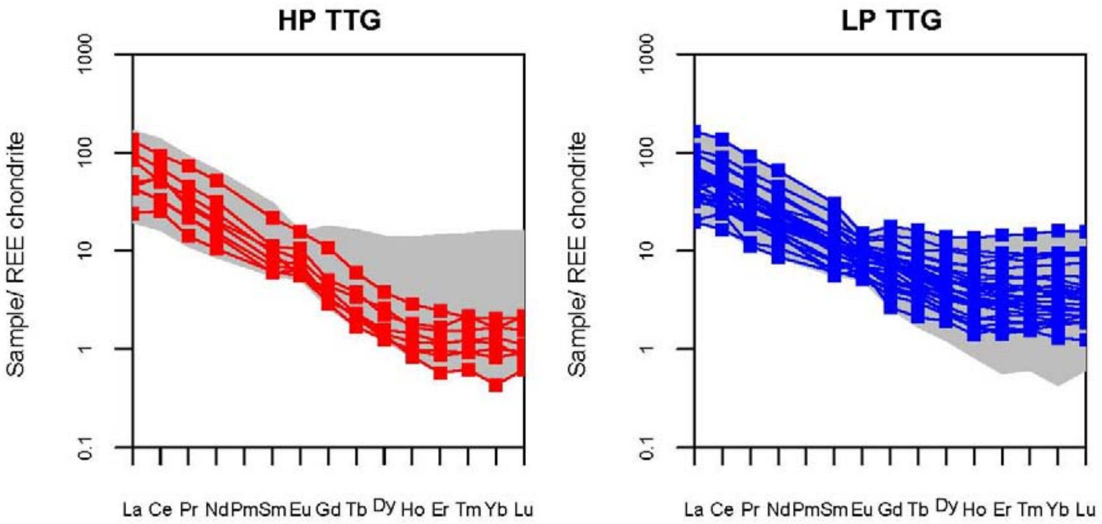

Figure 11. *The screened TTG samples are divided into a 'high pressure' (left-hand side) and 'low pressure' (right-hand side) according to their Sr/Y ratios. The two groups show different HREE patterns, which are consistent with higher proportions of residual garnet in the source of the high-pressure TTG samples.*

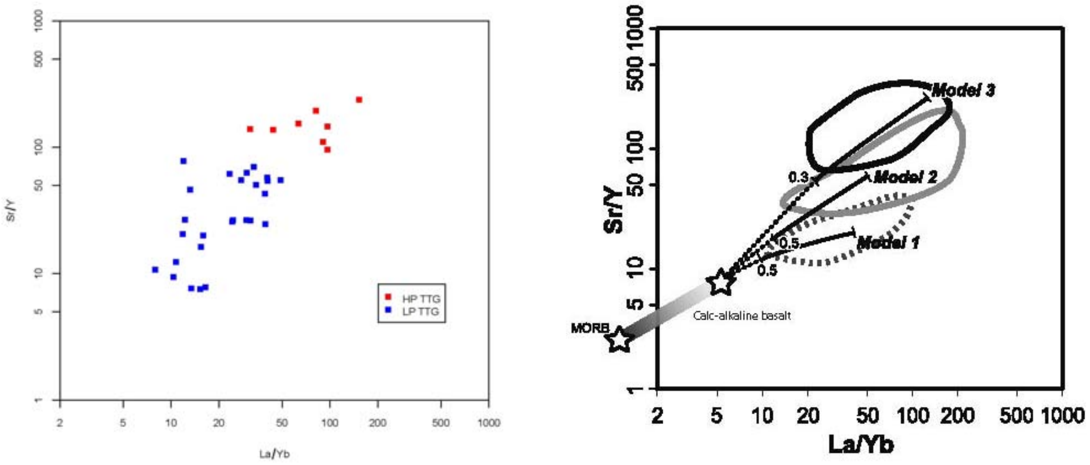

Figure 12. *Sr/Y vs. La/Yb for the SW Greenland TTG samples (left-hand side) show a positive correlation over a continuum of ratios that can be explained by partial melting over a pressure range, as demonstrated by the different melting models by Moyen (2011) (right-hand side): Model 1 is low pressure; Model 2 is intermediate pressure; and Model 3 is high pressure. The model of Moyen (2011) indicates that partial melting of a MORB source will not produce the enriched signature of the TTG's, whereas a slightly more enriched source is required, consistent with our melting modelling (see Figs. 8 and 9). Note log-scale on all axes.*

From the REE patterns (Fig. 11), it is not entirely clear if the two groups represent a distinct jump or actually form a continuum. However, in the Sr/Y vs. La/Yb plot (Fig. 10) it seems most likely that they form two distinct groups. This jump is not as distinct on the log-scale diagram (Fig. 12), but the significance of such a jump would be that two different pressure intervals must be responsible for the formation of the TTGs and thus perhaps two different settings (or processes) must be operating in the formation of the TTGs.

The modelling of the REE and Sr/Y variations of the SW Greenland TTG samples (Figs. 8-12) suggest that the melts formed by partial melting from a variably enriched basaltic source over a pressure range from mainly 8 to 16 kbar (~25-50km depth) and a distinct group at about 22 kbar (~70km depth). To further characterise the geological environment in which the TTG's formed we now discuss the evidence from the HFSE, as they may help to constrain the presence of certain accessory mineral phases diagnostic of the particular conditions prevailing under TTG formation.

The primitive mantle-normalised 'spidergram' (Fig. 5) shows significant negative anomalies in Nb and Ti, which is usually a diagnostic feature in arc-related volcanism where it is taken as an indication of fluid/melt LILE enrichment into a mantle wedge source whereas HFSE are retain in a residual phase such as rutile. However, negative HFSE anomalies have also been reported from dacitic rocks in Iceland HFSE with no obvious relation to a subduction zone environment, and this finding may seriously question the diagnostic ability of this feature as argued by Willbold et al. (2009). This also high-lights the potential problem assigning a specific tectonic setting using so-called diagnostic trace element ratios, an issue that is especially pronounced for Archaean rocks for which the basic uniformitarian principles might not apply, as the increased mantle temperature may have resulted in different tectonics regimes and thus change in these ratios (Pearce 2008).

Principally, negative anomalies for HFSE are likely to reflect the presence of HFSE-retaining minerals in the source region, such as rutile or ilmenite. The extent of the anomaly would be controlled by the governing factors for the stabilisation of these phases is water content, degree of melting and the P-T conditions (Green and Pearson 1986; Klemme et al. 2002; Xiong et al. 2006). The preferential partitioning of HFSE into these accessory phases would make them unavailable for the melt and thus would occur in lower relative abundances.

The distinct positive Zr (and Hf) anomalies are likely related to the presence of amphibole in the source region, as Zr has been shown to partition into amphibole, which is even capable of fractionating Zr and Hf from Nb and Ta (Foley et al. 2002). The strong positive anomaly seen for Zr therefore indicates an important role for amphibole in the generation of TTG melts of SW Greenland. Furthermore, this is consistent with the observations in modern arc magmas that have been explained by the 'amphibole sponge model' (Davidson et al. 2007). In this model amphibole fractionation in magma chambers is proposed to control much of the variation in arc magmas, in a cryptic manner due to the dissolution of amphibolte at lower pressure, which results in lack of this mineral as a phenocryst. However, as we stated in the first part of the discussion, there is good evidence from the correlation of the major element variations in our data with those of experimental data (Springer and Seck 1997) that the major element variation of the TTGs of SW Greenland are mainly controlled by the melt fraction/temperature. Thus fractionation in a magma chamber is not compatible with our model, which is also not likely given the high SiO_2 content of these melts. This does not change the fact that amphibole is a significant mineral in the source rock and is likely responsible for the positive Zr anomaly seen in Figure 5.

The melting models with purely tholeiitic source does not adequately explain the data, as this model requires much to high melt fractions to be realistic. The model that best explain the TTG data assume a moderately enriched source derived from a mixture of tholeiitic and calc-alkaline volcanic rocks and low to intermediate melting at pressures between 8 and 16 kbar, and a few samples derived at high pressures up to about 22 kbar. This is consistent with a few high Sr/Y vs. La/Yb samples indicative of high pressure (Fig. 12) and the majority plotting at lower pressures, according to the classification of Moyen

(2011), which also proposes that high pressure garnet-rich restites will lead to high Sr, Al_2O_3 and Na_2O and low Y and HREE.

The melting models based on a pure tholeiite source result in unrealistically low degrees of partial melting (1-5%) and thus does not explain the data adequately. Most of the data are explained better by a source of combined tholeiitic and calc-alkaline metabasalts, which is reasonable since this is also closer to the average composition of the majority of the supracrustal belt in SW Greenland (Szilas et al. 2011). The main protolith for the TTGs must have been garnet-amphibolite (low to intermediate pressure) rather than eclogite (high pressure), as seen by Figure 9 and 12, where model 1 represents melting at low pressure and model 3 at high pressure.

Figure 13 shows the REE patterns produced by the different melting models assuming a mixed tholeiitic and calc-alkaline source, which we consider more likely than a purely tholeiitic source. It can be seen from Figure 13 that the complete range of REE variation within TTGs from SW Greenland can be adequately explained by ~5-20% partial melting over a pressure range of 8-22 kbar, corresponding to ~25-70 km depth. As noted earlier, part of the overlap in REE content between the different TTGs could be achieved by fractional crystallisation that would increase the total REE contents and/or variable content of restite garnet in the source to lower the HREE content.

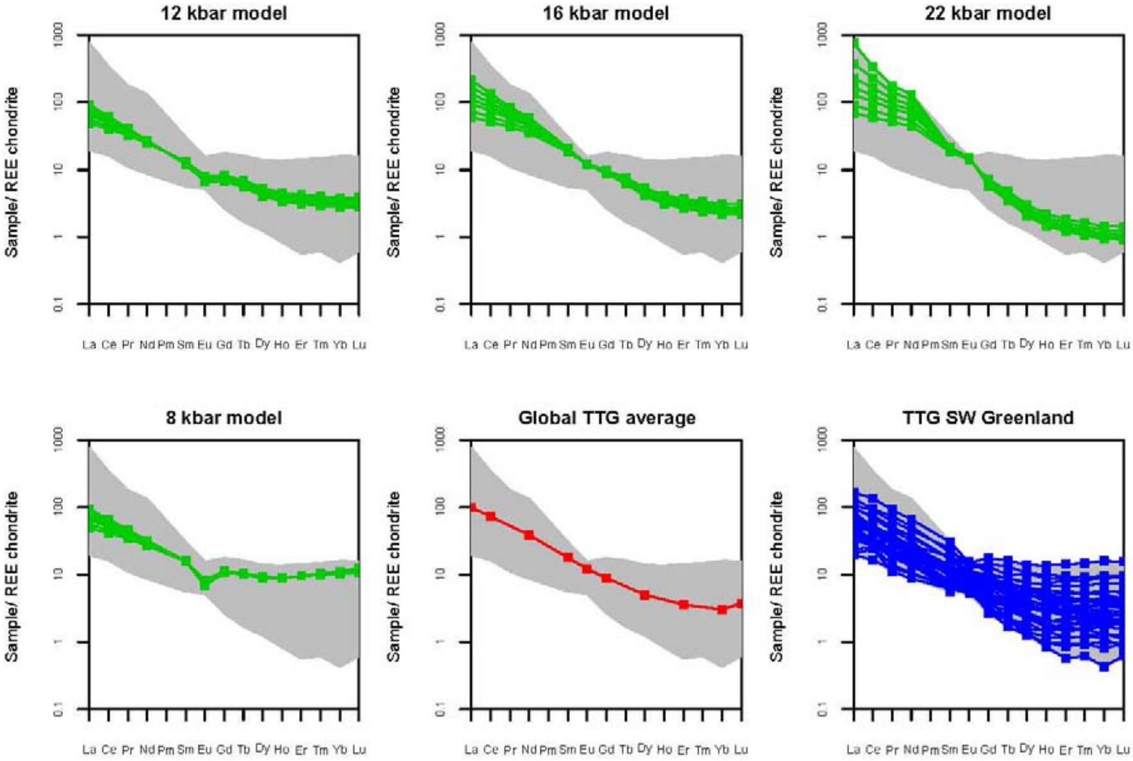

Figure 13. *Results of the melting models with the screened TTG data and an average of global TTGs for reference (Martin et al. 2005). The models are able to reproduce most of the variation in seen in the SW Greenland TTGs, by variable depth and degree of partial melting of a mixed tholeiitic-calc-alkaline basaltic source. Melt fractions for the models range from 1-40% as in Figure 9, although 10-20% is a more realistic range for TTGs (Hawkesworth and Kemp 2006; Moyen 2010).*

An interesting observation is that there seem to be a correlation between intrusion age and the major element chemistry, such that the oldest TTGs have higher MgO and lower SiO_2 and vice versa for the younger samples (Fig. 14). The same trend (not shown) is observed for FeO_t, TiO_2, P_2O_5, Al_2O_3, CaO, Cr, Ni, Y, and Sr, which are all inversely correlated with SiO_2 content as well as with time.

This could, as an initial hypothesis, be interpreted as being related to the general cooling of the Earth through the Archaean. If this was true then higher degrees of melting would be expected back in time and thus high MgO and lower SiO_2, but comparisment with samples from 3.7 Ga old TTGs from Isua (not shown in Fig. 14) does not support such a long term trend. This is also not supported by Martin and Moyen (2002), who showed that MgO content actually incease through time for TTGs, likely in response to an increase in the interaction with a mantle wedge.

It is thus more reasonably that the samples represent one single thermal event and that the cooling of this system is reflected by decreasing melt fractions. Alternatively this trend could be related to 'cratonisation', so that processes of crystal fractionation and reworking of crust were more likely in the later stages of intrusive activity in the crust.

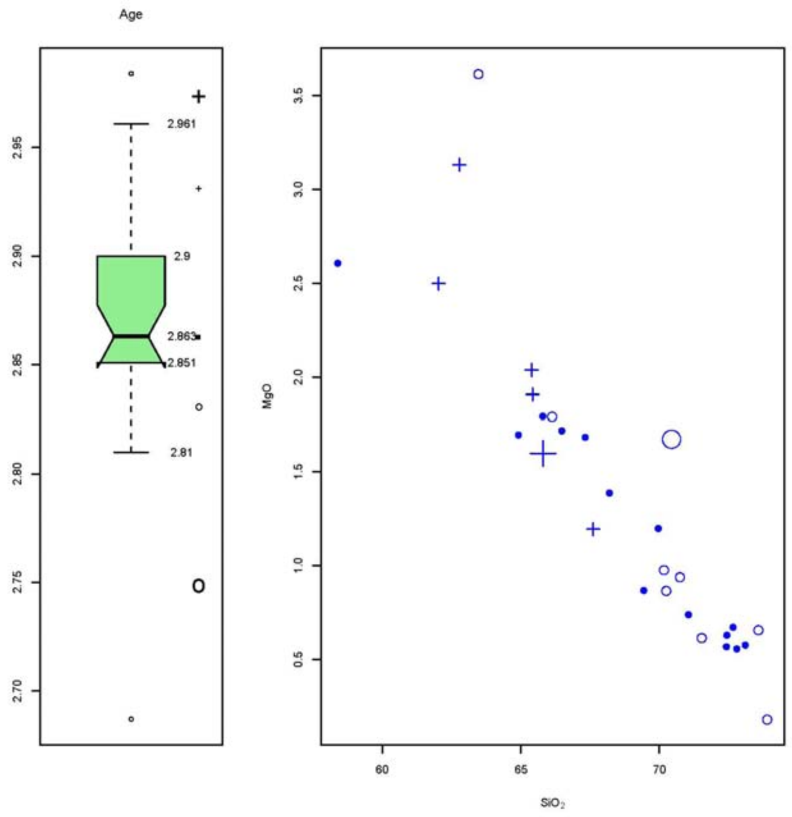

Figure 14. *MgO vs. SiO_2 for all unscreened samples that have been age dated. The symbols are related to the intrusion age of the samples as seen by the legend to the left.*

Proposed geodynamic models for TTG formation

TTGs have been related to a number of different geodynamic settings of which the most commonly promoted are 1) partial melting of subducted oceanic crust in an arc environment (Martin et al. 1986; Defant and Drummond 1990; Drummond et al. 1996; Foley et al. 2002; Martin et al. 2005), 2) melting of thickened lower mafic crust possibly aided by delamination of eclogite (Zegers and van Keken 2001; Condie 2005) and 3) oceanic plateau and continuous plume interaction (Bédard 2006; Smithies et al. 2009).

Model 1) proposes that the Archaean TTGs were produced in a subduction environment by direct melting of the subducting slab as seen in Figure 15.

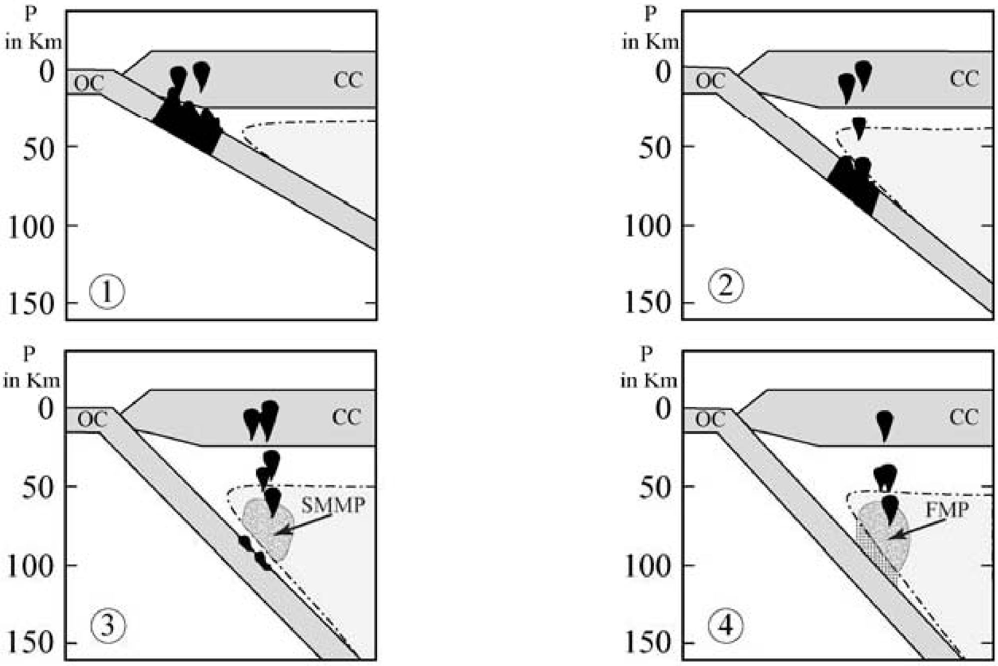

Figure 15. *TTG production in a subduction setting showing progressively more mantle wedge involvement through time as the angle of the subducting slab steepens due to the decreased buoyancy with decreasing temperature from the Archaean to the Proterozoic (from Martin and Moyen 2005).*

It was proposed by Martin (1999) that Archaean TTGs are the products of slab melts as they have large compositional overlaps with modern adakites and the characteristic Nb, Ta and Ti anomalies that are thought to be diagnostic of such a setting (Martin et al. 2005). In this model TTGs are formed by melting of the subducting hydrous mafic oceanic crust when conditions were anomalously hot such as during ridge-subduction. In the Archaean the greater geothermal gradient might have made this process much more common than today. Martin and Moyen (2002) present a compelling model for TTG-formation by slab melting, which would be able to explain the systematic changes of TTGs through time, by increased melt and mantle-wedge interaction.

A number of studies have argued that subduction and modern style plate tectonics were probably active by the late Archean (~2.7 Ga) and probably occurred prior to 3.2 Ga

(Smithies et al. 2005; Kerrich and Polat 2006; Wyman et al. 2008; Windley and Garde 2009).

It has also been noted that many eclogitic sub-continental lithospheric mantle (SCLM) xenoliths have a chemistry that correspond to the residues during melting of basalts to form TTG (Rollinson 1997). Continental crust and depleted mantle both have subchondritic Nb/Ta, Nb/La and Ti/Zr, which requires the existence of an additional reservoir with superchondritic ratios, such as eclogite residue produces by TTG production (Rudnick et al. 2000). This is also consistent with age constraints provided by Re-Os dates on peridotite xenoliths (Pearson et al. 1995; Pearson 1999), which suggest a correlation between crust formation and the age of SCLM xenoliths.

However, some problems do exist with the direct slab melting model. First of all it has been shown that adakites, the suggested modern analogue of TTGs, can be produced in a range of environments unrelated to a subduction zone setting (Castillo 2006). Secondly the greater buoyancy of the oceanic crust in the Archaean might have completely prevented the possibility of subducting this material in the first place until fairly late in the Archaean (van Hunen et al. 2008). The slab melting model is also contradicted to some degree by Lu-Hf isotopic data from zircons, which often indicates significant input from pre-existing crustal material to the TTGs (Næraa 2011). Also, since pillow lavas and dyke-complexes of the oceanic crust have been through low-temperature sea-floor alteration, as seen by variable $\delta^{18}O$ values of +5 to +10‰ (Muehlenbachs 1986; Staudigel et al. 1995), the restricted variation in $\delta^{18}O$ values obtained from the TTGs seem incompatible with an origin via direct partial melting of the upper portion of a slab. The general mantle-like $\delta^{18}O$ values also contradicts, that the crustal Hf signature observed in the TTGs is derived via a slab-derived sediment-melt component.

Additionally many TTGs from southern West Greenland have long residence times seen from Hf-isotope data in zircons (Næraa 2011), suggesting that a pre-existing crust was involved in the petrogenesis of the TTGs. This suggests that there was a decoupling between subduction, mantle metasomatism and the formation of TTGs and thus indicates that slab melting during subduction might not be a likely setting for the formation of these TTGs.

Model 2) relates TTG production to melting of the mafic lower crust during accretionary thickening and/or delamination as seen in Figure 16, but could occur in a number of tectonic environments.

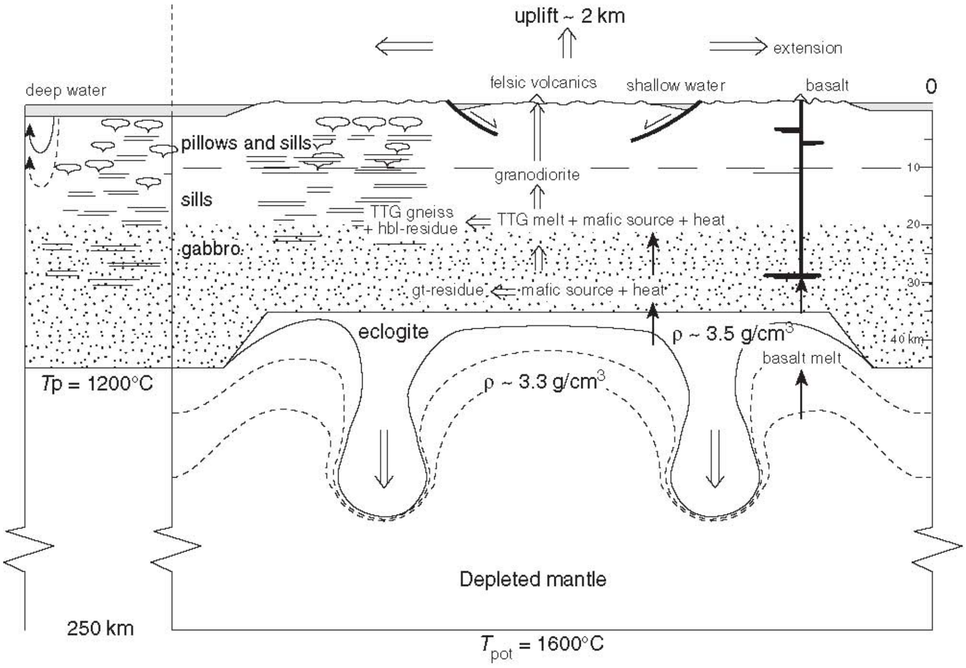

Figure 16. *Melting of the lower crust in a thickened mafic lithosphere possibly aided by delamination to cause asthenosphere upwelling and promote TTG formation (from Zegers and van Keken 2001).*

For post-Archaean TTG-like suites estimates of crustal thickness required to generate these melts from garnet amphibolite or eclogite residues within the lower crust range from 27 km (Tate and Johnson 2000) to >40 km (Petford and Atherton 1996). Thus the source for these rocks must have occupied a significant crustal section, possibly from the base of the crust to mid-crustal levels. The Hf signatures obtained from TTGs indicate that such an amphibolitic proto-crust must have been established long before the TTGs were formed (Næraa 2011). Thickened amphibolitic proto-crust could have formed by under-stacking of hydrated, buoyant upper oceanic lithosphere (Martin 1993; de Wit 1998) or by flake tectonics where oceanic crust was scraped off and stacked in collision zones (Hoffman and Ranalli 1988) while the lithospheric mantle was subducted (Davies 1992).

Zegers and van Keken (2001) proposed that the lower mafic crust could be within the eclogite stability field and might delaminate due to the much higher density (Fig. 16). Such delamination would result in upwelling asthenosphere that would provide heat to partially melt the lower amphibolitic crust and produce TTG melts.

Model 3) envisages mantle plume upwelling with anomalous hot asthenosphere to cause melting of thick oceanic plateaus as seen in Figure 17. This model is basically an extension of model 2), where thick oceanic crust is melted at the base by upwelling mantle, but in this case mantle plumes are the driving force.

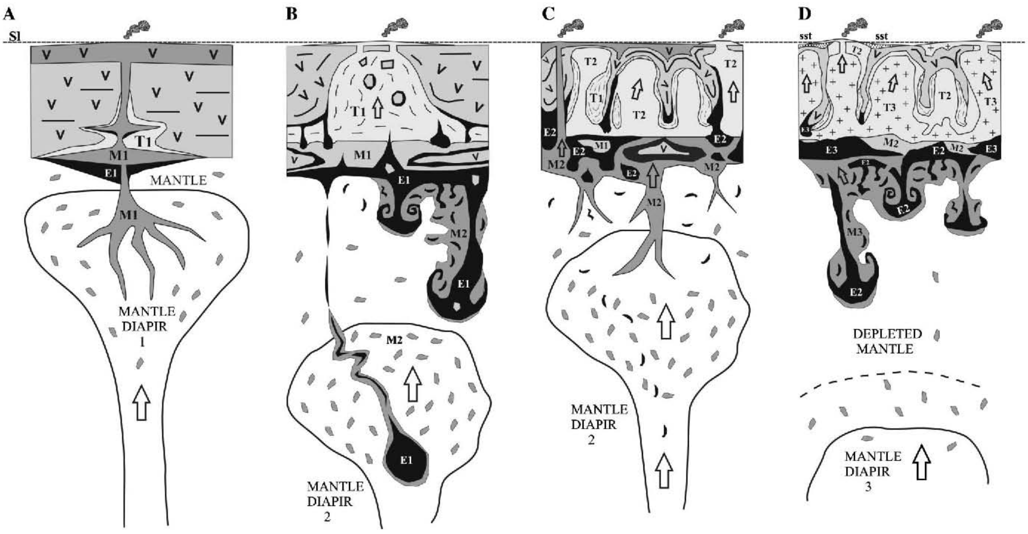

Figure 17. *Mantle plume cause melting of the base of an oceanic plateau and the restites delaminate into the mantle to cause further melt production (catalysis), which might explain the periodicity of the age populations often seen in TTG terranes (from Bédard 2006).*

Major mantle plumes or upwellings below oceanic plateaus could form TTG melts where repeated ascent of hot magma to the base of the oceanic plateau would cause partial melting, which would generate a differentiated crust by extraction of TTG magmas (Kröner 1991; Sandiford et al. 2004; Bédard 2006; Smithies et al. 2009). The internal structure of modern oceanic plateaus appears to be dominated by lavas, injected by increasing proportions of differentiated feeder dykes/sills towards their base (Saunders et al. 1996; Kerr et al. 1998). The arrival of a new plume beneath the established plateau could start a new cycle of primitive extrusive magmatism and partial melting at the base of the plateau (Smithies et al. 2009). Eclogite is dense and numerical, as well as, analogue models imply that such restites would be unstable and should delaminate and sink down into the mantle (Jull and Kelemen 2001; van Thienen et al. 2004). Such negative crustal restite diapirs could, depending on their size, move rapidly and might detach from the SCLM (Rudnick et al. 2000; van Thienen et al. 2004) to be recycled into deeper parts of the mantle, or could have mixed with the depleted mantle in the plume head. Such mixing could refertilise the mantle, allowing for further melting and the ascent of these melts to the base of the plateau could then trigger more crustal melting in the overlying plateau, generating a new generation of TTG melts (Bédard 2006). This ‘melt catalysis’ may occur because mantle melt productivity decreases when the easily fusible, high Ca-Al phases (e.g. garnet and clinopyroxene) are exhausted such that decompression-driven melting should tail off, possibly allowing for further melting if such phases are added (Bédard 2006).
This model is favoured for the formation of TTGs in the east Pilbara Craton as they are clearly related to plume activity (van Kranendonk et al. 2004).

To sum up the findings from the geochemical data presented in this report, we can relate them to the above models. There appears to be a spread in the data that is consistent with either variable melt fractions and/or fractional crystallisation processes. The source seem to be a heterogeneous mixture of both tholeiitic and calc-alkaline metavolcanic rocks resembling those found throughout the supracrustal belts in SW Greenland. This is consistent with the findings of Moyen (2011), who showed that a pure N-

MORB source would be too depleted to explain the TTG for a realistic range of melt fractions. The melt modelling show that the majority of the TTGs formed at low to intermediate pressures (8-16 kbar) without the presence of eclogitic residuum in the source and only few formed at a distinctly higher pressure (22 kbar).

The temporal correlation might represent one single thermal event and that the cooling of this system is reflected by decreasing melt fractions. Alternatively this trend could be related to ‘cratonisation’, so that processes of crystal fractionation and reworking of crust were more likely later in later stages of intrusions into the crust.

According to Hoffmann (2010) and Næraa (2011) the Hf isotopic data and trace elements of TTGs in SW Greenland are consistent with an early phase of melting at low to moderate pressures (5-15 kbar) of juvenile crust followed by later remelting at higher pressures (>15 kbar). This is consistent with the observation that our data mainly consists of low to moderate pressure melts and few high-pressure TTGs, which could reflect a growing/thickening craton.

In regard to the three models discussed above we can reject model 3) based on the fact that there is no evidence for plume-related volcanics in SW Greenland (Szilas et al. 2011) and strong evidence for horisontal tectonics and thrusting (Windley and Garde 2009). It is more difficult to distinguish model 1) and 2) as they would essentially result in magmas with similar compositions and characteristics.

In a recent model for Cordilleran orogenic systems Decelles et al. (2009) propose a model that contains elements from both model 1) and 2). They explain the cyclicity in magma production as a function of the build-up of eclogite restite from melting of the lower crust, which eventually delaminates and cause a period of compression and repeated restite build-up.

A similar process could be envisioned for the production of TTGs in the Archaean, if volcanic rocks were being accreted causing the base of this primarily mafic crust to melt to produce TTGs in a cyclic behaviour which is observed world wide for the crust formation (e.g. Stein and Hofmann 1994; Condie 1998; Kemp et al. 2006).

Conclusions

1. The TTG data from SW Greenland reported here are similar to those of TTG rocks found elsewhere in the North Atlantic Craton (Garde 1997) as well as global TTG data (Martin et al. 2005).
2. Our melt modelling suggests that the source composition for the TTGs in SW Greenland is a mixture of tholeiitic and calc-alkaline basaltic rocks in similar proportions as observed in the supracrustal belts of the region.
3. Our melt modelling further suggests that most TTGs mainly formed at pressures of 8-16 kbar and minor proportion at 22 kbar (Fig. 9).
4. Major element variation of the TTGs (Fig. 2) likely reflects melt derivation with variable melt fractions and possibly also involvement of fractional crystallisation, which would produce overlapping trends.
5. Trace element variation of the TTGs (Fig. 3) scatters considerably for the incompatible elements, although a slight positive correlation with SiO_2 is observed. We interpret this scatter to reflect a heterogeneous source consisting of both tholeiitic and calc-alkaline rocks. Compatible trace elements seem much less affected and follow expected trends related to melt fraction/fractionation.

6. Temporal correlation in the geochemical data (Fig. 14) suggests that ‘cratonisation’ or cooling during a single thermal event could be responsible for this covariance.
7. A likely model for the formation of TTGs in SW Greenland could involve a combination of subduction zone processes and delamination of eclogitic restites from the lower crust in a similar way as suggested for present Cordilleran orogenic systems (DeCelles et al. 2009).

Future work

Scientific work is in progress involving combined geochemical and geochronological work on the TTGs of SW Greenland to elucidate the petrogenetic processes in a temporal framework, and further to constrain the likely petrological model for the formation of TTGs in the Archaean.

Acknowledgements

We would like to acknowledge the Bureau of Minerals and Petroleum (BMP) for financial support of the field work and the analytical work. We would also like to thank Geocenter Danmark for funding of two PhD-projects at GEUS, which have contributed to this work.
Agnete Steenfelt is greatly acknowledged for reading through the draft version of this report, which helped to improve it.

References

Annen, C., Blundy, J.D. & Sparks, S.J. 2006: The genesis of intermediate and silicic magmas in deep crustal hot zones. Journal of petrology 47, 505-539.

Bea, F. 2010: Crystallization dynamics of granite magma chambers in the absence of regional stress: multiphysics modelling with natural examples. Journal of petrology 51, 1541-1569.

Bédard J.H. 2006: A catalytic delamination–driven model for coupled genesis of Archean crust and sub–continental lithospheric mantle. Geochim. Cosmochim Acta 70, 1188-1214.

Belousova, E.A., Kostitsyn, Y.A., Griffin, W.L., Begg, G.C., O’Reilly, S.Y. & Pearson, N.J. 2010: The growth of the continental crust: constraints from zircon Hf-isotopic data. Lithos 119, 457-466.

Boynton, W.V. 1984: Cosmochemistry of the rare earth elements: meteorite studies. In: Henderson, P. (Ed.), Rare Earth Element Geochemistry. Elsevier, Amsterdam, pp. 63–114.

Castillo, P.R. 2006: An overview of adakite petrogenesis. Chinese science bulletin 51, 257-268.

Condie K.C., 1998: Episodic continental growth and supercontinents: a mantle avalanche connection? Earth and planetary science letters 163, 97-108.

Condie K.C. 2005: TTGs and adakites: are they both slab melts? Lithos 80, 33–44.

Davies, G.F. 1992: On the emergence of plate tectonics. Geology 20, 963-966.

Davidson, J., Turner, S., Handley, H., Macpherson, C. & dosseto, A. 2007. Amphibole "sponge" in arc crust? Geology 35, 787-790.

de Wit, M.J. 1998: On Archean granites, greenstone, cratons and tectonics: does the evidence demand a verdict? Precambrian research 91, 181-226.

DeCelles, P.G., Ducea, M.N., Kapp, P. And Zandt, G. 2009: Cyclicity in Cordilleran orogenic systems. Nature geoscience 2, 251-257.

Defant M.J. & Drummond M.S. 1990: Derivation of some modern arc magmas by melting of young subducted lithosphere. Nature 347(6294), 662–665.

Drummond, M.S., Defant, M.J. & Kepezhinskas, P.K. 1996: Petrogenesis of slab-derived trondhjemite-tonalite-dacite/adakite magmas. Trans. R. Soc. Edinburgh-Earth Science 87, 205-215.

Foley S., Tiepolo M. & Vanucci R. 2002: Growth of early continental crust controlled by melting of amphibolite in subduction zones. Nature 417, 837–840.

Garde, A.A. 1997: Accretion and evolution of an Archaean high-grade grey gneiss – amphibolite complex: the Fiskefjord area, southern West Greenland. Geology of Greenland survey bulletin 177, 115 pp.

Green, T.H. & Pearson, N.J. 1986: Ti–rich accessory phase saturation in hydrous mafic-felsic compositions at high PT. Chemical geology 54, 185– 201.

Griffin, W.L., O'Reilly, S.Y., Afonso, J.C. & Begg, G.C. 2009: The composition and evolution of lithospheric mantle: A re-evaluation and its tectonic implications. Journal of Petrology 50, 1185-1204.

Griffin, W.L., O'Reilly, S.Y., Afonso, J.C. & Begg, G.C. 2010: The evolution and extent of Archean continental lithosphere: implications for tectonic models. In: Tyler, I.M and Knox-Robinson, C.M. 2010. Fifth international Archean symposium abstracts: geological survey of Western Australia, record 2010/18, 410 pp.

Hawkesworth, C.J. & Kemp, A.I.S. 2006: Evolution of the continental crust. Nature 443, 811-817.

Hawkesworth, C.J., Dhuime, B., Pietranik, A.B., Cawood, P.A., Kemp, A.I.S. & Storey, C.D. 2010: The generation and evolution of the continental crust. Journal of the Geological Society , London 167, 229-248.

Hoffman, P.F. & Ranalli, G. 1988: Archean oceanic flake tectonics. Geophysical research letters 15, 1077-1080.

Hoffmann, J.E. 2010: The development of the mantle-crust system in the early Archean. Unpublished PhD thesis, University of Bonn. 166 pp.

Jull, M. & Kelemen, P.B. 2001: On the conditions for lower crustal convective instability. Journal of Geophysical Research 106, 6423-6446.

Kerrich, R. & Polat, A. 2006: Archean greenstone-tonalite duality: Thermochemical mantle convection models or plate tectonics? Tectonophysics 415, 141-165.

Klemme, S., Blundy, J.D. & Wood, B.J. 2002: Experimental constraints on major and trace element partitioning during partial melting of eclogite. Geochimica et Cosmochima Acta 66, 3109-3123.

Kemp, A.I.S., Hawkesworth, C.J., Paterson, B.A. & Kinny, P. 2006: Episodic growth of the Gondwana supercontinent from hafnium and oxygen isotopes in zircon. Nature 439, 580-583.

Kemp, A.I.S., Hawkesworth, C.J., Foster, G.L., Paterson, B.A., Woodhead, J.D., Hergt, J.M., Gray, C.M. & Whitehouse, M.J. 2007: Magmatic and crustal differentiation history of granitic rocks from Hf-O isotopes in zircon. Science 315, 980-983.

Kerr, A.C., Tarney, J., Nivia, A., Marriner, G.F., Saunders, A.D., 1998: The internal structure of oceanic plateaus: inferences from obducted Cretaceous terranes in western Colombia and the Caribbean. Tectonophysics 292, 173–188.

Kokfelt T.F., Keulen, N. Næraa, T., Nilsson, M., Scherstén, A. Szilas, K. & Heijboer, T. 2011: Geochronological characterisation of the felsic rocks of the Archaean craton in South-West Greenland and southern West Greenland, 61°30′ - 64°N, Geological survey of Denmark and Greenland report 2011/12.

Kröner, A. 1991: Tectonic evolution in Archaean and Proterozoic. Tectonophysics 187, 393-410.

Martin, H. 1986: Effect of streeper Archean geothermal gradient on geochemistry of subduction–zone magmas. Geology 14, 753–756.

Martin, H. 1993: The mechanisms of petrogenesis of the Archaean continental crust – Comparison with modern processes. Lithos 30, 373–388.

Martin, H. 1999: Adakitic magmas: modern analogues of Archaean granitoids. Lithos 46, 411–429.

Martin, H. & Moyen, J.-F. 2002: Secular changes in TTG composition as markers of the progressive cooling of the Earth. Geology 30, 319–322.

Martin, H. & Moyen, J.-F. 2005: The Archaean-proterozoic transition: sanukitoid and closepet type magmatism. Mineralogical society of Poland special papers 26, 57-68.

Martin, H., Smithies, R.H., Rapp, R., Moyen, J.-F. & Champion, D. 2005: An overview of adakite, tonalite-trondhjemite-granodiorite (TTG) and sanukitoid: relationships and some implications for crustal evolution. Lithos 79, 1-24.

Moyen J.-F. & Stevens G. 2006: Experimental constraints on TTG petrogenesis: Implications for Archean geodynamics. In: Archean geodynamics and environments (eds. K. Benn, J.-C. Mareschall & K.C. Condie). American Geophysical Monograph 164, 149–175.

Moyen J.-F. 2011: The composite Archaean grey gneisses: Petrological significance, and evidence for a non-unique tectonic setting for Archaean crustal growth. Lithos (in press).

Muehlenbachs, K., 1986: Alteration of the oceanic crust and the 180 history of seawater. In: Stable Isotopes in High Temperature Geological Processes. Valley, J.W. et al., 1986. Rev. Mineral. 16, pp. 425-444

Næraa, T. 2011: Zircon U/Pb, Hf and O isotope systematics from the Archaean basement in the Nuuk region, southern West Greenland - Constrains on the early evolution of the continental crust. Unpublished PhD thesis. Geological Museum of Copenhagen. 205 pp.

O'Connor, J. T. 1965: A classification for quartz-rich igneous rocks based on feldspar ratios. In: US Geological Survey Professional Paper B525. USGS, 79-84.

Pearce, J.A., Harris, N.W. & Tindle, A.G. 1984: Trace element discrimination diagrams for the tectonic interpretation of granitic rocks. Journal of petrology 25, 956-983.

Pearce, J.A. 2008: Geochemical fingerprinting of oceanic basalts with applications to ophiolite classification and the search for Archean oceanic crust. Lithos 100, 14-48.

Pearson, D.G., 1999: The age of continental roots. Lithos 48, 171-194.

Pearson, D.G., Carlson, R.W., Shirey, S.B., Boyd, F.R. & Nixon, P.H., 1995: Stabilisation of Archaean lithospheric mantle: a Re-Os isotope study of peridotite xenoliths from the kaapvaal craton. Earth and planetary science letters 134, 341-357.

Petford, N., & Atherton, M., 1996: Na-rich partial melts from newly underplated basaltic crust: The Cordillera Blanca batholith, Peru. Journal of petrology 37, 1491-1521.

Rapp, R.P. & Watson, E.B. 1995: Dehydration melting of metabasalt at 8-32 kbar: Implications for continental growth and crust–mantle recycling. Journal of petrology 36, 891-931.

Rapp, R.P., Watson, E.B. & Miller, C.F. 1991: Partial melting of amphibolite/eclogite and the origin of Archean trondhjemites and tonalites. Precambrian research 51, 1-25.

Rapp, R.P., Shimizu, N. & Norman, M.D. 2003: Growth of continental crust by partial melting of eclogite. Nature 425, 605–609.

Rapp, R.P., Norman, M.D., Laporte, D.,Yaxley, G.M., Martin, H. & Foley, S.F. 2010: Continent Formation in the Archean and Chemical Evolution of the Cratonic Lithosphere: Melt-Rock Reaction Experiments at 3–4 GPa and Petrogenesis of Archean Mg-Diorites (Sanukitoids). Journal of petrology 51, 1237-1266.

Rudnick, R.L., Barth, M., Horn, I. & McDonough, W.F. 2000: Rutile-bearing refractory eclogites: missin link between continents and depleted mantle. Science 287, 278-281.

Rollinson, H.R. 1997: Eclogite xenoliths in West African kimberlites as residues from Archaean granitoid crust formation. Nature 389, 173-176.

Rollinson, H. 2008: Secular evolution of the continental crust: Implications for crust evolution models. Geochemistry Geophysics Geosystems 9, 14 pp.

Rollinson, H. 2010: Coupled evolution of Archean continental crust and subcontinental lithospheric mantle. Geology 38, no. 12, 1083-1086.

Sandiford, M., van Kranendonk, M. & Bodorkos, S. 2004: Conductive incubation and the origin of granite-greenstone dome and keel structure: the eastern Pilbara Craton, Australia. Tectonics 23.

Saunders, A.D., Tarney, J., Kerr, A.C., Kent, R.W., 1996: The formation and fate of large oceanic igneous provinces. Lithos 37, 81-95.

Shaw, D.M. 1970: Trace element fractionation during anatexis. Geochim. Cosmochim. Acta 34, 237–243.

Smithies, R.H., Champion, D.C., van Kranendonk, M.J., Howard, H.M. & Hickman, A.H. 2005: Modern-style subduction processes in the Mesoarchaean: geochemical evidence from the 3.12 Ga Whundo intra-oceanic arc. Earth and planetary science letters 231, 211-237.

Smithies, R.H., Champion, D.C. & Van Kranendonk, M.J. 2009: Formation of Palaeoarchean crust through infracrustal melting of enriched basalt. Earth and Planetary Science Letters 281, 298-306.

Springer, W. & Seck, H.A. 1997: Partial fusion of basic granulites at 5 to 15 kbar: implications for the origin of TTG magmas. Contributions to Mineralogy and Petrology 127, 30-45.

Staudigel, H., Davies, G.R., Stanley, R.H., Marchant, K.M. & Smith, B.M. 1995: Large scale isotopic Sr, Nd and O isotopic anatomy of altered oceanic crust: DSDP/ODP sites 417/418 Earth and Planetary Science Letters 130, 169-185.

Steenfelt, A., Garde, A.A. & Moyen, J.–F. 2005: Mantle wedge involvement in the petrogenesis of Archaean grey gneisses in Wes Greenland. Lithos 79, 207-228.

Stein, M. & Hofmann, A.W. 1994: Mantle plumes and episodic crustal growth. Nature 372, 63-68.

Sun, S. & McDonough, W.F. 1989: Chemical and Isotopic Systematics of oceanic basalts: implications for Mantle Composition and Processes. In A.D. Saunders & M.J. Norry (eds.) Magmatism in the Ocean Basins, Spec. Publ. Vol. Geol. Soc. Lond. , No. 42, 313-345.

Szilas, K., Kokfelt, T.F. & Scherstén, A. 2011: Geochemistry of Archaean supracrustals rocks in SW Greenland. Geological survey of Denmark and Greenland. Report 2011/10

Tate, M.C. & Johnson, S.E. 2000: Origins of voluminous tonalite in the Méxican Peninsular Ranges and other Cordilleran batholiths. Journal of Geology 108, 721-728.

van Hunen, J., van Keken, P.E., Hynes, A., & Davies, G.F., 2008: Tectonics of early Earth: Some geodynamic considerations. In Condie, K.C., & Pease, V., (eds.): When Did Plate Tectonics Begin on Planet Earth? Geological Society of America Special Paper 440, 157-171.

van Kranendonk, M.J., Collins, W.J., Hickman, A. & Pawley, M.J. 2004: Critical tests of vertical vs. horizontal tectonic models for the Archaean East Pilbara granite-greenstone terrane, Pilbara Craton, Western Australia. Precambrian Research 131, 173-211.

van Thienen, P., van den Berg, A.P. & Vlaar, N.J. 2004: Production and recycling of oceanic crust in the early Earth. Tectonophysics 386, 41-65.

Whalen, J.B., Percival, J.A., McNicoll, V.J. & Longstaffe, F.J. 2002: A mainly crustal origin for tonalitic granitoid rocks, Superior Province, Canada: implications for Late Archean tectomagmatic processes. Journal of petrology 43, 1551-1570.

Willbold, M., Hegner, E., Stracke, A. & Rocholl, A. 2009: Continental geochemical signatures in dacites from Iceland and implications for models of early Archaean crust formation. Earth and Planetary Science Letters 279, 44-52.

Windley, B.F. 1984. The evolving continents. Wiley, 399 pp.

Windley, B.F. & Garde, A.A. 2009: Arc-generated blocks with crustal sections in the North Atlantic craton of West Greenland: Crustal growth in the Archean with modern analogues. Earth-Science reviews 93, 1-30.

Wyman, D.A., O'Neill, C. & Ayer, J.A., 2008: Evidence for Modern-Style Subduction to 3.1 Ga: A Plateau-Adakite-Gold (Diamond) Association. GSA Special Paper 440, When Did Plate Tectonics Begin on Planet Earth? (ed. Condie, K.C. & Pease, V.), 129-148.

Xiong, X.L., Adam, J. & Green, T.H. 2005: Rutile stability and rutile/melt HFSE partitioning during partial melting of hydrous basalt: Implications for TTG genesis. Chemical Geology 218, 339–359.

Zegers, T.E. & van Keken, P.E. 2001: Middle Archaean continent formation by crustal delamination. Geology 29, 1083-1086.

Residues in a TTG area and their metamorphic overprint

Alfons Berger (1), Thomas F. Kokfelt (2), Martin B. Klausen (3)

(1) Department of Geography and Geology, University of Copenhagen, Øster Voldgade 10, 1350 Copenhagen K, Denmark.(Ab@geo.ku.dk), (2) Geological Survey of Denmark and Greenland (GEUS), Øster Voldgade 10, 1350 Copenhagen K, Denmark (tfk@geus.dk), (3) Department of Earth Sciences, University of Stellenbosch, Private Bag X1, Matieland 7602, South Africa (klausen@sun.ac.za)

Introduction

The genesis of the large volumes of TTG (tonalite–trondhjemite–granodiorite) magmas is still a matter of debate (e.g., Martin & Moyen 2002, Clemens et al. 2006). Therefore, the potential investigation of relics from the magmatic evolution will give insights in the process of production and modification of these magmas. In several TTG areas, different sized bodies of ultramafic and mafic rocks are common. One group of relics can easily be identified as former crustal rocks (often available as amphibolites with calc-silicates and/or schists). In addition, other mafic and ultramafic bodies have primary magmatic origin related to fractionation processes or pieces of incorporated mantle. In any case, the combination of mafic/ultramafic lenses in a quartzofeldspatic matrix leads often to metasomatic zones. These may introduce problems for the reconstructing the magmatic evolutions using the compositions of the mafic and ultramafic rocks. Such metasomatic zones are well investigated in terms of so-called “blackwalls” (e.g., Sanford 1981, Barnes et al. 2002, Miller et al. 2009). Most blackwalls are related to serpentine and/or chlorite rich cores of mafic/ultramafic lenses. The dehydration of these minerals allows the mass transport required for metasomatic changes and the related development of the blackwalls. However, original water poor ultramafic lenses show only minor metasomatic exchange. Such lenses are common in fractionated plutonic rocks. The distinction between the chemical signatures originating from magmatic differentiation versus metasomatic processes is a key-issue; here we investigate chemical variations in such bodies to address the issue of in situ melt extraction and the production and evolution of TTG magmas. In addition, the mineralogical studies of such rims around ultramafic bodies can be complicated by second metamorphic overprint. The potential metamorphic overprint in such areas can be described as metamorphism related to repeated intrusion of the TTG magmas into a given area. In such field areas, deformation and metamorphic overprint of the slightly older plutonic rocks are common, but also relics and small scale intrusion relationships can be preserved.

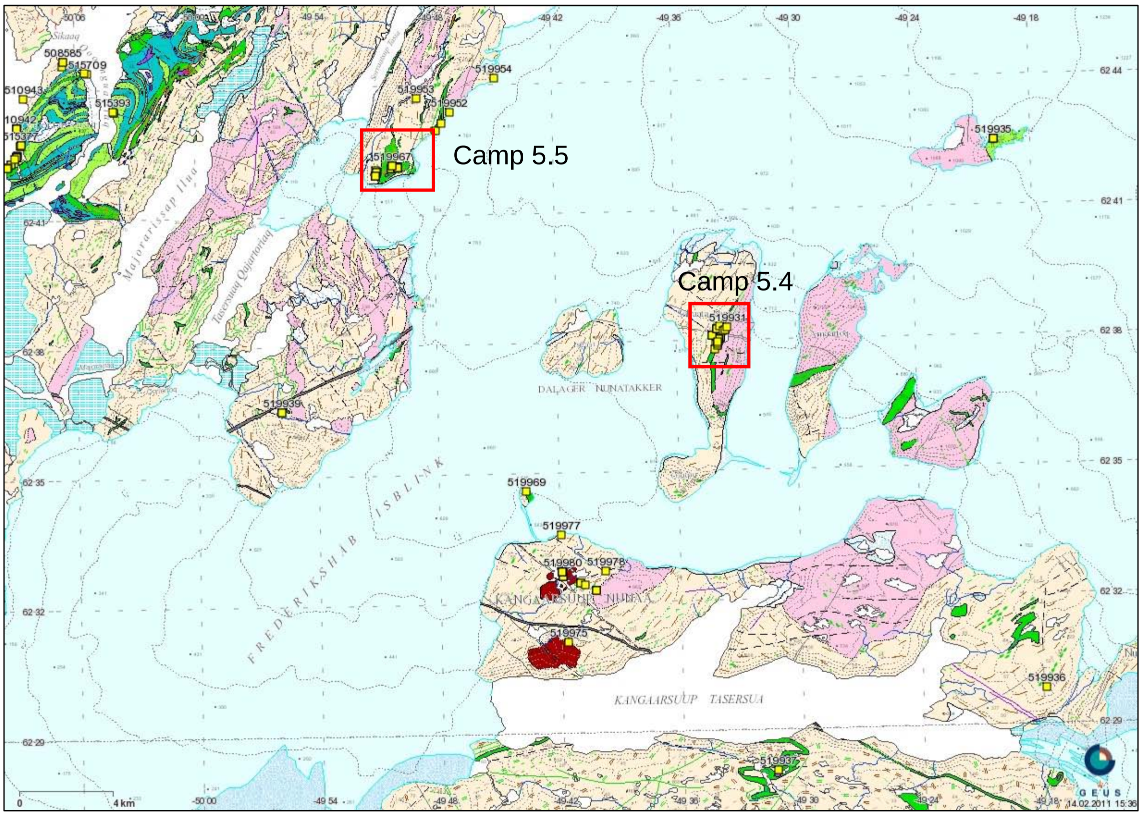

Figure 1. *Geological map of the Frederikshåb Isblink area, including Dalager's Nunatakker. The main study areas are Saliaata Nunaa (camp 5.4) and south-west of Sorraatsup Tasia (camp 5.5). Sample locations are indicated (yellow squares).*

The selected example is located around Frederikshåb Isblink, which was investigated from two camps in summer 2010 (Fig. 1). The TTG's have a metamorphic overprinting as documented in local migmatitic structures and recrystallisation of the rock forming minerals inside the TTG gneisses. In addition, the role of mass transfer during this metamorphism by metasomatic processes or partial melting is unclear.

Field relations and sample description

The area is characterized by migmatitic TTG gneisses. These show different amounts and sizes of leucosomes and different intensities of foliation development. The structural evolution includes folding and developed different type of shear zones (e.g., Keulen et al. 2009, Windley and Garde 2009). In addition, the area contains two different types of lenses and bands: (1) amphibolites with minor amount of metasediments (often calc-silicates); and (2) ultramafic bodies. In the latter group, hornblendites are the main rock type, but peridotitic compositions also occur. The ultramafic bodies are often lens-shaped with diameters between several decimetres to several tens of meters (Fig. 2). Some of these bodies are layered and their composition varies from more peridotitic (pyroxene and olivine) towards hornblendites (Fig. 3). In addition, different local interaction zones occur, which include veins of former melt and potential metasomatism. Sample 519906 represents such a migmatite, including small scale restitic composition and leucosomes in the cm scale. This sample differs from the granitoid migmatites of the TTG areas in general, because it is located inside an amphibolite body. Sample 519914 represents a metasomatically overprinted rock, which is taken from a ~1.5 meter sized irregular, ultrabasic body. The surrounded ultramafic rock contains pyroxenes that are partly replaced by amphiboles. In the metasomatic sample, minor amounts of K-feldspar have been detected and sphene is a common phase. The main rock forming minerals are epidote and chlorite. The epidotes are characterized by symplectitic intergrowth with quartz.

Figure 2. *Lenses of ultrabasic bodies inside TTG gneiss. Example from the area directly north of Frederikshåb Isblink.*

Figure 3. *Layering inside an ultramafic body and layer parallel intrusion of more evolved melts (TTG-type melts).*

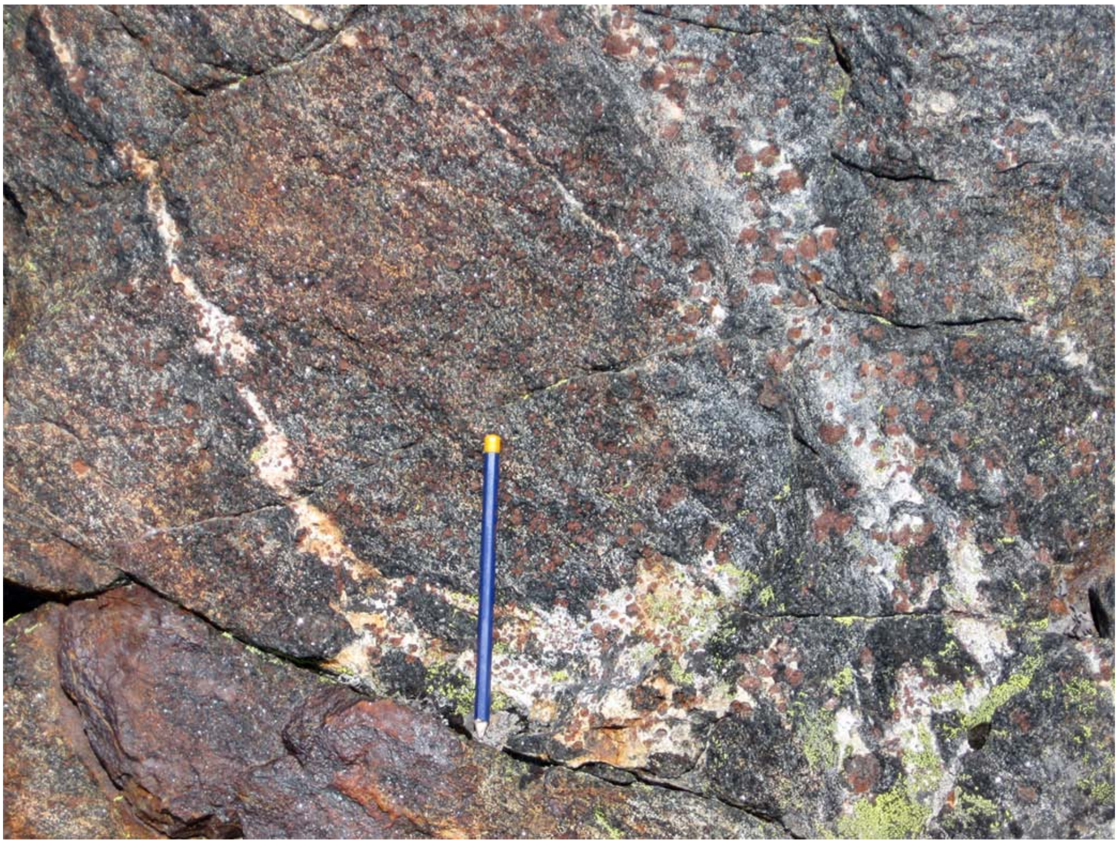

Figure 4. *Garnet amphibolite with local leucosomes.*

The most common mafic rocks are amphibolites. They contain hornblende and plagioclase as the rock forming minerals, but also garnet-bearing layers occur (Fig. 4). The garnet-bearing layers may help to estimate P/T conditions for the metamorphic overprinting event.

Methods

We analyzed whole rocks in Stellenbosch using standard XRF technique on glass pellets for the major elements. Trace elements are analysed with LA-ICPMS techniques (see Appendix for more details). Mineral chemistry data are measured on a JEOL JXA 8200 superprobe at the University of Copenhagen. Minerals are measured at 15 kV and 15 nA using natural and synthetic standards.

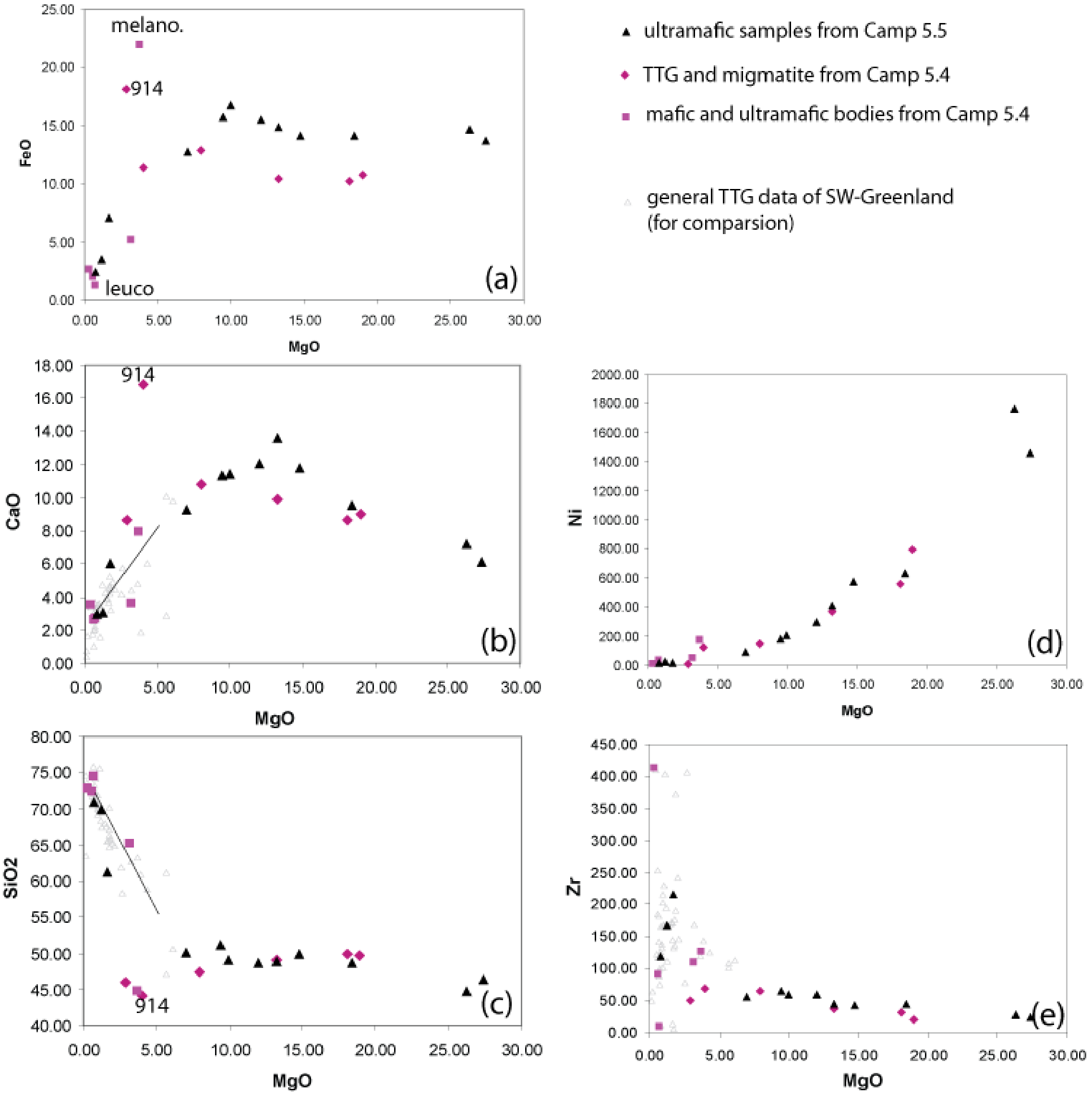

Figure 5. *Geochemical co-variation diagrams for major and trace elements. Major elements in wt%, trace elements in p.p.m.. (a) FeO versus MgO. (b) MgO versus CaO; (c) MgO versus SiO$_2$; (d) MgO versus Ni; (e) MgO versus Zr. leuco = leucosome and melano.= melanosome of sample* 519906. *914 refer to sample 519914 the metasomatic sample. Note the deviation from the fractionation trend of this sample.*

Bulk rock chemistry

The different samples are collected with two aims: (1) discussing possible mass transfer during metasomatism; and (2) investigate magmatic processes related to the origin of TTG. The main parts of the mafic to ultramafic samples show correlations between CaO-MgO. They have similar SiO_2 contents at highly variable MgO contents (Fig. 5). The MgO have a positive correlation with most transition metals (e.g., Ni, V, Cr) as expected for magmatic evolutions (Fig. 5). The constant SiO_2 content excludes a classical metasomatic origin for most of the investigated rocks, because the differences in chemical potential for Si is large and drives most of the metasomatism in blackwalls (Sanford 1982). With the exception of the migmatite sample (519906) and the metasomatic sample (519914), the other samples can be investigated as metamorphic overprinted magmatic rocks.

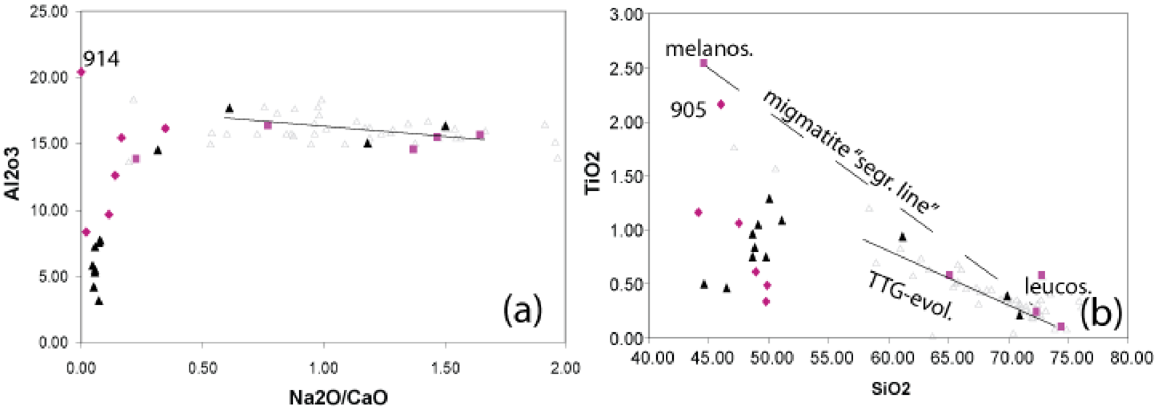

Figure 6. *(a) Correlation diagram of Al_2O_3 versus Na_2O/CaO. (b) Correlation diagram of SiO_2 versus TiO_2. All concentrations in wt%, symbols as in figure 5.*

The TTG gneisses, away from any ultramafic bodies, show only a small spread of fractionation (Fig. 6). This is biased by the sampling. However, most TTG areas show a larger spread in composition (e.g., Martin et al. 2005), which fall in the range between 55 and 75 wt% SiO_2 (Martin et al. 2005; Clemens et al. 2010). The general trend of the measured TTG fits also with larger evolution of the samples in SW Greenland (small grey triangles in Figs. 5 and 6). The REE pattern of the different samples can be clearly grouped in the ultramafic bodies and the TTG, but the two chemically altered samples (519914, 519906) differ clearly (Figs. 5, 6 and 7). These compositions cannot be explained as mixing lines between these two rock groups. The metasomatic sample and the migmatite differ besides the major and trace elements, also in their REE pattern (Fig. 7; see discussion below).

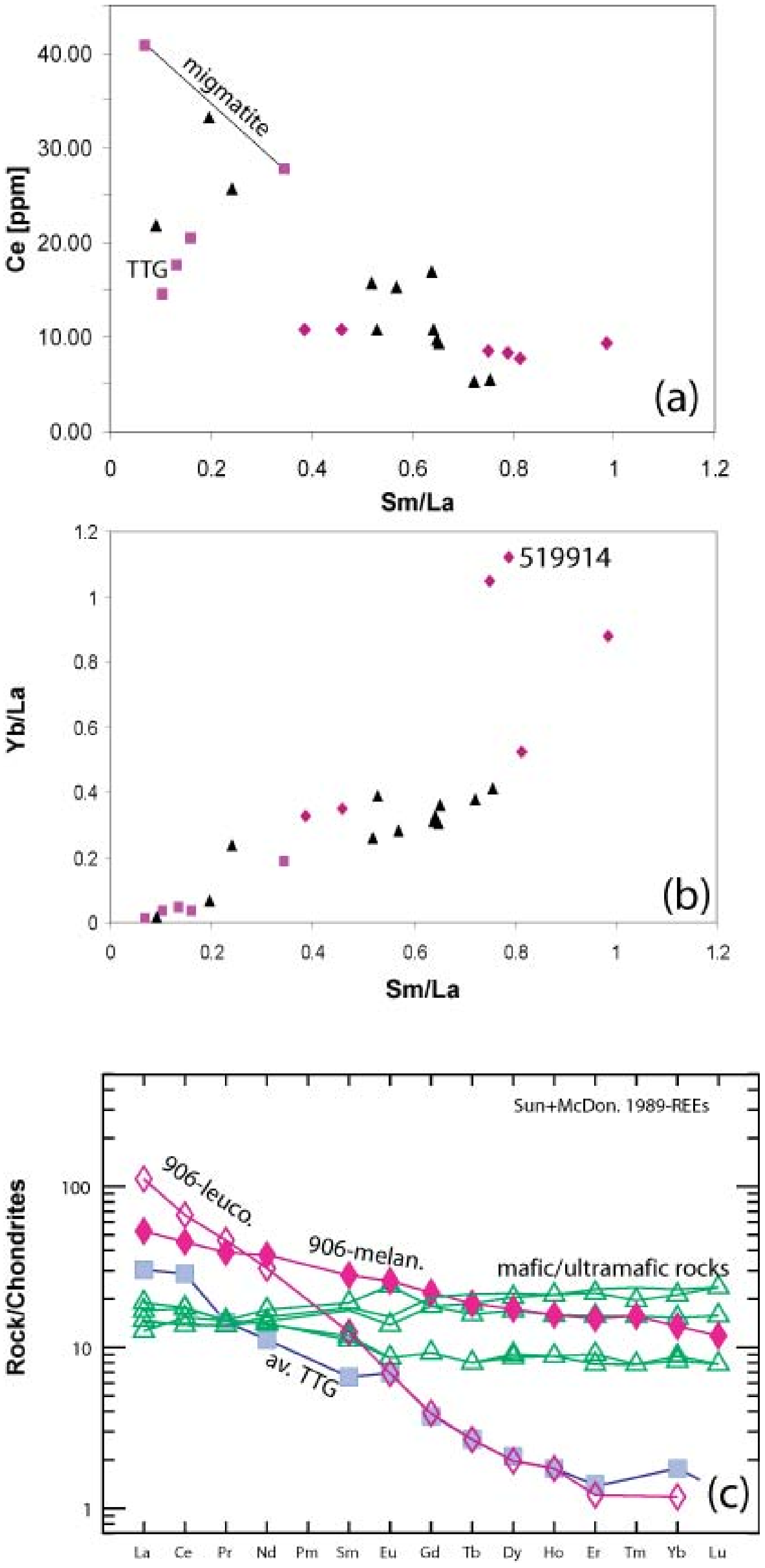

Figure 7. *Presentation of the evolution of the REE. Symbols as in figure 5. (a) Ce versus Sm/La. (b) Yb/La versus Sm/La; (c) REE spider diagram after Sun and McDonald (1989).*

Magmatic evolution

The pyroxene rich rocks and the hornblendites have textural and geochemical characteristics to be part of the magmatic evolution. The TiO_2, Al_2O_3 and Ni content exclude the peridotite bodies as relics from mantle. The geochemical data and the textural data indicate relics of residues as developed in layered intrusions (Fig. 4). The major elements evolution indicates a calc-alkaline type of fractionation (e.g., correlation diagrams MgO versus CaO, Al_2O_3 versus Na_2O/CaO). Some of the ultrabasic rocks represent the residue, whereas some of the metagabbros and amphibolites are part of the intermediate position along fractionation lines. The main (and often investigated) fractionation of the TTG series itself is not covered in this data set. Combining the data from the TTG in a larger area of SW Greenland and the ultramafic bodies, the ultramafic rocks can serve as residues of the magmatic process. This can further constrains by the REE concentrations and patterns. The high SiO_2 TTG shows the LREE enriched pattern. In contrast, the hornblendite show the slightly HREE-enriched pattern (Fig. 7). The mafic rocks have flat chondrite-normalised REE patterns or slightly enriched in the LREE. This indicates that the hornblendites are the residue from a mafic parent melt towards LREE enriched TTG (Fig. 7). The evolution of different fractionation can be best illustrated in Ce versus Sm/La diagram, illustrating the change in REE pattern as well as in concentration (Fig. 7a). The migmatite differ from this trend and is not part of the magmatic evolution. These differences may be related to the major occurrence of REE-dominated accessory phases in REE enriched systems (i.e. monazite, allanite).

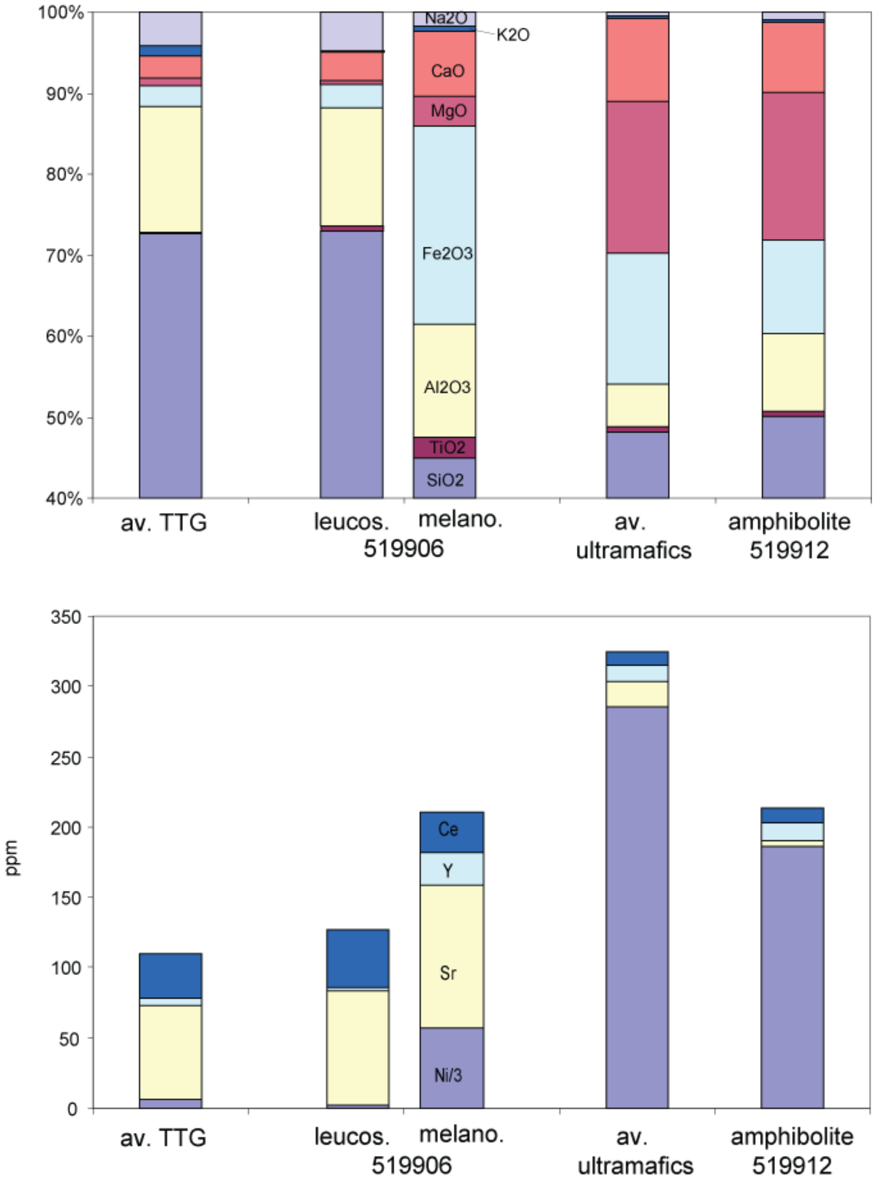

Figure 8. *Normalized bulk rock chemistry of selected samples. Colour coding is shown inside the column of sample 519906 (a) major elements in wt% oxides normalized to 100% (b) selected trace elements. Note the similarity between the leucosome of the migmatite and the average TTG and the difference between the melanosome and the average ultrabasic rocks.*

Metamorphic evolution

The migmatites of the area include possible local partial melting of the amphibolites and/or intrusions of the TTG melts. The leucosome of the migmatite sample fits the composition of the surrounded TTG in major and trace elements (Fig. 8). However, the melanosome differ from the ultramafic and mafic rocks in the surroundings. The different Mg# (= MgO/(MgO+FeO^{tot})) between the melanosome and the larger rock bodies indicate a different processes for the genesis of these two rock types, but Mg# are similar between leucosome and melanosome. A similar Mg# between segregated melt and local residues is known from migmatites near the solidus (e.g. Stevens et al. 1997). This would also explain the different trace elements and TiO_2 content between the melanosome and the ultramafic bodies (Fig. 6 and 7). The REE patterns of the ultramafic bodies differ also from the melanosome. The geochemical characteristics indicate different origins for the melanosome in comparison to the frequent occurring mafic/ultramafic lenses. One explanation for the chemical signature of these melanosome is local partial melting of the amphibolites, which has been introduced by water influx (see below). Another mafic sample has the same chemical characteristic, which is not taken from a migmatite directly (sample 519905; e.g. Fig. 6b). This indicate, this overprint process occur locally at different positions and may not always be easy to recognize in the field. Partial melting at water saturated conditions is possible for tonalites or amphibolites between 650°C and 700°C at intermediate pressures (see summary in Moyen and Stevens 2006). These conditions are consistent with the metamorphic assemblage of the garnet amphibolites. However, the local preserved mafic migmatite did not represent an analogue to the production of the TTG of the area. It occurs during the metamorphic overprint of the area, which is also responsible for the migmatite structure of the TTG in general.

The garnet amphibolite contains no quartz and has typical amphibolite composition. In a basaltic composition the minimum pressures to stabilize garnet is in the range of 8 kbar (Moyen & Stevens 2006). The garnets of the garnet-amphibolite are almandine-rich garnets with X_{Pyrope} ~0.06 and $X_{Grossular}$ of ~0.25. These garnets coexist with a hornblende containing 12.8 wt% Al_2O_3 and ~1.7 wt% Na_2O (Table 1). The garnets are nearly unzoned as the hornblende. The composition indicate metamorphic equilibration in the garnet-amphibolite facies.

Conclusions

The geochemical study of ultramafic lenses and their alteration zone indicate that some of these bodies related to primary magmatic fractionation processes. The ultramafic bodies can be interpreted as residues of a fractionation processes. This would coincidence with REE pattern and REE concentrations. The melt contain the LREE, whereas the HREE are slightly enriched in the ultramafic bodies. Magmatic fractionation alone cannot explain all measured compositions and additional processes are necessary to understand the evolution of the TTG magmas (e.g., Clemens et al. 2010).

In addition, all rocks are overprinted by metamorphic processes, which include metasomatism and partial melting. The role of partial melting is restricted to small areas, where water saturated conditions meets temperatures around 700°C. Except for the special locations of partial melting or metasomatic exchange, the ultramafic bodies will give insights in the magmatic evolution of the TTG.

Table 1: Mineral chemistry of sample 519905.

mineral	Hbl	Hbl	Hbl	Hbl	Hbl	Hbl	Grt	Grt	Grt	Grt
SiO_2	39.81	39.74	39.95	40.09	39.70	40.13	38.05	37.59	36.75	38.10
TiO_2	0.31	0.47	0.53	0.56	0.50	0.52	bdl	bdl	bdl	bdl
Al_2O_3	13.51	12.80	12.73	12.83	12.66	12.60	20.95	20.49	20.76	20.32
Fe_2O_3	3.24	2.43	2.17	2.50	2.27	2.63	1.01	1.51	1.98	1.47
FeO	22.65	22.71	23.12	22.81	22.67	23.03	28.82	28.38	27.29	29.07
MnO	0.18	0.14	0.28	0.13	0.25	0.30	2.02	1.87	1.89	1.66
MgO	4.65	4.76	4.65	4.80	4.65	4.80	1.65	1.53	1.52	1.56
CaO	11.32	11.45	11.35	11.62	11.45	11.35	9.17	9.31	9.33	9.40
Na_2O	1.67	1.77	1.72	1.71	1.67	1.76				
K_2O	1.03	1.03	1.06	1.08	1.09	1.03				
H_2O	1.93	1.91	1.91	1.93	1.90	1.92				
Total	100.33	99.20	99.47	100.06	98.82	100.08	101.74	100.71	99.54	101.67
Si	6.183	6.243	6.266	6.244	6.263	6.258	2.995	2.993	2.957	3.008
Ti	0.036	0.055	0.063	0.066	0.059	0.061	0.004	0.001	0.000	0.004
Al	2.473	2.370	2.353	2.356	2.354	2.316	1.943	1.923	1.969	1.891
Fe^{3+}	0.379	0.287	0.256	0.293	0.270	0.309	0.060	0.091	0.120	0.088
Fe^{2+}	2.942	2.983	3.032	2.971	2.991	3.004	1.896	1.889	1.836	1.919
Mn	0.024	0.019	0.037	0.017	0.033	0.040	0.135	0.126	0.129	0.111
Mg	1.076	1.115	1.087	1.114	1.093	1.116	0.194	0.181	0.182	0.184
Ca	1.884	1.927	1.907	1.939	1.935	1.896	0.773	0.794	0.804	0.795
Na	0.503	0.539	0.523	0.516	0.511	0.532				
K	0.204	0.206	0.212	0.215	0.220	0.204				
H	2.000	2.000	2.000	2.000	2.000	2.000				
X Pyrope							0.06	0.06	0.06	0.06
X Almandine							0.61	0.60	0.57	0.60
X Grossular							0.25	0.25	0.25	0.25
X Spessartine							0.04	0.04	0.04	0.03

References

Barnes, J. D., Selverstone, J., and Sharp, Z. D. (2004) Interactions between serpentinite devolatilization, metasomatism and strike-slip strain localization during deep-crustal shearing in the Eastern Alps J. metamorphic Geol., 22, 283–300.

Clemens, J., Yearron, L.M. Stevens, G. (2006) Barberton (South Africa) TTG magmas: Geochemical and experimental constraints on source-rock petrology, pressure of formation and tectonic setting Precambrian Geology, 151, 53-78.

Clemens, J.D. Belcher, R., Kisters, A.F.M. (2010) The Heerenveen Batholith, Barberton Mountain Land, South Africa: Mesoarchaean, Potassic, Felsic Magmas Formed by Melting of an Ancient Subduction Complex Journal of Petrology 51, 1099-1120.

Keulen, N., Scherstén, A., Schumacher, J.C., Næraa, T. & Windley, B.F., (2009) Geological observations in the southern West Greenland basement from Ameralik to Frederikshåb Isblink in 2008. Bulletin of the Geological Survey of Denmark and Greenland 17, 49–52.

Martin, H., Moyen, J.-F., (2002) Secular changes in TTG composition as markers of the progressive cooling of the Earth. Geology 30 (4), 319– 322.

Martin, H., Smithies, R.H. Rapp, R., Moyen, J.-F. Champion, D., (2005) An overview of adakite, tonalite–trondhjemite–granodiorite (TTG), and sanukitoid: relationships and some implications for crustal evolution. Lithos 79 1 – 24.

Miller, D. Marschall, H., Schumacher, J.C. (2009) Metasomatic formation and petrology of blueschist-facies hybrid rocks from Syros (Greece): Implications for reactions at the slab–mantle interface. Lithos 107 53–67.

Moyen, J.-F. and Stevens, G. (2006) Experiemental constrains on TTG Petrogenesis: Implicaitons for Archean Geodynamiccs. Physical monograph 164. 149-175.

Sanford, R.F., 1982. Growth of ultramafic reaction zones in greenschist to amphibolite facies metamorphism. American Journal of Science 282, 543–616.

Stevens, G., Clemens. J.D. and Droop. G.T.R. (1997) Melt production during granulite facies anatexis: experimental data from primitive protoliths. Contrib. Mineral. Petrol. 128, 352-370.

Sun, S.S., McDonough, W.F., (1989) Chemical and isotopic systematics of oceanic basalts: implications for mantle composition and process. In: Saunders, A.D., Norry M.J. (Eds.), Magmatism in the ocean basins, Geological Society Special Publication 42, 313–345.

Windley, B.F. & Garde, A.A., (2009) Arc-generated blocks with crustal sections in the North Atlantic craton of West Greenland: Crustal growth in the Archean with modern analogues. Earth Science Reviews 93, 1-30.

Acknowledgements

We like to thank the persons working in the GEUS laboratories that helped with preparing the samples for chemical analysis; Fiorella Aquilera, Mozgan Alaei, Jørgen Kystol and Michael Nielsen, as well as several students at GEUS.

The technical employees the University of Stellenbosch are thanked for conducting a great job in running the rock samples through the laboratories.

Agnete Steenfelt is greatly acknowledged for careful reading through the draft version of this report, which helped to improve it.

Appendices

A. Analytical methods and data quality

A.1. Major and trace elements analysed at Stellenbosch University

Major element compositions have been obtained by XRF analysis on La-free glass beads (Phillip's PW1404w at Stellenbosch University). *Fluorescence (XRF).* The instrument used is an Axios from PANalytical with a 2.4kW Rh X-ray tube. The gas-flow proportional counting detector and scintillation detector, or a combination of the two, are used to cover the elements fluorine to uranium. Major elements (Na_2O, MgO, SiO_2, K_2O, CaO, TiO_2, MnO, P_2O_5, Al_2O_3, Cr_2O_3 and Fe_2O_3T (total iron) are analyzed on fused glass beads. A wide range of international (NIST®) and national (SARM®) standards are used in the calibration procedures and quality control (precision and accuracy) for both major and trace element analyses. Detection limits for the elements quoted, depending on the matrix (combination of elements present), are approximately 0.5 ppm for trace elements on a pressed pellet and approximately 0.001 wt% for major elements on a fused bead.

Fusion bead method for Major element analysis:

- Weigh 1.0000g ± 0.0009g of milled sample
- Place in oven at 110 ºC for 1 hour to determine H_2O^-
- Place in oven at 1000 ºC for 1 hour to determine LOI (loss on ignition)
- Add 10.0000g ± 0.0009g Claisse flux and fuse in M4 Claisse fluxer for 23 minutes.

The loss on ignition (LOI) comprises contributions from the volatile compounds H_2O+, OH-, CO_2, F, Cl, S; and added O_2 due to oxidation, mainly of FeO to Fe_2O_3.

The following standard reference materials were used: NIM-N, -G, -S, -P, -D; AGV-1; BHVO-1; GA; GH; GSN; SY-2, -3; BCR.

Detection limits and uncertainties:

Analyte	Al_2O_3	CaO	Fe_2O_3	MgO	MnO	P_2O_5	K_2O	SiO_2	Na_2O	TiO_2	LOI
Uncertainty	0.11688	0.07288	0.14672	0.02416	0.00904	0.00364	0.0172	0.3506	0.10448	0.02096	0.03
Units	Wt%	Wt%	Wt%	Wt%	Wt%	Wt%	Wt%	Wt%	Wt%	Wt%	Wt%
LOD	0.06	0.04	0.01	0.04	0.01	0.01	0.01	0.03	0.01	0.02	0.01
Units	Wt%	Wt%	Wt%	Wt%	Wt%	Wt%	Wt%	Wt%	Wt%	Wt%	Wt%

Table A.1. *Tests for maximum contamination during sample processing*

Sample	Al2O3	CaO	Cr2O3	Fe2O3	K2O	MgO	MnO	Na2O	P2O5	SiO2	TiO2	Sum
Unit	(wt%)	(wt%)	(wt%)	(wt%)	(wt%)	(wt%)	(wt%)	(wt%)	(wt%)	(wt%)	(wt%)	(wt%)
Quartz Standard bought (not milled at US)	0.168	0.035	0.003	0.015	0.027	0.065	0.003	0.151	0.015	99.823	0.004	100.31
Quartz (WC mill pot)	0.044	0.003	0.003	0.019	0.006	0.025	0.002	0.010	0.006	99.379	0.003	99.50
Quartz (Steel mill pot)	0.041	0.013	0.056	0.392	0.003	0.035	0.002	0.012	0.005	99.966	0.000	100.53
Quartz (Agate mill pot)	0.041	0.01	0.017	0.025	0.011	0.036	0.001	0.016	0.004	99.317	0.001	99.48

Sample	V	Cr	Co	Ni	Cu	Zn	Ga	Rb	Sr	Y	Zr	Nb	Ba	La	Ce	Nd	Pb	Th	U
Unit	(ppm)	(ppm)	(ppm)	(ppm)	(ppm)	(ppm)	(ppm)	(ppm)	(ppm)	(ppm)	(ppm)	(ppm)	(ppm)	(ppm)	(ppm)	(ppm)	(ppm)	(ppm)	(ppm)
Quartz Standard bought (not milled at US)	4	9	0	6	2	5	1	2	8	3	89	3	16	2	2	2	11	1	1
Quartz (WC mill pot)	0	22	204	8	3	5	1	3	5	2	12	3	1	1	6	4	9	0	1
Quartz (Steel mill pot)	0	217	1	33	2	3	1	2	5	1	13	2	5	2	9	5	11	2	3
Quartz (Agate mill pot)	0	10	0	4	4	2	1	2	6	1	13	2	3	0	0	0	11	2	2

Tests were performed on clean quartz in the various mill pots to test for maximum contamination. Quartz chips were too small for the steel jaw crusher, but the maximum contamination due to steel was simulated by using the steel mill pot.

Table A2. *Accuracy of trace element analysis of BCR standard (glass and powder) at Stellenbosch University*

		Sc	V	Cr	Co	Ni	Cu	Zn	Rb	Sr	Y	Zr	Nb	Mo	Sn	Cs	Ba
LA QC std	**Certified BCR glass**	**33**	**425.00**	**17**	**38**	**13**	**21**	**125**	**47**	**342**	**35**	**184**	**12.5**	**270**	**2.6**	**1.16**	**683**
	SD			**2**			**5**	**5**							**0.4**		
	Average Analysed	35.34	434.56	15.30	37.73	12.14	17.43	158.91	46.50	343.66	33.35	181.12	12.61	262.98	2.15	1.16	685.93
	% Deviation	***7.09***	***2.25***	***10.01***	***0.71***	***6.65***	***17.02***	***27.13***	***1.06***	***0.48***	***4.72***	***1.56***	***0.86***	***2.60***	***17.23***	***0.13***	***0.43***
Fusion control std	**Certified BCR powder**	**33**	**416.00**	**18**	**37**	**18**	**21**	**127**	**46.9**	**340**	**37**	**184**	**12.6**	**250**		**1.1**	**677**
	Average Analysed	37.07	445.29	19.36	37.76	16.02	21.16	119.98	46.10	355.62	35.11	188.72	12.93	275.55	2.63	1.11	703.26
	% Deviation	***12.32***	***7.04***	***7.57***	***2.05***	***10.99***	***0.75***	***5.53***	***1.70***	***4.60***	***5.11***	***2.57***	***2.58***	***10.22***		***1.17***	***3.88***

		La	Ce	Pr	Nd	Sm	Eu	Gd	Tb	Dy	Ho	Er	Tm	Yb	Lu	Hf	Ta	W	Pb	Th	U
LA QC std	**Certified BCR glass**	**24.7**	**53.3**	**6.7**	**28.9**	**6.59**	**1.97**	**6.71**	**1.02**	**6.44**	**1.27**	**3.7**	**0.51**	**3.39**	**0.503**	**4.84**	**0.78**	**0.50**	**11**	**5.90**	**1.69**
	SD																	**0.07**		**0.30**	
	Average Analysed	25.30	53.20	6.61	29.13	6.75	1.96	6.53	1.00	6.44	1.30	3.67	0.54	3.45	0.52	4.72	0.82	0.61	10.82	6.66	1.74
	% Deviation	***2.45***	***0.18***	***1.31***	***0.81***	***2.37***	***0.39***	***2.68***	***2.29***	***0.05***	***2.08***	***0.89***	***6.00***	***1.62***	***3.15***	***2.39***	***4.58***	***22.69***	***1.60***	***12.81***	***3.00***
Fusion control std	**Certified BCR powder**	**24.9**	**52.9**	**6.7**	**28.7**	**6.58**	**1.96**	**6.75**	**1.07**	**6.41**	**1.28**	**3.66**	**0.54**	**3.38**	**0.503**	**4.9**	**0.74**		**11**	**5.7**	**1.69**
	Average Analysed	26.16	54.10	6.77	29.93	7.00	2.02	6.91	1.03	6.72	1.35	3.82	0.56	3.61	0.53	4.89	0.83	0.76	10.10	6.38	1.74
	% Deviation	***5.05***	***2.27***	***1.01***	***4.30***	***6.34***	***3.11***	***2.36***	***3.46***	***4.87***	***5.35***	***4.41***	***3.46***	***6.88***	***5.95***	***0.30***	***11.58***		***8.19***	***11.87***	***2.80***

Trace element compositions have been obtained from the same fused beads as the major elements by applying the method described by Eggins (2003) and analysed using an Agilent 7500ce ICP-MS coupled with a Nd-YAG 223 nm New Wave LASER ablation (LA) system operating at a 12 Hz frequency with a mixed He-Ar carrier gas. Three analyses (each comprising a 30 s blank followed by data collection for 60 s) on each whole rock fused disc were obtained using a 100 µm diameter aperture, and the results averaged.
After every three samples (i.e. every 10th analysis) a National Institute of Standards and Technology NIST612 (Pearce et al. 1997) glass bead was analysed as calibration standard, in addition to fused discs of Nim-G (granite) and BhVO-1 (basalt) as secondary standards. Data were collected in time-resolved mode and, were reduced using an Excel calculation spreadsheet using the SiO_2 content measured by XRF as the internal standard. For each element the reproducibility of replicate analyses of the samples, and deviation from the certified values of the secondary standards are better than 10%, and mostly below 5% relative.

For the crushing of the rocks a steel mill pot was used. Table A1 reports tests that were performed in the laboratory to assess contamination induced by grinding/powdering during sample preparation. The tests were performed on clean quartz in the various mill pots to test for maximum contamination. Quartz chips were too small for the steel jaw crusher, but the maximum contamination due to steel was simulated by using the steel mill pot. These tests show that the steel mill may introduce significant amounts of Fe2O3 and Cr, as well as smaller amounts of Ni, Pb and Zr. The results in Table A.1 represent a “worst case scenario” due to the hardness of the tested material, and generally it is believed that the contamination is minor. No correction has been attempted implemented to the analysed samples.

A.2. Major and trace elements analysed at Acmelab

The whole rock analyses carried out at ACMELabs followed the analytical method termed “Group 4A & 4B – lithogeochemical whole rock fusion” and is summarised below based on the description available on the homepage (www.acmelab.com) and on information obtained upon personal request from the company.

Prepared samples are mixed with $LiBO_2/Li_2B_4O_7$ flux. Crucibles are fused in a furnace. The cooled bead is dissolved in ACS grade nitric acid.

Group 4A: Total abundances of the major oxides and several minor elements are reported on a 0.2g sample analysed by ICP-emission spectrometry following a Lithium metaborate/tetraborate fusion and dilute nitric digestion. Loss on ignition (LOI) is determined by igniting a sample split at 1000°C then measuring the weight loss.

Group 4B: Total Trace Elements by ICP-MS. This package comprises two separate analyses. Rare earth and refractory elements are determined by ICP mass spectrometry following a Lithium metaborate / tetraborate fusion and nitric acid digestion of a 0.2g sample (same decomposition as Group 4A). In addition a separate 0.5g split is digested in Aqua Regia and analysed by ICP Mass Spectrometry to report the precious and base metals (in highlight). Sample splits of 0.5g are leached in hot (95°C) Aqua Regia.

Tables A.3. Lower and upper detection limits of analysed major and minor elements at ACMELabs, analytical Group 4A.

Element	Group 4A Detection	Upper Limit
SiO_2	0.01 %	100 %
Al_2O_3	0.01 %	100 %
Fe_2O_3	0.04 %	100 %
CaO	0.01 %	100 %
MgO	0.01 %	100 %
Na_2O	0.01 %	100 %
K_2O	0.04 %	100 %
MnO	0.01 %	100 %
TiO_2	0.01 %	100 %
P_2O_5	0.01 %	100 %
Cr_2O_3	0.002%	100 %
LOI	0.1 %	100 %
C	0.01 %	100 %
S	0.01 %	100 %

Tables A.4. Lower and upper detection limits of analysed trace elements at ACMELabs, analytical Group 4B.

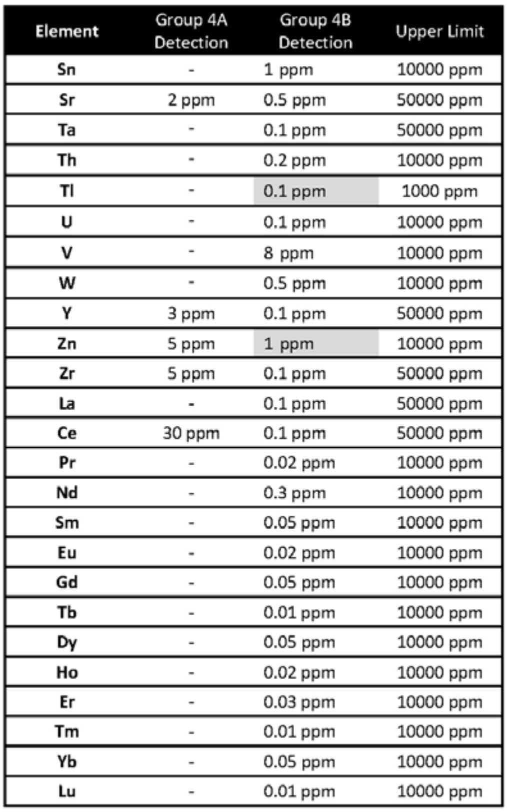

Element	Group 4A Detection	Group 4B Detection	Upper Limit
Sn	-	1 ppm	10000 ppm
Sr	2 ppm	0.5 ppm	50000 ppm
Ta	-	0.1 ppm	50000 ppm
Th	-	0.2 ppm	10000 ppm
Tl	-	0.1 ppm	1000 ppm
U	-	0.1 ppm	10000 ppm
V	-	8 ppm	10000 ppm
W	-	0.5 ppm	10000 ppm
Y	3 ppm	0.1 ppm	50000 ppm
Zn	5 ppm	1 ppm	10000 ppm
Zr	5 ppm	0.1 ppm	50000 ppm
La	-	0.1 ppm	50000 ppm
Ce	30 ppm	0.1 ppm	50000 ppm
Pr	-	0.02 ppm	10000 ppm
Nd	-	0.3 ppm	10000 ppm
Sm	-	0.05 ppm	10000 ppm
Eu	-	0.02 ppm	10000 ppm
Gd	-	0.05 ppm	10000 ppm
Tb	-	0.01 ppm	10000 ppm
Dy	-	0.05 ppm	10000 ppm
Ho	-	0.02 ppm	10000 ppm
Er	-	0.03 ppm	10000 ppm
Tm	-	0.01 ppm	10000 ppm
Yb	-	0.05 ppm	10000 ppm
Lu	-	0.01 ppm	10000 ppm

Note: Highlighted elements by 1DX Aqua Regia – ICP-MS analysis

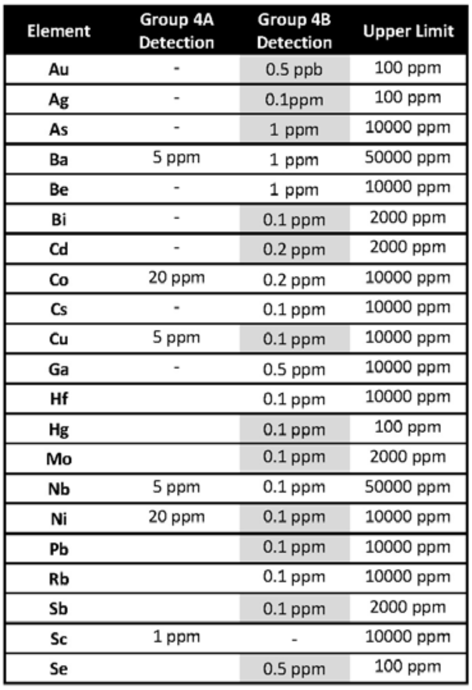

Element	Group 4A Detection	Group 4B Detection	Upper Limit
Au	-	0.5 ppb	100 ppm
Ag	-	0.1ppm	100 ppm
As	-	1 ppm	10000 ppm
Ba	5 ppm	1 ppm	50000 ppm
Be	-	1 ppm	10000 ppm
Bi	-	0.1 ppm	2000 ppm
Cd	-	0.2 ppm	2000 ppm
Co	20 ppm	0.2 ppm	10000 ppm
Cs	-	0.1 ppm	10000 ppm
Cu	5 ppm	0.1 ppm	10000 ppm
Ga	-	0.5 ppm	10000 ppm
Hf		0.1 ppm	10000 ppm
Hg		0.1 ppm	100 ppm
Mo		0.1 ppm	2000 ppm
Nb	5 ppm	0.1 ppm	50000 ppm
Ni	20 ppm	0.1 ppm	10000 ppm
Pb		0.1 ppm	10000 ppm
Rb		0.1 ppm	10000 ppm
Sb		0.1 ppm	2000 ppm
Sc	1 ppm	-	10000 ppm
Se		0.5 ppm	100 ppm

A3. Comparison of the Disko-1 standard

Table A.5 provides the compiled data for the Disko-1 standard obtained from the different laboratories involved in the analytical program.

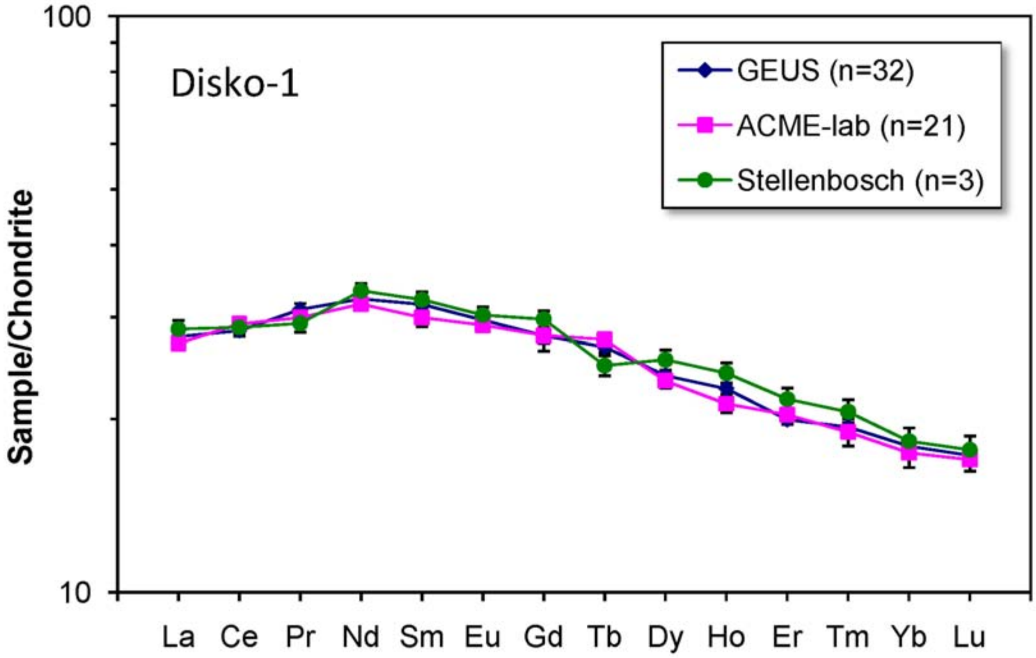

Figure A1. Comparison of the rare earth element contents in the Disko-1 basalt standard from three laboratories by different methods. In general the results from the various laboratories agree well and are generally within the analytical uncertainty. Results from Stellenbosch show a slight more “bumpy” pattern with higher values for Gd to Tm, except for Tb which is lower compared to GEUS and ACMELabs. Part of this deviation might reflect a comparatively much smaller statistical basis for the Stellenbosch dataset (n = 3) than the GEUS (n = 32) and ACMELabs (n = 21).

Table A.5. Comparison of trace element data for the Disko-1 'in house' standard

	GEUS (2003-2010)[1]				ACME lab (2008-2010)[2]				Stellenbosch (2010-11)[3]				ACME/GEUS	Stell/GEUS	Stell/ACME
Element	**Avg**	**±1σ (abs.)**	**±1σ (%)**	**n**	**Avg**	**±1σ (abs.)**	**±1σ (%)**	**n**	**Avg**	**±1σ (abs.)**	**±2σ (%)**	**n**	**(% diff.)**	**(% diff.)**	**(% diff.)**
Sc	40.9	1.3	3.3	32	41.8	0.9	2.2	21	45.5	1.7	3.7	3	2.1	11.1	8.8
V	412	12	2.9	32	434	17	3.9	21	436	2	0.5	3	5.5	6.0	0.5
Cr	126	3	2.5	32	129	5	3.7	21	129	8	6.5	3	2.7	2.4	-0.2
Co	56.7	1.0	1.7	32	51.9	4.9	9.4	21	54.4	1.0	1.9	3	-8.5	-4.1	4.8
Ni	60.1	2.1	3.5	32	61.0	7.1	11.7	19	63.4	2.7	4.2	3	1.6	5.6	4.0
Cu	226	3	1.5	32	222	10	4.4	21	195	6	3.0	3	-1.8	-13.5	-12.0
Zn	106	2	2.2	32	62.2	5.1	8.1	21	75.2	1.5	2.1	3	-41.1	-28.8	20.9
Ga	20.8	0.2	1.0	32	20.1	1.0	5.0	21	na.				-3.4		
Rb	3.30	0.05	1.6	32	3.57	0.51	14.4	21	3.01	0.07	2.2	3	8.1	-8.8	-15.6
Sr	213	3	1.4	32	224	7	3.1	21	222	1	0.3	3	5.4	4.4	-0.9
Y	33.8	0.6	1.7	32	30.6	1.2	3.8	21	32.2	0.4	1.3	3	-9.5	-4.8	5.2
Zr	122	3	2.3	32	111	5	4.3	21	119	1	1.2	3	-8.7	-2.0	7.3
Nb	4.46	0.09	1.9	32	4.16	0.35	8.3	21	4.25	0.12	2.7	3	-6.8	-4.7	2.2
Cs	0.059	0.003	4.5	32	0.121	0.043	35.1	14	0.066			1	106.2	12.1	-45.6
Ba	46.5	1.1	2.4	31	47.9	4.4	9.2	21	48.4	1.8	3.8	3	3.0	4.1	1.1
La	6.58	0.08	1.2	32	6.41	0.32	5.0	21	6.78	0.08	1.1	3	-2.6	3.0	5.8
Ce	17.4	0.3	1.7	32	17.9	1.0	5.5	21	17.7	0.4	2.0	3	2.8	1.4	-1.4
Pr	2.87	0.07	2.4	32	2.78	0.11	4.1	21	2.72	0.02	0.8	3	-3.2	-5.4	-2.3
Nd	14.7	0.3	2.0	32	14.4	0.8	5.4	21	15.2	0.1	0.4	3	-2.1	3.3	5.5
Sm	4.67	0.09	1.9	32	4.43	0.20	4.4	21	4.76	0.16	3.3	3	-5.1	1.9	7.5
Eu	1.67	0.04	2.5	32	1.64	0.06	3.8	21	1.70	0.04	2.1	3	-2.0	2.0	4.1
Gd	5.54	0.32	5.8	32	5.55	0.26	4.7	21	5.92	0.17	2.8	3	0.1	6.8	6.7
Tb	0.963	0.019	2.0	32	0.991	0.040	4.0	21	0.894	0.011	1.3	3	2.9	-7.2	-9.8
Dy	5.86	0.10	1.6	32	5.73	0.20	3.6	21	6.24	0.17	2.7	3	-2.1	6.5	8.8
Ho	1.23	0.03	2.3	32	1.16	0.05	4.0	21	1.31	0.04	3.1	3	-5.9	6.5	13.1
Er	3.19	0.06	1.8	32	3.26	0.16	4.9	21	3.47	0.06	1.6	3	2.0	8.6	6.4
Tm	0.479	0.009	1.8	32	0.469	0.030	6.4	21	0.509	0.026	5.0	3	-2.0	6.3	8.4
Yb	2.89	0.04	1.5	32	2.81	0.14	5.1	21	2.95	0.16	5.4	3	-2.6	2.1	4.8
Lu	0.425	0.012	2.9	32	0.419	0.029	7.0	21	0.435	0.019	4.5	3	-1.6	2.3	3.9
Hf	3.26	0.06	1.8	32	3.27	0.31	9.5	21	3.21	0.12	3.7	3	0.3	-1.7	-2.0
Ta	0.305	0.017	5.4	32	0.276	0.089	32.2	21	0.297	0.015	5.2	3	-9.4	-2.6	7.5
W	n.a.				83.3	5.2	6.2	9	89.0	0.5	0.6	3			6.9
Pb	1.24	0.08	6.5	32	1.17	1.57	134.9	21	1.31	0.12	9.4	3	-5.9	5.4	12.0
Th	0.594	0.024	4.0	32	0.790	0.232	29.4	21	0.630	0.017	2.6	3	33.0	6.0	-20.3
U	0.147	0.005	3.1	32	0.186	0.096	51.9	21	0.147	0.010	7.1	3	26.2	-0.1	-20.8

1: Based on total digestion solution ICP-MS; 2: Total fusion ICP-MS; 3: LA-ICP-MS on fused glass discs

References

Eggins, S. 2003: Laser ablation ICP-MS analysis of geological materials prepared as lithium borate glasses. Geostand Geoanal Res **27**,147–162.

Pearce, N.J.G., Perkins, W.T., Westgate J.A., Gorton M.P., Jackson S.E., Meal C.R. & Chenery, S.P. 1997: A compilation of new and published major and trace element data for NIST SRM 610 and NIST SRM 612 glass reference materials. Geostand Newsl **21**,115–144.

Appendix B. Whole rock geochemical data

Table B.1. Major and trace element data for felsic rocks of SW Greenland

Sample	511816	511840	511890	468759	468761	468767	468770	468771	468787	508221
Rock type	Bt-Grt gneiss	Bt gneiss	Bt gneiss	Tonalitic biotite-aplite	Hornblende-rich tonalite gneiss	Tonalitic biotite-gneiss	Felsic aplite	Tonalitic biotite-gneiss	Felsic aplite	Mgt-bearing tonalitic gneiss
TTG sensu Martin et al. (2005)				TTG	TTG	TTG	TTG	TTG	TTG	TTG
Latitude (°N)	62.45909	62.32680	61.82258	62.72217	62.72103	62.73602	62.73602	62.73602	62.71577	63.34923
Longitude (°W)	-49.83878	-49.19086	-48.84778	-50.15438	-50.15605	-50.14936	-50.14936	-50.14936	-50.17662	-50.68017
Age (Ma) *	2916	2850	2930							
±2σ	4	4	5							
Collector	JCS	JCS	JCS	KSZ	KSZ	KSZ	KSZ	KSZ	KSZ	KSZ
Laboratory **	1	1	1	1	1	1	1	1	1	1
SiO2	65.02	73.02	65.10	69.43	63.50	74.40	75.15	75.79	71.87	69.49
Al2O3	17.28	14.92	15.82	15.66	16.39	14.00	13.83	13.50	15.18	16.21
Fe2O3	4.55	2.18	5.99	3.42	5.56	2.19	1.77	1.86	2.69	2.99
MgO	1.90	0.65	2.03	1.07	2.62	0.29	0.54	0.25	0.76	0.51
CaO	4.94	3.72	4.52	2.93	4.47	2.73	2.76	2.29	3.27	2.29
Na2O	3.99	3.54	3.84	4.32	4.20	4.92	4.47	4.41	4.57	4.74
K2O	1.03	0.70	1.46	1.51	1.48	0.60	0.43	1.22	0.61	2.69
TiO2	0.47	0.41	0.58	0.38	0.55	0.11	0.11	0.10	0.26	0.23
P2O5	0.14	0.07	0.14	0.13	0.14	0.07	0.03	0.04	0.09	0.10
MnO	0.06	0.03	0.08	0.03	0.08	0.04	0.04	0.02	0.04	0.07
LOI	0.24	0.52	0.46	1.00	0.80	0.60	0.70	0.40	0.50	0.60
SUM	99.61	99.78	100.02	99.88	99.79	99.95	99.83	99.88	99.84	99.92
Cr	27.97	16.76	44.82	13.68	47.89	13.68	0.00	0.00	0.00	13.68
Sc	9.05	5.54	14.25	5.00	10.00	1.00	1.00	1.00	4.00	2.00
Ba	351.36	324.53	334.21	312.00	453.00	300.00	325.00	373.00	808.00	467.00
Co	12.92	6.08	14.38	18.10	26.80	24.80	2.50	1.40	4.70	3.30
Cs	0.36	1.00	1.90	0.60	2.90	1.40	0.60	0.70	0.20	0.80
Ga	n.a.	n.a.	n.a.	18.60	20.00	21.50	15.40	15.50	18.90	16.60
Hf	5.90	2.88	3.39	4.30	4.10	3.60	2.30	2.90	5.10	5.90
Nb	3.21	2.55	3.08	5.70	6.40	7.00	4.30	5.50	5.70	6.40
Rb	29.82	14.28	43.26	58.40	49.60	38.30	17.00	39.50	24.60	62.60
Sr	380.05	223.11	293.08	160.30	178.40	230.60	236.40	182.10	136.00	252.10
Ta	0.13	0.06	0.12	0.00	0.00	0.00	0.00	0.00	0.00	0.40
Th	0.29	0.29	0.44	2.90	2.90	3.90	4.00	7.00	4.70	7.50
U	0.09	0.38	0.11	0.70	0.70	0.80	0.80	0.70	1.00	1.10
V	61.02	27.59	80.12	40.00	87.00	8.00	8.00	8.00	26.00	8.00
W	1.11	0.40	0.23	0.00	0.00	0.00	0.00	0.00	0.00	7.80
Zr	242.86	120.03	145.94	171.30	168.30	151.10	86.40	90.00	167.90	219.90
Y	8.96	1.14	12.66	6.20	13.30	8.70	4.10	3.30	11.00	15.50
La	13.58	7.22	7.86	12.60	19.10	21.40	14.90	13.00	10.20	29.30
Ce	29.15	12.38	20.16	20.30	37.80	37.80	27.20	40.20	21.80	60.40
Pr	3.64	1.09	2.62	2.51	4.40	4.16	2.60	2.42	2.23	6.30
Nd	15.47	3.61	11.82	9.40	17.40	16.30	8.50	9.00	8.00	21.50
Sm	3.21	0.60	2.97	1.50	3.12	2.36	1.22	1.09	1.50	3.35
Eu	0.81	0.48	0.96	0.52	0.87	0.58	0.38	0.48	0.49	0.85
Gd	2.71	0.33	2.79	1.30	2.63	1.76	0.91	0.69	1.64	2.48
Tb	0.33	0.04	0.39	0.20	0.41	0.26	0.14	0.10	0.29	0.42
Dy	1.81	0.21	2.47	1.05	2.26	1.30	0.72	0.62	1.54	2.36
Ho	0.30	0.03	0.47	0.21	0.44	0.26	0.12	0.10	0.35	0.52
Er	0.84	0.15	1.31	0.59	1.34	0.72	0.32	0.35	0.89	1.73
Tm	0.11	0.02	0.17	0.09	0.20	0.11	0.05	0.05	0.13	0.26
Yb	0.89	0.15	1.27	0.52	1.22	0.72	0.37	0.47	0.95	1.90
Lu	0.11	0.03	0.17	0.08	0.19	0.10	0.06	0.07	0.13	0.31
Cu	62.14	7.07	9.10	13.10	2.20	4.40	3.70	3.10	10.80	23.40
Pb	4.24	5.16	6.18	0.70	0.80	1.00	3.00	6.40	1.80	0.90
Zn	56.15	53.91	67.67	55.00	70.00	47.00	42.00	50.00	43.00	40.00
Ni	31.97	16.08	29.27	8.10	26.70	0.70	7.00	2.20	5.80	0.10

* Age derived from zircon U/Pb ages at GEUS (Kokfelt et al. 2011)

** Code: 1: Acme lab, Vancouver, Canada (www.acmelab.com); 2: Stellenbosch University, South Africa (http://academic.sun.ac.za/saf/04_icp/services.html); 3: Major elements: Philips PW 1480 X-ray spectrometer at Universität Bonn; Trace elements: Agilent 7500cs quadrupole ICP-MS at Universität Kiel

† Samples were crushed at GEUS using WC swing mill; elevated W values in these samples reflect contamination during powder preparation

n.a. = not analysed

Table B.1. Major and trace element data for felsic rocks of SW Greenland, continued

Sample	510912	510941	510943	511110	511137	512255	515820	515829	468793(2)	519732
Rock type	Tonalitic aplite dyke	Tonalitic biotite-aplite	Tonalitic biotite-aplite	Tonalitic gneiss	Mgt-bearing tonalite gneiss	Chloritised tonalite gneiss	Biotite-tonalite	Muscovite-rich tonalite	Tonalitic biotite-gneiss	Granitic gneiss, pale foliated
TTG sensu Martin et al. (2005)	TTG		TTG	TTG	TTG	TTG	TTG	TTG	TTG	
Latitude (°N)	62.66926	62.72408	62.74703	63.34450	61.90532	61.45335	62.65993	62.65206	62.71362	62.67149
Longitude (°W)	-50.26474	-50.15079	-50.14311	-50.67997	-48.59158	-48.75517	-50.28880	-50.28170	-50.17589	-49.58555
Age (Ma) *										
±2σ										
Collector	KSZ	KSZ	KSZ	KSZ	KSZ	KSZ	KSZ	KSZ	KSZ	MBK
Laboratory **	1	1	1	1	1	1	1	1	1	2
SiO2	72.43	71.23	67.19	75.47	74.07	75.29	70.80	75.59	71.20	70.87
Al2O3	15.09	15.11	16.07	12.86	13.59	12.86	15.92	14.09	15.63	16.05
Fe2O3	2.53	2.69	4.20	1.55	2.25	2.82	2.18	2.13	2.35	1.83
MgO	0.49	0.62	1.46	0.48	0.28	0.55	0.68	0.22	0.75	0.66
CaO	2.69	2.54	4.03	1.36	1.19	1.11	2.85	2.36	3.19	3.22
Na2O	5.47	3.68	4.08	2.79	3.71	3.88	5.35	5.06	4.67	3.77
K2O	0.54	2.02	1.58	4.51	3.58	1.93	1.03	0.14	0.92	1.92
TiO2	0.21	0.29	0.43	0.17	0.15	0.29	0.25	0.08	0.28	0.23
P2O5	0.07	0.10	0.14	0.03	0.05	0.06	0.09	0.04	0.10	0.05
MnO	0.04	0.04	0.07	0.01	0.05	0.04	0.03	0.05	0.03	0.03
LOI	0.30	1.60	0.60	0.60	0.90	1.00	0.70	0.10	0.70	1.06
SUM	99.86	99.92	99.85	99.83	99.82	99.83	99.88	99.86	99.82	99.69
Cr	13.68	13.68	20.53	13.68	13.68	14.00	13.68	0.00	13.68	18.42
Sc	2.00	3.00	8.00	5.00	6.00	9.00	3.00	1.00	3.00	2.89
Ba	402.00	650.00	370.00	815.00	676.00	458.00	172.00	314.00	539.00	435.49
Co	5.70	7.80	12.90	4.50	2.20	3.10	23.40	0.80	21.40	3.48
Cs	1.60	0.50	2.00	2.40	1.00	1.60	1.20	0.40	0.50	0.35
Ga	16.80	19.80	21.10	15.50	14.20	14.00	22.50	18.60	22.20	n.a.
Hf	4.40	4.60	4.70	6.80	5.40	6.90	4.60	3.50	4.60	2.16
Nb	5.50	6.30	6.60	8.90	6.40	5.50	2.80	6.10	5.90	1.61
Rb	35.50	70.60	81.70	133.40	88.90	56.50	62.30	5.10	39.40	65.82
Sr	192.40	112.50	247.00	126.80	213.60	197.80	234.00	174.80	252.80	388.62
Ta	0.00	0.00	0.00	1.00	0.40	0.30	0.00	0.00	0.00	0.07
Th	5.60	4.40	2.90	10.10	10.10	13.90	2.10	5.90	4.20	1.14
U	1.40	1.10	0.50	2.80	1.40	1.10	1.20	1.40	0.70	0.18
V	21.00	23.00	58.00	11.00	8.00	8.00	25.00	8.00	30.00	23.88
W	0.00	0.00	0.00	18.50	9.70	5.70	0.00	0.00	0.00	0.31
Zr	147.40	175.80	172.60	202.60	182.00	253.40	156.00	93.30	206.90	74.80
Y	7.30	6.90	12.30	15.70	28.30	15.50	3.80	7.10	4.60	0.62
La	19.60	18.90	16.90	30.90	51.00	93.40	6.30	22.30	18.10	3.46
Ce	38.20	36.40	34.50	63.70	109.30	183.90	19.50	42.40	43.20	5.27
Pr	3.85	3.71	3.50	6.62	11.13	17.90	1.37	4.72	4.10	0.53
Nd	12.60	12.90	12.50	23.80	39.50	57.80	5.20	16.10	15.10	1.71
Sm	2.23	2.06	2.36	3.75	5.95	7.46	1.19	2.69	2.15	0.30
Eu	0.70	0.60	0.67	0.67	1.10	1.13	0.41	0.71	0.52	0.37
Gd	1.84	1.42	2.15	3.16	4.57	5.00	1.02	1.92	1.40	0.25
Tb	0.28	0.21	0.35	0.49	0.77	0.62	0.16	0.29	0.18	0.03
Dy	1.33	1.27	2.07	2.55	4.49	3.06	0.79	1.40	0.87	0.13
Ho	0.24	0.21	0.36	0.54	0.98	0.55	0.12	0.23	0.15	0.02
Er	0.63	0.61	1.11	1.58	3.02	1.68	0.30	0.58	0.41	0.06
Tm	0.10	0.07	0.17	0.22	0.48	0.24	0.05	0.09	0.06	0.02
Yb	0.62	0.58	1.06	1.34	3.34	1.47	0.27	0.57	0.37	0.10
Lu	0.09	0.07	0.14	0.20	0.51	0.23	0.04	0.08	0.06	0.01
Cu	9.30	11.50	0.80	16.40	2.70	6.50	0.40	7.80	1.60	7.80
Pb	1.60	1.20	1.00	2.50	3.40	5.50	1.00	1.80	1.50	9.05
Zn	51.00	53.00	68.00	27.00	38.00	38.00	60.00	13.00	42.00	42.19
Ni	1.40	1.40	18.80	2.90	0.80	1.10	3.50	2.70	3.90	14.01

Table B.1. Major and trace element data for felsic rocks of SW Greenland, continued

Sample	519733	511503	511619	519405	519699	508233	508243	508245	508262	509965
Rock type	Banded gneiss, granitic	Grt gneiss, migmatite	Grt-Bt-Ath gneiss	Hbl-Grt-Bt schist	Bt gneiss, granodiorite	Diopside-bearing felsic gneiss	Bt gneiss, tonalite	Bt gneiss, granodiorite	Bt-Hbl gneiss, tonalite	Bt gneiss
TTG sensu Martin et al. (2005)	TTG							TTG	TTG	TTG
Latitude (°N)	62.66276	61.81957	61.89491	61.82870	62.11154	63.20536	63.20859	63.20253	63.21701	62.94428
Longitude (°W)	-49.57475	-48.34800	-48.23675	-48.33367	-48.92133	-49.30214	-49.29609	-49.29874	-50.16305	-49.76942
Age (Ma) *						2687	2810	2866	2818	2900
±2σ						3		3	10	6
Collector	MBK	NTK	NTK	NTK	NTK	TFK	TFK	TFK	TFK	JCS
Laboratory **	2	1	1	2	2	1 †	1 †	1 †	1 †	1 †
SiO2	71.83	59.46	60.86	46.69	74.28	69.87	65.27	70.39	69.67	67.42
Al2O3	15.53	17.91	14.88	18.25	14.25	15.70	15.63	16.03	16.09	15.64
Fe2O3	2.25	9.51	11.38	13.69	1.02	3.23	4.79	1.96	2.51	4.00
MgO	0.59	3.73	5.58	5.55	0.08	1.66	1.77	0.73	0.86	1.37
CaO	2.63	1.89	2.97	10.08	0.86	5.27	3.24	3.21	3.22	4.34
Na2O	4.34	1.88	1.58	2.18	3.73	3.18	4.02	4.95	4.86	4.18
K2O	1.68	1.96	0.88	0.57	4.79	0.14	2.89	1.45	1.48	1.27
TiO2	0.23	0.81	0.92	1.75	0.08	0.05	0.63	0.25	0.35	0.44
P2O5	0.07	0.08	0.06	0.06	0.01	0.01	0.42	0.07	0.12	0.14
MnO	0.05	0.16	0.15	0.28	0.05	0.07	0.05	0.02	0.03	0.05
LOI	0.27	2.68	0.96	0.70	0.29	0.60	0.90	0.70	0.60	0.90
SUM	99.48	100.07	100.23	99.80	99.45	99.78	99.61	99.76	99.79	99.75
Cr	14.64	360.38	539.16	64.55	12.37	20.70	20.79		0.00	20.76
Sc	4.61	35.84	33.89	40.39	4.72	4.00	5.00	2.00	4.00	7.00
Ba	529.56	274.65	115.46	44.79	272.13	92.00	1037.00	388.00	318.00	299.00
Co	4.38	28.98	57.04	26.87	1.13	143.30	77.80	108.40	73.10	111.70
Cs	0.60	4.91	2.45	6.10	4.48	<0.1	1.10	0.60	0.70	1.70
Ga	n.a.	n.a.	n.a.	n.a.	n.a.	15.00	22.40	20.60	18.90	18.80
Hf	2.26	3.89	2.68	2.56	1.96	<0.1	8.90	3.50	5.10	4.90
Nb	2.42	5.90	4.09	26.50	9.62	0.40	10.40	3.00	4.90	6.20
Rb	46.47	115.51	27.40	35.15	211.05	3.80	109.50	39.10	54.30	45.40
Sr	396.84	132.38	88.11	92.83	57.24	253.40	637.70	357.00	462.80	207.80
Ta	0.10	0.48	0.32	1.59	0.88	0.50	0.70	0.40	0.50	0.90
Th	1.20	5.25	3.38	0.44	5.71	0.30	15.80	1.90	4.20	2.90
U	0.30	1.12	0.94	0.18	2.38	<0.1	0.80	0.10	0.50	0.60
V	25.39	209.18	254.65	425.82	11.02	27.00	66.00	28.00	29.00	67.00
W	0.37	0.37	0.39	3.88	0.49	1058.30	568.00	791.30	595.50	814.80
Zr	90.24	142.31	101.40	107.34	49.21	4.20	374.60	125.10	203.40	169.70
Y	2.85	21.28	17.75	60.31	5.40	2.80	10.10	1.50	4.20	10.10
La	7.49	17.16	15.07	14.06	4.69	2.60	40.50	13.70	30.70	10.40
Ce	20.46	34.77	32.20	42.68	12.20	3.30	121.20	26.50	56.00	26.60
Pr	1.72	4.16	3.88	6.71	1.37	0.38	10.76	2.62	5.58	2.76
Nd	6.28	17.54	16.51	34.53	5.03	1.00	39.60	9.20	19.10	11.80
Sm	1.21	3.44	4.01	9.56	1.02	0.26	6.30	1.37	2.17	2.49
Eu	0.41	1.07	1.07	2.59	0.20	0.25	1.29	0.48	0.77	0.79
Gd	0.78	3.64	3.27	10.12	0.92	0.36	3.87	0.87	1.31	2.25
Tb	0.11	0.58	0.52	1.65	0.12	0.07	0.50	0.10	0.18	0.35
Dy	0.51	4.12	3.44	11.44	0.82	0.44	2.25	0.45	0.71	1.85
Ho	0.10	0.81	0.67	2.25	0.20	0.10	0.35	0.06	0.13	0.34
Er	0.25	2.52	2.17	6.56	0.62	0.27	0.88	0.12	0.35	0.95
Tm	0.04	0.35	0.32	0.97	0.08	0.06	0.12	0.02	0.07	0.14
Yb	0.24	2.34	2.24	6.07	0.66	0.36	0.71	0.09	0.34	0.88
Lu	0.03	0.36	0.31	0.84	0.11	0.06	0.11	0.02	0.07	0.12
Cu	48.79	71.37	115.09	14.99	7.31	34.70	26.00	1.30	5.40	22.90
Pb	11.65	7.76	9.24	6.51	32.39	0.40	5.70	1.00	2.70	1.70
Zn	55.10	86.90	125.02	233.21	23.26	8.00	93.00	40.00	52.00	55.00
Ni	10.81	109.44	237.55	47.17	9.25	6.40	14.00	7.60	4.00	12.70

Table B.1. Major and trace element data for felsic rocks of SW Greenland, continued

Sample	510007	510138	510169	511535	511545	511558	512803	512804	512805	512810
Rock type	Hbl-Bt gneiss	Granodiorite	Granodiorite	Bt gneiss, tonalite	Bt gneiss, tonalite	Hbl-Bt gneiss, tonalite	Hbl-Gt gneiss, granulite	Bt-Hbl gneiss, granulite?	Hbl-Opx-Gt gneiss, granulite?	Banded migmatite gneiss
TTG sensu Martin et al. (2005)	TTG		TTG	TTG						
Latitude (ºN)	61.58668	62.95327	62.94428	61.81604	61.91274	61.92770	63.21480	63.19665	63.20264	61.62914
Longitude (ºW)	-49.25825	-49.76064	-49.76942	-48.58667	-48.37373	-48.31041	-50.25087	-50.33217	-50.36908	-49.08290
Age (Ma) *	2961		2900	2856	2854	2935	2863	2866	2841	2870
±2σ	3		3	9	5	4	5	6	8	9
Collector	JCS	NTK	NTK	TFK	TFK	TFK	TFK	TFK	TFK	TFK
Laboratory **	1†	1†	1†	2	2	2	1†	1†	1†	1†
SiO2	66.81	45.43	65.36	71.79	57.82	61.26	68.90	65.85	73.50	72.11
Al2O3	17.01	31.53	15.54	14.94	17.67	17.44	16.47	16.61	15.00	15.00
Fe2O3	3.01	2.55	5.72	2.85	7.58	6.39	2.80	3.61	0.81	1.60
MgO	1.18	1.57	1.78	0.62	2.58	2.47	0.86	1.70	0.18	0.55
CaO	4.78	16.23	4.53	2.25	5.78	4.21	3.62	4.25	1.74	2.85
Na2O	4.71	1.62	3.98	4.72	4.37	3.72	4.88	4.83	4.12	3.93
K2O	0.89	0.10	1.52	1.46	1.37	2.42	1.17	1.49	4.03	2.71
TiO2	0.31	0.19	0.68	0.32	1.19	0.57	0.36	0.45	0.08	0.20
P2O5	0.08	0.02	0.14	0.09	0.54	0.16	0.13	0.21	0.02	0.08
MnO	0.04	0.03	0.08	0.05	0.10	0.11	0.03	0.04	<0.01	0.02
LOI	1.00	0.70	0.50	0.50	0.55	1.29	0.50	0.60	0.30	0.60
SUM	99.82	99.97	99.83	99.61	99.55	100.04	99.72	99.64	99.78	99.65
Cr	0.00	55.13	0.00	13.68	48.66	50.77	0.00	20.72	0.00	0.00
Sc	6.00	10.00	10.00	6.63	14.95	19.19	3.00	6.00		2.00
Ba	252.00	15.00	381.00	438.57	805.07	498.73	351.00	653.00	600.00	1456.00
Co	91.10	25.90	60.50	4.47	18.25	15.91	105.40	104.30	78.80	121.70
Cs	0.70	1.50	1.50	1.38	0.60	2.27	0.10		0.10	0.90
Ga	17.00	19.40	19.50	n.a.	n.a.	n.a.	17.30	17.90	15.70	16.40
Hf	2.80	0.50	5.60	4.40	8.08	2.05	4.50	3.70	1.80	3.50
Nb	2.50	0.20	7.50	5.20	8.95	4.88	1.70	2.90	0.50	1.60
Rb	21.50	2.70	55.70	95.52	27.00	114.91	25.90	40.60	65.30	78.10
Sr	428.90	80.90	210.00	309.64	629.75	532.55	550.20	678.90	368.50	375.70
Ta	0.20	0.10	0.70	0.38	0.40	0.25	0.30	0.30	0.30	0.40
Th	0.60	<0.2	3.70	6.94	9.25	6.56	2.40	4.70	2.60	4.70
U	0.20	<0.1	0.60	1.06	0.43	0.28		0.10	0.10	0.30
V	32.00	77.00	79.00	29.84	100.78	92.10	29.00	58.00		14.00
W	676.60	110.80	387.20	0.39	0.34	0.38	785.70	748.40	624.80	962.90
Zr	110.30	12.20	190.30	182.60	407.79	77.59	166.40	136.10	62.60	117.00
Y	5.50	4.60	19.50	7.21	19.19	11.44	2.30	5.10	0.60	1.40
La	6.10	0.50	14.80	30.14	91.43	43.46	24.60	42.80	11.10	18.80
Ce	13.30	1.20	42.00	57.89	176.66	77.81	53.10	83.30	20.40	43.80
Pr	1.48	0.17	3.98	6.08	21.68	8.37	5.12	8.62	2.07	4.08
Nd	6.40	1.10	16.10	22.81	82.69	30.75	17.40	29.00	6.90	14.70
Sm	1.29	0.35	3.65	3.39	12.79	4.79	2.10	3.72	1.00	1.87
Eu	0.52	0.27	0.99	0.71	2.39	1.01	0.68	1.00	0.44	0.45
Gd	1.22	0.61	3.71	2.21	7.91	3.29	1.17	2.14	0.51	1.00
Tb	0.19	0.11	0.63	0.25	0.84	0.41	0.13	0.27	0.06	0.11
Dy	1.01	0.69	3.41	1.71	4.41	2.40	0.61	1.12	0.20	0.44
Ho	0.20	0.18	0.72	0.28	0.75	0.44	0.08	0.18	0.03	0.05
Er	0.59	0.47	1.99	0.76	1.77	1.19	0.20	0.44	0.04	0.09
Tm	0.08	0.08	0.30	0.11	0.22	0.15	0.02	0.06		0.01
Yb	0.51	0.48	1.86	0.77	1.44	0.99	0.20	0.36	0.07	0.12
Lu	0.08	0.07	0.29	0.11	0.20	0.15	0.03	0.05	0.01	0.02
Cu	6.20	30.70	27.40	9.67	53.75	29.21	5.80	12.70	0.50	19.50
Pb	1.60	0.50	1.40	13.65	7.70	12.87	1.30	1.50	1.90	5.80
Zn	40.00	2.00	57.00	46.54	74.13	82.06	37.00	35.00	16.00	29.00
Ni	11.80	15.50	13.20	9.58	33.80	29.12	4.90	21.10	1.20	3.60

Table B.1. Major and trace element data for felsic rocks of SW Greenland, continued

Sample	512814	512817	512820	512822	512826	512829	512831	519425	519427	519431
Rock type	Bt gneiss, tonalite	Bt gneiss, tonalite	Grt-Hbl-Bt gneiss	Bt-Hbl gneiss, tonalite	Bt gneiss, granite	Bt-Hbl schist	Bt gneiss, tonalite	Hbl-Bt gneiss tonalite	Hbl-Bt gneiss tonalite	Bt-Hbl gneiss tonalite
TTG sensu Martin et al. (2005)	TTG	TTG		TTG	TTG		TTG			TTG
Latitude (°N)	61.62403	61.62567	62.21152	62.01375	62.07259	61.52027	61.80831	61.82252	61.87026	61.86299
Longitude (°W)	-49.09962	-49.09344	-49.91029	-49.72796	-48.95181	-48.30324	-49.28795	-48.34714	-48.61597	-48.62221
Age (Ma) *		2855	2833	2867	2892	2942	2850			
±2σ		3	7	3	4	42	4			
Collector	TFK	TFK	TFK	TFK	TFK	TFK	TFK	TFK	TFK	TFK
Laboratory **	1[†]	1[†]	1[†]	1[†]	1[†]	1[†]	1[†]	2	2	2
SiO2	67.90	64.37	62.80	72.48	71.58	61.92	69.99	69.31	71.43	72.77
Al2O3	16.56	17.68	15.65	15.02	15.02	16.39	15.90	14.71	16.40	14.06
Fe2O3	3.01	4.02	6.37	1.83	1.88	5.39	2.38	4.05	1.38	2.82
MgO	1.12	1.68	3.58	0.57	0.66	3.09	0.93	0.87	0.48	0.50
CaO	3.38	4.59	4.82	2.63	2.11	4.43	2.92	3.17	2.64	1.87
Na2O	4.83	4.50	3.51	5.14	4.60	4.28	4.87	3.46	5.05	3.67
K2O	1.60	1.55	1.37	1.11	2.29	2.06	1.49	1.53	1.51	3.39
TiO2	0.44	0.58	0.63	0.25	0.22	0.73	0.35	0.31	0.19	0.36
P2O5	0.15	0.13	0.12	0.08	0.10	0.26	0.09	0.09	0.06	0.09
MnO	0.02	0.05	0.10	0.03	0.04	0.07	0.03	0.10	0.03	0.08
LOI	0.70	0.60	0.70	0.60	1.20	1.00	0.80	1.90	0.25	0.19
SUM	99.69	99.73	99.71	99.73	99.70	99.63	99.73	99.49	99.42	99.79
Cr	0.00	0.00	62.23	0.00	0.00	83.24	0.00	21.38	13.28	12.08
Sc	4.00	7.00	15.00	3.00	4.00	13.00	4.00	8.54	4.95	8.69
Ba	526.00	526.00	433.00	207.00	571.00	635.00	442.00	383.45	472.32	735.59
Co	103.50	71.80	89.50	131.90	142.40	72.30	102.80	7.05	3.37	3.30
Cs	1.10	27.70	0.20	1.50	2.50	9.00	3.70	6.49	2.03	2.16
Ga	19.00	20.70	18.90	17.30	16.40	18.70	19.00	n.a.	n.a.	n.a.
Hf	4.70	4.20	3.70	4.20	3.00	4.70	6.00	6.17	3.15	4.59
Nb	2.10	3.90	3.70	3.80	3.80	6.70	3.20	23.02	2.97	7.87
Rb	58.40	195.80	39.00	51.90	79.80	64.90	54.70	125.57	63.69	123.16
Sr	468.10	417.00	278.00	339.10	289.60	712.30	389.30	93.35	632.03	142.69
Ta	0.50	0.70	0.20	0.40	0.50	0.50	0.30	2.67	0.22	0.55
Th	5.80	2.00		2.90	3.90	7.20	2.90	12.71	3.98	6.88
U	0.50	0.70	0.10	0.50	0.70	1.40	0.30	2.25	0.65	0.89
V	38.00	63.00	111.00	14.00	19.00	96.00	24.00	29.15	15.18	17.14
W	778.30	478.60	609.50	999.50	1134.80	446.10	819.70	0.33	1.17	0.35
Zr	194.80	176.50	119.20	141.00	99.20	167.90	230.60	216.35	122.01	184.70
Y	3.40	9.00	14.80	2.20	4.60	17.20	2.00	61.00	2.79	18.34
La	15.40	9.90	10.00	13.30	12.00	43.90	13.90	22.97	16.36	33.17
Ce	43.90	22.20	24.50	26.80	27.80	100.80	46.10	83.94	43.03	72.87
Pr	3.68	2.68	3.20	2.69	2.68	11.48	3.36	6.39	3.56	7.56
Nd	12.10	11.30	15.70	8.50	9.50	43.00	11.50	24.07	12.44	27.32
Sm	2.03	2.29	3.18	1.17	1.55	6.97	1.56	6.85	1.94	4.74
Eu	0.60	0.75	0.85	0.47	0.41	1.64	0.54	1.21	0.58	0.92
Gd	1.13	2.18	2.97	0.74	1.07	4.47	0.85	7.37	1.08	3.45
Tb	0.16	0.32	0.49	0.08	0.16	0.66	0.10	1.36	0.13	0.47
Dy	0.84	1.63	2.62	0.40	0.76	3.35	0.41	10.04	0.58	3.30
Ho	0.12	0.32	0.54	0.07	0.14	0.58	0.07	2.18	0.10	0.64
Er	0.32	0.86	1.48	0.20	0.47	1.75	0.18	6.90	0.21	1.80
Tm	0.05	0.13	0.22	0.03	0.07	0.25	0.03	1.09	0.04	0.30
Yb	0.35	0.75	1.51	0.21	0.40	1.60	0.17	7.24	0.28	2.01
Lu	0.05	0.12	0.23	0.03	0.07	0.25	0.03	1.04	0.04	0.31
Cu	2.70	7.70	16.60	1.00	4.30	30.50	3.50	7.01	18.07	5.82
Pb	3.50	2.50	1.40	2.70	2.90	4.80	2.00	9.18	23.34	14.21
Zn	58.00	74.00	57.00	45.00	21.00	66.00	55.00	55.15	39.34	54.29
Ni	6.90	10.30	37.30	3.80	4.40	57.20	8.50	20.81	12.88	10.52

Table B.1. Major and trace element data for felsic rocks of SW Greenland, continued

Sample	519901	519915	519921	519951	519906(2)	468636	484622	484623	496442	498005
Rock type	Augen Bt gneiss, granodiorite	Tonalitic gneiss	Tonalitic gneiss	Tonalitic gneiss	Hbl migmatite, leucosome	Migmatitic gneiss	Dioritic gneiss	Undeformed tonalite	Tonalitic gneiss	Gt-bearing tonalitic gneiss
TTG sensu Martin et al. (2005)	TTG				TTG			TTG		
Latitude (°N)	62.11170	62.65018	62.65196	62.73553	62.65092	64.18740	64.16661	64.15720	64.07642	64.33435
Longitude (°W)	-48.92116	-49.56468	-49.56963	-49.79308	-49.56323	-51.04245	-50.98580	-50.99588	-50.36895	-49.54595
Age (Ma) *	2900			2854				2862	2851	2851
±2σ	4			3				4	6	5
Collector	TFK	TFK	TFK	TFK	TFK	TOMN	TOMN	TOMN	JEH	JEH
Laboratory **	2	2	2	2	2	1	1	1	3	3
SiO2	69.13	73.13	71.75	69.77	71.84	75.95	58.02	66.84	70.60	70.30
Al2O3	14.33	15.20	15.79	14.96	14.37	11.85	15.61	15.71	15.00	15.60
Fe2O3	2.19	1.36	2.18	3.83	2.87	3.43	8.44	4.58	2.19	3.39
MgO	0.54	0.73	0.87	1.19	0.36	1.04	4.18	1.67	0.59	0.98
CaO	1.99	2.67	3.55	3.06	3.44	1.71	6.03	4.71	2.88	3.70
Na2O	4.04	3.94	4.54	3.62	4.72	3.66	3.26	4.08	4.00	4.40
K2O	2.83	1.11	0.49	2.74	0.22	1.51	1.94	1.05	2.46	1.29
TiO2	0.26	0.10	0.18	0.39	0.56	0.35	0.69	0.46	0.25	0.32
P2O5	0.08		0.08	0.08	0.19	0.02	0.12	0.11	0.05	0.08
MnO	0.06	0.03	0.05	0.07	0.04	0.04	0.11	0.06	0.03	0.07
LOI	0.50	1.25	0.41	0.32	0.49	0.30	1.40	0.60	0.34	0.49
SUM	95.95	99.53	99.90	100.04	99.10	99.86	99.80	99.87	98.39	100.62
Cr	13.25	34.62	21.87	26.68	10.04	13.68	116.31	27.37	0.00	0.00
Sc	7.14	3.84	7.65	8.81	6.20	6.00	19.00	9.00	14.54	6.40
Ba	598.62	226.75	294.96	558.90	32.84	116.00	321.00	306.00	306.71	396.80
Co	4.27	5.05	6.14	8.38	5.87	5.60	26.30	13.10	9.99	5.91
Cs	4.96	0.12	0.16	1.09	0.08	2.20	1.40	0.50	1.00	0.78
Ga	n.a.	n.a.	n.a.	n.a.	n.a.	19.50	20.40	19.00	10.62	16.97
Hf	2.33	0.35	2.24	4.18	8.32	12.60	3.50	3.20	2.44	4.24
Nb	6.72	1.47	1.15	6.16	3.30	12.60	7.80	4.20	3.41	3.69
Rb	116.13	30.58	4.37	80.50	5.27	175.20	67.70	26.90	37.19	25.43
Sr	211.18	121.26	319.56	177.43	326.91	99.70	207.90	232.80	98.70	97.83
Ta	0.47	0.46	0.03	0.38	0.24	0.40	0.60	0.30	0.25	0.20
Th	4.50	8.05	0.22	3.61	2.61	15.10	1.10	0.30	2.42	3.13
U	1.03	0.73	0.13	0.50	0.73	1.50	1.00	0.20	0.47	0.33
V	25.93	14.04	23.43	43.25	13.44	23.00	126.00	65.00	111.17	24.73
W	0.52	0.87	0.53	0.33	1.08	0.50	0.50	0.50	0.14	0.10
Zr	87.48	9.92	101.31	167.58	412.68	405.20	124.20	131.30	95.33	167.79
Y	7.96	1.49	1.09	11.48	2.23	15.30	21.10	8.70	10.45	12.78
La	18.64	4.44	8.35	15.63	26.40	42.70	7.40	9.90	12.03	20.47
Ce	42.46	14.47	16.89	33.14	40.73	100.90	24.50	22.40	23.36	32.63
Pr	4.06	0.75	1.46	3.78	4.38	10.56	2.73	2.53	2.73	3.65
Nd	15.01	2.41	4.50	14.74	14.54	38.90	12.00	10.00	10.64	12.37
Sm	2.40	0.46	0.69	3.06	1.88	6.40	3.12	2.06	2.26	2.11
Eu	0.51	0.10	0.43	0.73	0.41	0.61	0.88	0.69	0.63	0.81
Gd	1.64	0.39	0.44	2.60	1.07	5.03	3.54	1.92	2.22	2.63
Tb	0.19	0.06	0.03	0.36	0.11	0.67	0.61	0.31	0.34	0.43
Dy	1.32	0.27	0.24	2.31	0.46	3.64	3.74	1.58	2.05	2.47
Ho	0.24	0.06	0.05	0.42	0.08	0.62	0.73	0.30	0.42	0.49
Er	0.63	0.15	0.14	1.14	0.24	1.64	2.11	0.82	1.15	1.41
Tm	0.11	0.02	0.02	0.17	0.04	0.23	0.30	0.13	0.17	0.22
Yb	0.76	0.16	0.11	1.08	0.27	1.55	2.15	0.81	1.16	1.52
Lu	0.13	0.02	0.01	0.16	0.04	0.24	0.31	0.12	0.17	0.24
Cu	7.42	17.05	11.61	13.64	11.58	0.50	18.40	4.10	15.09	1.92
Pb	22.78	7.94	5.51	6.64	6.12	6.10	1.60	5.90	2.81	8.83
Zn	55.88	12.73	41.73	49.42	23.76	90.00	73.00	60.00	22.67	45.29
Ni	12.25	31.77	39.14	28.44	5.50	2.90	63.90	19.20	17.67	9.07

Table B.1. Major and trace element data for felsic rocks of SW Greenland, continued

Sample	499339	468793(1)	499221	499228
Rock type	Tonalitic gneiss	Felsic dyke	Migmatitic gneiss	Migmatitic gneiss
TTG sensu Martin et al. (2005)		TTG		
Latitude (°N)	64.19212	62.71362	63.96848	63.89559
Longitude (°W)	-51.70357	-50.17589	-50.20956	-50.54223
Age (Ma) *	2984		2881	
±2σ	11		4	
Collector	CM	TOMN	HST	HST
Laboratory **	3	1	1	1
SiO2	66.30	70.80	69.93	71.80
Al2O3	16.30	15.68	14.71	15.32
Fe2O3	4.00	2.53	4.69	1.49
MgO	1.61	0.76	0.61	0.42
CaO	3.80	2.95	3.58	2.48
Na2O	4.89	4.92	3.96	3.57
K2O	1.38	0.98	1.42	4.06
TiO2	0.53	0.30	0.45	0.18
P2O5	0.19	0.10	0.10	0.06
MnO	0.04	0.03	0.08	0.01
LOI	0.50	0.80	0.30	0.40
SUM	99.54	99.85	99.53	99.39
Cr	0.00	13.68	13.68	34.21
Sc	4.17	4.00	16.00	1.00
Ba	810.39	497.00	296.00	942.00
Co	8.13	4.90	5.20	2.80
Cs	0.35	0.50	0.10	0.50
Ga	18.30	19.20	20.00	18.60
Hf	3.40	4.50	9.40	3.90
Nb	2.20	5.00	6.80	3.00
Rb	16.61	36.70	25.80	111.00
Sr	460.36	216.60	237.50	217.70
Ta	0.09	0.50	0.30	0.20
Th	3.58	3.90	6.90	8.60
U	0.24	0.70	0.40	0.60
V	56.40	29.00	16.00	18.00
W	-0.02	0.50	0.50	0.50
Zr	144.22	165.00	423.00	141.50
Y	4.80	4.00	13.90	1.60
La	41.37	15.80	45.30	15.30
Ce	75.96	46.20	92.20	34.50
Pr	8.88	3.77	8.84	3.03
Nd	31.22	12.80	28.90	9.40
Sm	4.21	1.86	4.20	1.34
Eu	1.15	0.51	1.23	0.58
Gd	2.80	1.13	3.20	0.68
Tb	0.29	0.17	0.49	0.08
Dy	1.23	0.74	2.59	0.31
Ho	0.21	0.12	0.48	0.05
Er	0.52	0.38	1.49	0.15
Tm	0.07	0.06	0.24	0.03
Yb	0.43	0.39	1.70	0.18
Lu	0.07	0.06	0.27	0.03
Cu	27.70	3.00	12.40	5.20
Pb	5.93	2.30	2.60	7.30
Zn	49.55	55.00	51.00	29.00
Ni	9.76	5.00	4.40	4.10